

Chapter 2

Searching Dark Matter: The Quest for the Missing Mass

An increasing number of observations indicates the existence of *dark matter*, which led to one of the greatest discoveries of modern physics: the well known normal matter is only a minor contribution to the total matter and energy content of the Universe. The major matter content of the Universe is of an unknown type. This results in a central question: what is the particle nature for dark matter? The fact that it cannot be one of the constituents of known matter is one of the strongest hints to a new kind of physics beyond the standard model of particle physics. Several experiments look for hints of this new physics, e.g. *direct searches* for dark matter like EDELWEISS.

One prominent candidate for dark matter is a *weakly interacting massive particle* (WIMP). If WIMPs are the constituents of dark matter, direct searches have to be sensitive to a very rare signal, i.e. around one interaction per tonne detector mass and per year observation time. Therefore, a detailed understanding of the background is needed to decrease the background rate below the expected interaction rate.

A central background for direct searches are muon-induced neutrons. To motivate the significance of muon-induced neutrons as background for the direct dark matter search with EDELWEISS, a summary of dark matter induced signals, and hence the properties of dark matter itself, is needed.

We will first review evidences for and properties of WIMP-like dark matter in Sect. 2.1. In Sect. 2.2, we give an overview of the current state of direct dark matter searches. Finally, in Sect. 2.3 experimental aspects of direct searches for WIMPs are discussed in more detail on the example of EDELWEISS. As an important background for direct searches, muon-induced neutrons will be the topic of Chap. 3.

2.1 Motivation for WIMP-Like Dark Matter

In this section we will motivate WIMP-like dark matter as solution of the *missing mass problem*. The defining property of *dark matter* is its non-luminosity as opposite to the luminous matter visible in astronomical observations, originally referred only to

the visible light [259], nowadays extended to other wavelength ranges like infrared, X-rays, gamma-rays, and even particles like ν_e from the Sun or neutrinos from supernovae, often described as a *multi messenger approach* in astroparticle physics. Under the assumption that Newtonian physics is valid for the description of non-relativistic dynamics, the dynamical behaviour of gravitationally bound systems can not be explained by their visible mass alone, raising the *problem of missing mass*.

Astronomical indications for dark matter as solution for the missing mass problem will be given in Sect. 2.1.1. Thereafter, we introduce a supersymmetric WIMP as one possible particle candidate for dark matter (Sect. 2.1.2).

To detect dark matter and to specify its properties, three experimental approaches are viable: *accelerator based* experiments including the search for the missing transverse momentum associated with the production of dark matter (Sect. 2.1.3), *indirect detection* experiments searching for the products of dark matter self-annihilation (Sect. 2.1.4), and *direct detection* experiments searching for the scattering of galactic dark matter off terrestrial targets (Sect. 2.1.5).

We will review the first two approaches briefly and will focus on direct detection with the example of EDELWEISS in the next two Sects. 2.2 and 2.3.

2.1.1 Dark Matter as Solution for the Missing Mass Problem

We will first motivate dark matter as solution to the problem of missing mass via a historic review of classic indications relying on the dynamical behaviour of gravitationally bound systems, like galaxy clusters and galaxies,^{1,2} Afterwards, we will discuss the standing of the dark matter paradigm against the alternative solution of modified gravity on the example of weak gravitational lensing. Possible particle candidates for dark matter will be discussed in Sect. 2.1.2.

In the original meaning as non-visible mass, F. Zwicky used the term in 1933 to describe the discrepancy between the mass of luminous matter and the total, dynamic mass he observed in the Coma cluster, a gravitationally bound group of galaxies [325, pp. 124f.], [326].

F. Zwicky's original intention was to determine the velocity of Coma for a further validation of Hubble's law, the proportionality between distance and velocity of an astronomical object. In his work F. Zwicky noted an unusual great spread of the single galaxies within the cluster. By applying the virial theorem³

¹We find it convenient to the focus on gravitationally bound systems like our Galaxy in contrast to cosmological arguments because the experiments reported in Sect. 2.2 search for dark matter in the galactic halo.

²Besides these selected cases, further indications for dark matter in the sense of missing mass related to the dynamics in gravitationally bound astronomical systems, e.g. binary galaxies, are listed in [312].

³In his original work, F. Zwicky denotes Newtons gravitational constant, nowadays usually abbreviated as G , with Γ .

$$M = \frac{5R}{3G} \overline{v^2} \quad (2.1)$$

on the mean velocity of the clusters galaxies $\sqrt{\overline{v^2}} = 1000 \text{ km s}^{-1}$ he found a dynamical mass M within the cluster radius R of 400-times the mass of luminous matter of the cluster. The latter one he approximated as the number of cluster galaxies times the averaged galaxy mass. The discrepancy between dynamical mass and luminous mass he attributed to a non-luminous, hence *dark*, mass that contributes to the dynamics of the cluster.

The discrepancy observed by F. Zwicky was confirmed over the last 80 years and is still valid. After his introduction of the virial theorem in astronomy [86], other galaxy clusters and groups were weighted with the same technique. So find R. Carlberg et al. [140] by averaging over 16 clusters with roughly 1000 galaxies a mass-to-luminosity ratio of $M/L = (295(53)) h M_{\odot} L_{\odot}^{-1}$ where h is the Hubble constant and M_{\odot} (L_{\odot}) the mass (luminosity) of the sun. For galaxy groups, like the local group containing the Milky Way, a smaller ratio of $M/L \approx 12 M_{\odot} L_{\odot}^{-1}$ is found [209, 230]. The difference in M/L can be explained by assuming that big galaxy clusters are dominated by the dark matter distributed throughout their gravitational well, whereas small-size galaxy groups are dominated by dark matter concentrated around the single galaxies [209].

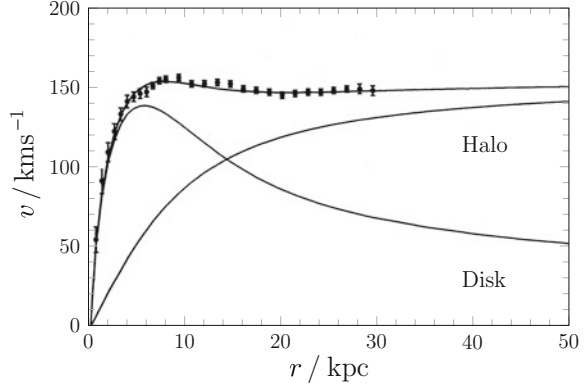
The concept of dark matter concentrated around single galaxies was first applied in 1970 by K.C. Freeman for the galaxies M33 and NGC300. Again, a discrepancy between luminous matter and dynamical mass could be derived. In the *rotation curves* $v - r$, see e.g. Fig. 2.1 for a more recent example, he recognized a deviation of the orbits of stars around the galaxy centre from the Keplerian predictions (the *disk-curve* in Fig. 2.1): beyond a characteristic radius that depends on the actual mass-density profile of the galaxy, a drop of rotation velocity v inversely proportional to the radius r of the orbit is expected: $v^2 \propto 1/r$. He found no such drop in the rotation curve $v - r$ over the whole visible galaxy (visible light and radio emissions) and concluded the existence of additional ‘undetected matter’, extending further than the luminous matter [184, p. 828], [185].

In 1974, the dark matter within the galaxy clusters was connected to the dark matter in individual galaxies. The existence of ‘coronas’ [167] or ‘spheres’ [260] of dark matter around galaxies were postulated after it was found that the stars orbits could be explained by a spherical distribution of additional dark matter. These *dark halos* as they are called today are therefore also contributing to the mass of the host galaxy cluster. For example, Fig. 2.1 shows a fit of a spherical dark halo on the rotation curve of NGC 3198.⁴

Finally V.C. Rubin, N. Thonnard, and W.K. Ford Jr. showed in 1980 by the then largest systematic observation of galactic rotations that the anomalous rotation curves were no exception. Contrary, they found out of 21 spiral galaxies no single one that followed the expected Keplerian behaviour [274]. Five years later, V.C. Rubin et al.

⁴Albeit J. Einasto, A. Kaasik, and E. Saar provide an earlier fit of a dark halo to a rotation curve in [167], we chose the example of [48] for the sake of clarity as it shows the individual components.

Fig. 2.1 Observed rotation curve of NGC 3198 (data points), i.e. circular velocity v of stars as function of their distance to the galaxy centre r , fitted by a combination of an exponential disk containing the visible mass and a dark, spherical halo. Figure adapted from [48, Fig. 4]



could describe the rotation curves for all spiral galaxies of a given type and luminosity L with one general formula, after the radius r is scaled to the optical radius r_{opt} , at which the luminosity drops under a certain threshold. Additionally, the similarity between these general curves was noted [275]. And in the 1990s, it was shown by M. Persic and P. Salucci that the rotation curve $v(r/r_{\text{opt}})$ of all spiral galaxies can be described by the same formula after they were normalized to the total luminosity L_* , assuming a visible disk and a dark halo [262, 263]. This universal rotation curve was then reproduced in 1996 by numerical simulation of the galaxy formation, assuming a *Navarro-Frenk-White* (NFW)-distribution of the dark matter density $\rho(r)$ [250, 251], which can be parametrized as [121]

$$\rho = \frac{\rho_0}{\left(\frac{r}{R}\right)^\gamma \left[1 + \left(\frac{r}{R}\right)^\alpha\right]^{(\beta-\gamma)/\alpha}} \quad (2.2a)$$

$$\alpha = 1.0, \quad \beta = 3.0, \quad \gamma = 1.0, \quad R = 20 \text{ kpc} \quad (2.2b)$$

with the dark matter density of the halo ρ_0 and a characteristic scale R . However, the behaviour of the rotational curve near the galactic centre is debatable, see the reviews in [121, 206], and several models for the halo exist, see references in [97, 169, 207]. Also the existence of substructure of dark matter clumps is discussed [107]. Nevertheless, the given NFW-model fits well the outer parts of the galaxies, as Fig. 2.2 shows for the example of our Galaxy. The existence of dark matter in our Galaxy indicates also the possibility to detect dark matter with earth based experiments, which will be discussed in Sect. 2.1.5.

The cluster and rotation curves are clear indications of missing matter, but no final proofs. The observed discrepancy may be explained not only by dark matter, i.e. correcting our experimental knowledge about the source distribution of gravity, but also by modifying gravity, i.e. correcting our theoretical model of gravity.

To explain the missing mass problem without an introduction of an additional kind of matter, M. Milgrom proposed in 1983 a modification of Newton's second law [242]. As M. Milgrom pointed out, all experimental validation of Newton's

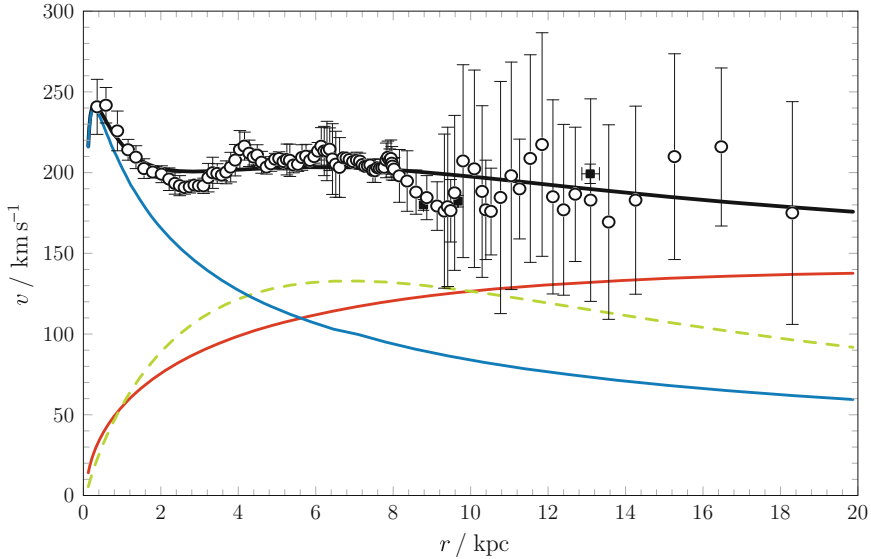


Fig. 2.2 Rotation curve of the Milky Way, i.e. circular velocity v as function of the distance r to the galactic center, for the innermost 20 kpc. Fitted to the data points are the sum (black line) of three components: A visible bulge (blue line) and disk (dashed green line), together with a dark halo based on a NFW-parametrisation (red line). Figure adapted from [293, Figs. 2 and 5], references for the data compilation therein

second law were made within the range of our solar system and for accelerations higher than the typically intra-galactic accelerations. Therefore it may be possible that on intra-galactic scales the inertial force and the gravitational mass of a body is not anymore related by Newton's second law, but by a more generalized function $\mu(x)$ [242, p. 366]:

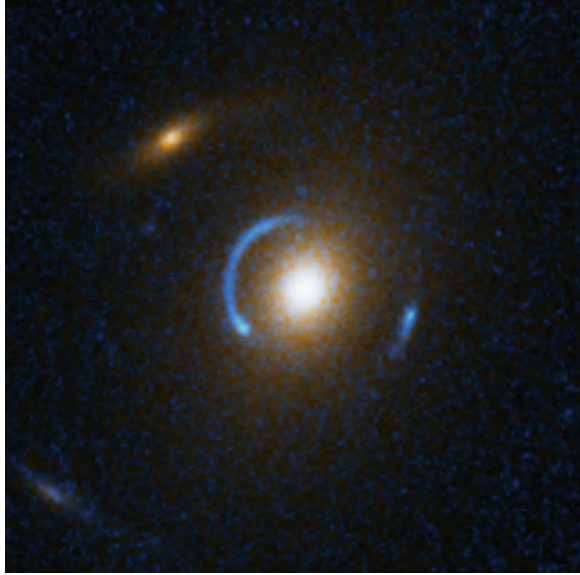
$$\vec{F} = \vec{a} \cdot \mu(a/a_0) \cdot m_g \quad (2.3)$$

known as *Modified Newtonian Dynamics* (MOND). By demanding that for accelerations higher than a threshold a_0 Newton's second law is valid $\mu(x \gg 1) \approx 1$, and that for accelerations below the threshold a modification $\mu(x \ll 1) \approx x$ occurs, the function $\mu(x)$ is constrained.

M. Milgrom noted a good reproduction of the rotation curves for $a_0 \approx 2 \cdot 10^{-8} \text{ cm s}^{-2}$ without the need of non-visible mass [243]. As all the systems under considerations are bound by gravity the modified dynamics (Eq. 2.3) can be expressed by a modified gravitational field [242]: But as M. Milgrom stated himself: The modification “can at most be considered an effective working formula. [...] We are thus still in need of a theory for the modified dynamics even in the nonrelativistic regime” [242, p. 366].

A non-relativistic theory of gravity leading to Eq. 2.3 was first given by Bekenstein and Milgrom [92], and named AQUAL (derived from *AQUadratic Lagrangian* [95]):

Fig. 2.3 Einstein ring SDSS J120540.43+491029.3: Multiple, arc-like images of a background galaxy (*blue*) caused by strong gravitational lensing from a foreground galaxy (*center, yellow*) [187]. Picture reprinted from [294]. Credit NASA, ESA, A. Bolton (Harvard-Smithsonian CfA) and the SLACS Team



the Lagrangian leading to the Poisson equation for the gravitational potential Φ is no longer quadratic in $\nabla\Phi$, but depends on $f((\nabla\Phi)^2/a_0^2)$ instead. For $f(x^2) = \mu(x)$, the dynamics described by Eq. 2.3 follow. AQUAL fits the rotation curves of several hundred galaxies as successfully as MOND [95, 278], but it is challenged by results from *gravitational lensing*: the gravitational potential of a mass in the foreground causes a distortion of background light sources, ranging from a slight shearing of the background image (*weak gravitational lensing* [201]) to the split into multiple images (*strong gravitational lensing* [311]). Strong lensing is in tension with MOND/AQUAL, as it reveals a missing mass problem also in regions of galaxies where $a > a_0$, i.e. where MOND/AQUAL behaves by definition Newtonian, leading again to the need of dark matter [176]. However, the possibility remains that gravitational lensing in a relativistic formulation of AQUAL could behave differently [176]. A relativistic theory of MOND/AQUAL is TeVeS (derived from *Tensor-Vector-Scalar* [93]), in the sense that the non-relativistic limit is AQUAL. The success of TeVeS to explain strong lensing is controversial. It is claimed [95, 154], that TeVeS can explain strong lensing systems like SDSS J120540.43+491029.3 [154], see Fig. 2.3, with an additional amount of neutrinos with $m_\nu \approx 2\text{eV}$ [150]. However, even with such massive neutrinos, more recent investigations claim that TeVeS will fail to explain strong lensing without additional, non-neutrino dark matter [178]. Contrary, dark matter can explain the observed strong lensing, like Fig. 2.3 [177], without modifying gravity.

The challenge for theories like TeVeS is even greater for *weak gravitational lensing*: An example for a system showing weak gravitational lensing is the galaxy cluster 1E 0657–558, named *Bullet Cluster*, which consists of two sub-cluster, one less massive than the other [156], see Fig. 2.4. Both are moving away from each other, after

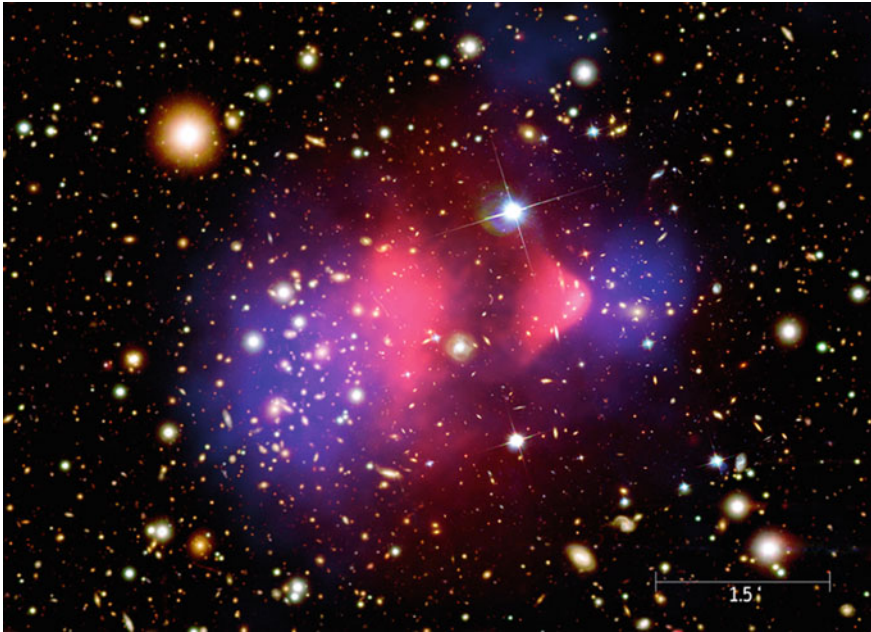


Fig. 2.4 Galaxy cluster merger 1E 0657–558 (‘bullet cluster’) observed via X-rays (*red*) and the corresponding shear map (*blue*) obtained via weak gravitational lensing [156]. Via self-interaction, the hot intracluster medium was slowed down and is nowadays located in the centre of the cluster. In the dark matter paradigm, the shear field shows that most of the gravitating mass is different from the intracluster medium and located at the position of the sub-clusters. In modified gravity paradigm, the difference between the peaks in shear field are caused by the intracluster medium via position dependent gravitational coupling. For details see text. Picture reprinted from [198]. *Credit* X-ray: NASA/CXC/CfA/M.Markevitch et al.; Optical: NASA/STScI; Magellan/U.Arizona/D.Clowe et al.; Lensing Map: NASA/STScI; ESO WFI; Magellan/U.Arizona/D.Clowe et al.

the cluster cores passed through each other in a collision roughly 100 million years ago [156]. While the single galaxies of the sub-clusters were not affected by the collision, acting as collision-less particles, the hot intracluster medium, containing most of the visible mass [248], acts fluid-like and was heated. The location and extension of the intracluster medium therefore can be tracked by the X-ray emission. The total gravitational mass of the cluster can be traced by weak gravitation lensing which causes a distortion of the shape of a background object. As the original shape of a single background object is unknown, the average shape over a sample of background objects away from the cluster can serve as reference and can then be compared with the average shape of background objects behind the cluster. The resulting shear map is related with the mass density map via the theory of gravitation under consideration, for an overview over weak lensing see [201]. The X-ray observations reveal that the intracluster medium is located roughly in the middle between the visible centres of the sub-clusters. In contrast, the mass-density map revealed from the weak lensing

observations shows two centres coincident with the centres of the visible sub-cluster. The superposition of both observations results in the famous Fig. 2.4, resembling a blue bullet (mass density of the smaller cluster) punching through a red wall (X-ray emission of intracluster medium), hence the popular name of the cluster.⁵

Whereas the astronomical observation could be reproduced with other clusters (see [130] and references therein), the interpretation of the observations depends on the used paradigm. Supporters of both paradigms agree that nearly the total of the luminous mass is traced via X-ray emission. But the interpretation of the shear map is different:

For a MOND based theory like TeVeS, the centre of baryonic matter should coincide with the measured centres of shear [94, 170, 304], which is not the case. This is accepted by supporters of MOND, like J. D. Bekenstein:

[TeVeS] does not account for the observed distortion [of weak lensing] without the help of invisible matter [=dark matter] in addition to a reasonable dose of massive neutrinos. [...] dramatized by a handful of colliding clusters, [...] MOND has never dealt perfectly with the dynamics of clusters. So TeVeS, which was designed with MOND in mind, could not [be] expected to do well in this business, and modification of it may be in order. [...] clusters may well contain large amounts of as yet invisible [baryonic] matter [95, p. 559c]

However, more generalized theories of gravity can accommodate to this difference by introducing a position dependent gravitational coupling [245].

Within the dark matter paradigm, the centres of the shear map are coincident with the centres of collisional-less dark matter. As the dark matter halos of the sub-cluster do not interact with each other during the collision, like the visible cluster content, they are already separated again, and coincident with the centre of the visible sub-clusters [156]. If the dark matter paradigm is correct, such cluster merger would allow to measure the self-interaction rate of dark matter [267]. In general, weak lensing is a suitable tool to map the large scale distribution of dark matter [164, 270], e.g. in galaxy clusters like Cl0024+17 [205], see Fig. 2.5.

In summary, over the last 80 years, astronomical observations from galaxies clusters and single galaxies showed strong evidence for a gap between the visible mass and the dynamic mass of the system, leading to the problem of missing mass. Proposed solutions are additional *dark matter* or a modified theory of gravity like *MOND*. Strong and weak gravitational lensing reject the simpler MOND-like theories. The remaining, more complex theories are forced to incorporate an additional amount of dark matter in form of massive neutrinos and baryonic matter, contrary to their original intention. Albeit this does not disprove theories of modified gravity as possible explanation for the missing mass problem, it certainly reduces their attractiveness. The identification of a new kind of particles leading to the density distributions needed to substitute the dark halos would be a strong support for the dark matter paradigm and disfavour an explanation of the missing mass problem by modified gravity. Needed properties for such a particle candidate and its galactic distribution are the topic of Sect. 2.1.2.

⁵Some of the X-ray features, like the red bow shock behind the blue bullet in Fig. 2.4, are also visible by radio observations of the cluster [232, 286].

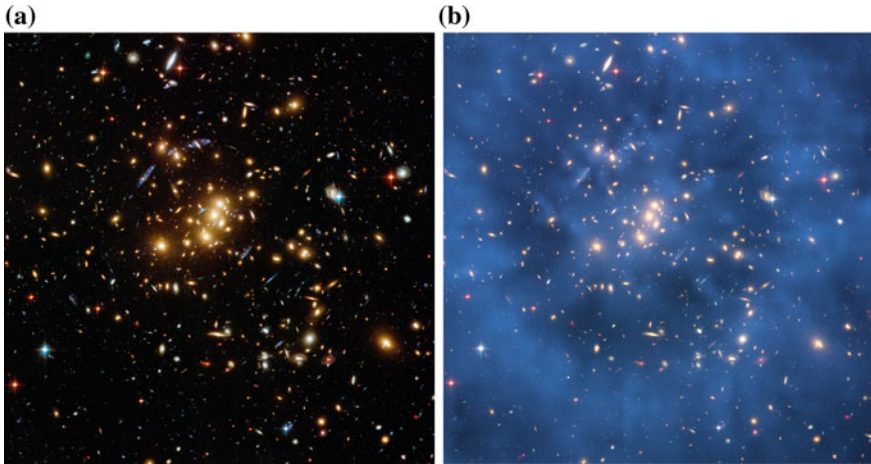


Fig. 2.5 **a** The rich galaxy cluster Cl0024+17 features both weak and strong gravitational lensing, the latter is visible as *arc* like structure around the centre of the image. *Credit* NASA, ESA, M.J. Jee and H. Ford (Johns Hopkins University). **b** Based on weak and strong gravitational lensing, the projected distribution of dark matter is obtained as *ring* like structure (*blue*) around the cluster center. The ring structure may be the result of a high-speed collision of two clusters along the line-of-sight [205]. *Credit* NASA, ESA, M.J. Jee and H. Ford (Johns Hopkins University). Pictures reprinted from [295]

2.1.2 Supersymmetric WIMPs as Dark Matter Candidates

The astronomical observations discussed in the previous section, ranging from velocity dispersion in galaxy clusters over galactic rotation curves to weak lensing maps of rich galaxy clusters, are strong evidences for dark matter. However, these observations do not reveal the constituents of dark matter. In this section, we will shortly review the properties for such constituents, deduced from astrophysical and cosmological observations. Subsequently, we list well motivated particle candidates for dark matter, focusing on the classic example of supersymmetric particles like the neutralino. In the next section we will review the impact of the Higgs discovery and the latest LHC results on the parameter space for supersymmetric *weakly interacting massive particles* (WIMPs) as candidates for cold, non-baryonic dark matter.

The observations reported in Sect. 2.1.1 show that dark matter is non-luminous and has a small self-interaction, as shown by merging clusters (Fig. 2.4). The merging clusters also show that at this length scale dark matter is mostly *non-baryonic*: the main mass is distinct from the intercluster medium [248], which contains most of the baryonic mass of a galaxy cluster [193] especially if it is traced until the outskirts of the cluster [290]. This is further supported by observations on galactic scale. A possible source for non-luminous, baryonic matter on galactic scale could be *massive compact halo objects* (MACHOs), e.g. in form of stellar remnants [141]. However, searches for microlensing events caused by the transit of such an MACHO in front

of a star could limit the MACHO contribution to the mass of the galactic halo to less than 8 % [307].

Large scale structures and their distribution can solve the question whether the dark matter was non-relativistic (*cold*) or relativistic (*hot*) at the time of recombination. The free-streaming of *hot dark matter*, like neutrinos, suppresses the growth of structures below a certain scale [124]. The comparison between observed and simulated matter power spectra ruled out a major contribution of hot dark matter [58, 305]. This is further supported by the success of N-body simulations based on *cold dark matter* (CDM) to reproduce the observed hierarchical clustering [252] from individual galaxies [196, 214] over galaxy clusters [216] to super clusters [298] in the local universe. An often quoted disadvantage of CDM structure formation is the over-prediction of smaller dark halos (see [215] and references therein). If they are identified as hosts of dwarf galaxies, then the simulated numbers are often in disagreement with the observed number of dwarf galaxies. However, recent simulations reduce the predicted numbers of dwarf galaxies by tidal disruption caused by bigger galaxies nearby [166, 291] and by feed-back of star formation, supernovae wind, and ultraviolet radiation of the luminous matter [188, 194]. Also newer observations increased significantly the number of ultra-faint dwarf galaxies [99, 308] and dark matter dominated satellites [314]. Combining both effects, an agreement between simulations and observations seems possible. Recent weak lensing observation confirms also the predicted filaments of CDM between individual galaxies [164].

From studies of the *cosmic microwave background* (CMB), the energy density Ω in units of the critical density (see Eq. A.7) of the total non-relativistic matter (Ω_m), of the baryonic matter (Ω_b), and of active neutrinos (Ω_ν) can be deduced on cosmological scale. As neutrinos affect the matter power spectrum, Ω_ν can be deduced from its effect on the CMB via weak gravitational lensing since the time of recombination [226]. The peak-height ratio of the acoustic oscillations in the CMB power spectrum (Fig. 2.6) are sensitive to Ω_m , Ω_b at the time of recombination [203, 277]. Consequently, the cold dark matter density can be calculated: $\Omega_{\text{cdm}} = \Omega_m - \Omega_b$. Observation of the CMB with the PLANCK satellite [28] gives the latest values for the energy densities⁶:

$$\Omega_m = 0.313 \quad (2.4a)$$

$$\Omega_{\text{cdm}} = 0.263 \quad (2.4b)$$

$$\Omega_b = 0.0486 \quad (2.4c)$$

$$\Omega_\nu < 0.0156 \quad (2.4d)$$

⁶The energy densities for matter, cold dark matter, and baryons are calculated from the PLANCK best fit values $\Omega_m h^2 = 0.1423$ [28, Eq. 15], $\Omega_{\text{cdm}} h^2 = 0.1196$ [28, Eq. 18], and $\Omega_b h^2 = 0.02207$ [28, Eq. 17] with a Hubble constant of $H_0 = h \cdot 100 \text{ km s}^{-1} \text{ Mpc}^{-1} = 67.4 \text{ km s}^{-1} \text{ Mpc}^{-1}$ [28, Eq. 13]. The energy density of active neutrinos is based on $\Omega_\nu h^2 = \sum_i m_i / 93.14 \text{ eV}$ [226, 296] with $\sum_i m_i < 0.66 \text{ eV}$ [28, Eq. 69]. All densities are given to three decimal places.

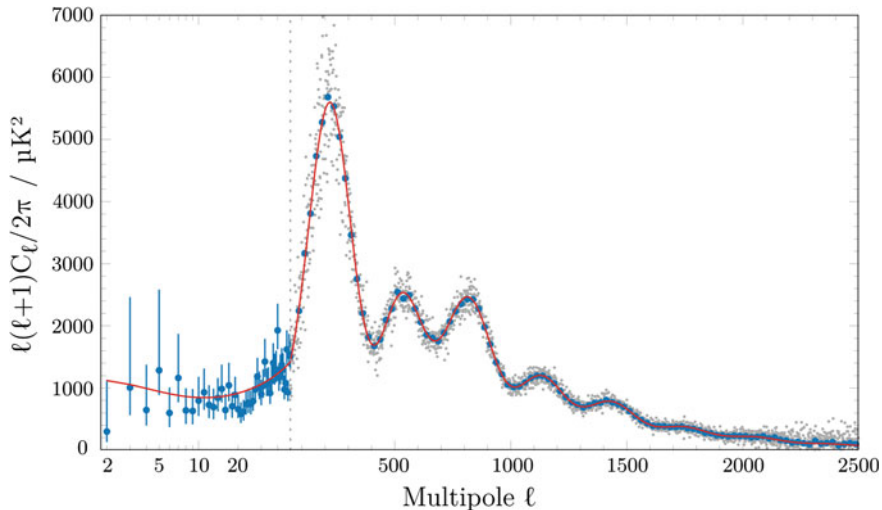


Fig. 2.6 Foreground-subtracted temperature power spectrum on a logarithmic-linear hybrid scale as observed by Planck. Power spectrum shown as multipole-by-multipole (*grey points*) and averaged over width of 31 (*blue*). The *red line* shows the temperature spectrum for the best-fit based ΛCDM cosmology. The *dashed line* indicates the change from logarithmic scale to linear scale. Figure and description adapted from [28, Fig. 1]

The relative small contribution of baryonic matter is in agreement with results from the big bang nucleosynthesis [301]. These numbers clearly show that most of the matter content of the Universe is provided by non-baryonic, cold dark matter.

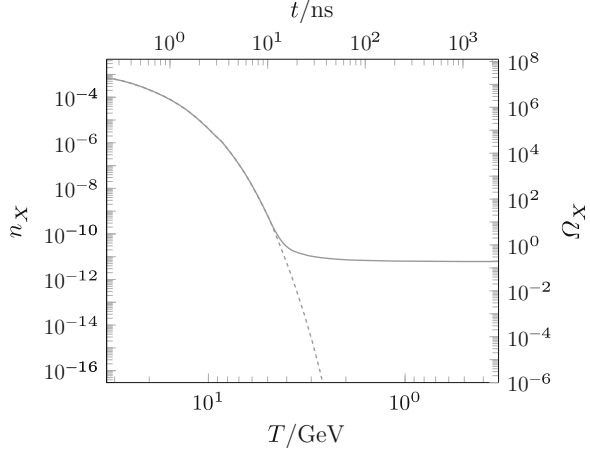
According to the production process, candidates for nonbaryonic CDM are divided into two groups, either being produced in nonthermal processes or produced in thermal equilibrium in the early universe, hence called *thermal relict*. Even particles from both categories may contribute to the observed Ω_{cdm} in context of multicomponent scenarios [120, 173].

An example for nonthermally produced candidates is the *axion*. It is the pseudo-Nambu-Goldstone boson of the Peccei-Quinn symmetry postulated to solve the strong CP problem [212, 261]. If the Peccei-Quinn symmetry exists, it would be broken by the Peccei-Quinn phase transition when the Universe cools below the axion decay constant f_a , resulting in the nonthermal production of axions with mass m_a . As the axion is not yet observed, the observed Ω_{cdm} can be produced by a wide range of the axion parameter space [173]:

$$\begin{aligned} 10^{12} \text{ GeV} \theta^{-2} &\gtrsim f_a \gtrsim 10^9 \text{ GeV} \\ 6 \mu\text{eV} \theta^2 &\lesssim m_a c^2 \lesssim 6 \text{ meV}, \end{aligned} \tag{2.5}$$

where $\theta \lesssim 1$ depends on the phase transition.

Fig. 2.7 Comoving number density n_X and resulting relic density Ω_X as function of the temperature T and age t of the Universe for a WIMP with 100 GeV. The *solid line* is the number density of a particle that freezes out, the *dashed line* for a particle that remains in thermal equilibrium. Figure adapted from [173, Fig. 2]



A thermal relic particle X produced in the early universe, was initially in thermal equilibrium. When the temperature T drops below the particle mass m_X , its comoving number density n_X becomes Boltzmann suppressed: $n_X \sim (m_X T / 2\pi)^{3/2} \exp(-m_X / T)$ [173, 206]. As the Universe expands with the inverse Hubble's constant $1/H$, the particles eventually become chemically decoupled [269], and they *freeze out* as their number density approaches a constant *relic density* [153, 323]. The actual evolution of the number density n_X is described by the Boltzmann equation [173, 206],

$$\frac{dn_X}{dt} = -3Hn_X - \langle \sigma_a v \rangle (n_X^2 - n_{X,\text{eq}}^2) \quad (2.6)$$

where $\langle \sigma_a v \rangle$ is the thermal average of the annihilation cross section times the relative velocity and $n_{X,\text{eq}}$ is the number density in thermal equilibrium. A numerical solution is shown in Fig. 2.7. The number density $n_f = H / \langle \sigma_a v \rangle$ at decoupling can be approximated as [173]

$$n_f \simeq \frac{T_f^2}{m_{\text{Pl}} \langle \sigma_a v \rangle}, \quad (2.7)$$

with the Planck mass m_{Pl} and the freeze-out temperature T_f . This leads to a present day relic density of [173]:

$$\Omega_X \sim \frac{m_X T_0^3}{\rho_c m_{\text{Pl}} T_f} \langle \sigma_a v \rangle^{-1}. \quad (2.8)$$

For a weakly interacting particle, the cross section can be approximated in leading order by [173]

$$\sigma_a v \approx \frac{g^4}{16\pi^2 m_X^2} \begin{cases} 1, & \text{S-wave annihilation} \\ v^2, & \text{P-wave annihilation} \end{cases} \quad (2.9)$$

with the weak interaction gauge coupling $g \simeq 0.65$. As a consequence, the *WIMP miracle* [173, 206] occurs: Each *weakly interacting massive particle* (WIMP) with $m_X \sim 1 \text{ TeV}$ can produce the observed amount ($\Omega_X \sim \Omega_{\text{cdm}}$) of cold ($T_f \approx m_X/20$ [186, 206]) dark matter. To reproduce the observed dark matter abundance (Eq. 2.4b), an annihilation cross section of [264]

$$\langle \sigma_a v \rangle \approx 3 \times 10^{-26} \text{ cm}^3 \text{ s}^{-1} \quad (2.10)$$

is necessary.

Several theories like universal extra dimensions or *supersymmetry* (SUSY) can motivate particle candidates that qualify as WIMPs [173]. In the following we will focus on the classical example of supersymmetric WIMPs.

SUSY is a symmetry between bosons and fermions: it transforms each boson (fermion) of the standard model of particle physics, called *particle*, in a yet undiscovered fermion (boson), called *sparticle*, and vice versa [240]. Supersymmetry is motivated by the *gauge hierarchy problem* of the standard model: the loop-corrections Δm_h^2 of the Higgs mass $m_h^2 = m_{h0}^2 + \Delta m_h^2$ are only limited by an ultraviolet momentum cut-off Λ . The cut-off is assumed to be on the order of the Planck mass m_{Pl} where the standard model is expected to break down [173, 240]:

$$\Delta m_h^2 \sim \frac{\lambda^2}{16\pi^2} \int^\Lambda \frac{d^4 p}{p^2} \sim \frac{\lambda^2}{16\pi^2} \Lambda^2, \quad (2.11)$$

with a dimensionless coupling $\lambda \sim \mathcal{O}(1)$.

However, the recent discovery of the Higgs boson [2, 147] fixed its mass to $126 \text{ GeV} \ll m_{\text{Pl}}$, i.e. the single contributions to the loop correction must cancel out within 1 part in 10^{36} [173]. As the contribution of fermions to Eq. 2.11 differs from the contribution of bosons by a sign change, an exact SUSY would lead to the needed cancellation as it provides a fermionic (bosonic) sparticle for every bosonic (fermionic) particle. As up to now no sparticles were detected, they must be heavier than the standard model particle, and hence SUSY must be broken with a mass splitting between particles m_{SM} and corresponding sparticle m_{SUSY} . This results in a loop correction to the Higgs mass of [173, 240]:

$$\Delta m_h^2 \sim \frac{\lambda^2}{16\pi^2} \int^\Lambda \frac{d^4 p}{p^2} \Big|_{\text{SM}} - \frac{\lambda^2}{16\pi^2} \int^\Lambda \frac{d^4 p}{p^2} \Big|_{\text{SUSY}} \quad (2.12)$$

$$\sim \frac{\lambda^2}{16\pi^2} \left(m_{\text{SUSY}}^2 - m_{\text{SM}}^2 \right) \ln \frac{\Lambda}{m_{\text{SUSY}}}, \quad (2.13)$$

and therefore stabilizes the gauge hierarchy problem for $m_{\text{SM}} \sim m_{\text{SUSY}} \ll m_{\text{Pl}}$. From the experimental constraints on the Higgs mass, one can deduce the mass splitting, and therefore the mass of the *lightest supersymmetric particle* (LSP), to be of $\mathcal{O}(1 \text{ TeV})$. This is the same mass scale needed for a WIMP to produce the observed relic density Ω_{cdm} . Quantitative constraints on the WIMP mass from global fits of SUSY to recent observations will be discussed in Sect. 2.1.3.

As further advantage, the LSP is stable in SUSY theories with preserved R -parity. The R -parity P_R of a given particle or sparticle is a discrete symmetry [240]

$$P_R = (-1)^{3(B-L)+2s} \quad (2.14)$$

$$= \begin{cases} +1, & \text{particle} \\ -1, & \text{sparticle} \end{cases} \quad (2.15)$$

associated with baryon-number B , lepton-number L , and spin s . It is motivated to prevent any baryon- and lepton-number violation, as under conserved R -parity only pairs of sparticle can be produced or annihilate. Consequently, a stable LSP results.

The *minimal supersymmetric standard model* (MSSM) contains all sparticle partners to the known particles, the latter are extended by an extra Higgs doublet [206], and it conserve R -parity [240]. Depending on the parameter space, the MSSM-LSP χ is usually the lightest of four *neutralinos* $\tilde{\chi}_1^0, \dots, \tilde{\chi}_4^0$, i.e. it is a linear combination of *gauginos* (\tilde{B}, \tilde{W}^3) and *higgsinos* ($\tilde{H}_1^0, \tilde{H}_2^0$) [206, 240]:

$$\chi = n_{10}^* \tilde{B} + n_{20}^* \tilde{W}^3 + n_{30}^* \tilde{H}_1^0 + n_{40}^* \tilde{H}_2^0. \quad (2.16)$$

Here, \tilde{B}, \tilde{W}^3 are the supersymmetric partners of the $U(1)$ gauge field B and the third component of the $SU(2)$ gauge field W^3 that mix to the photon and Z^0 boson, and $\tilde{H}_1^0, \tilde{H}_2^0$ are neutral Higgs bosons [206].

Therefore, the neutralino provided by the MSSM is the classic example of a supersymmetric WIMP as particle candidate for non-baryonic, cold dark matter.

2.1.3 Constraints on the WIMP Parameter Space Including Latest LHC Results

As discussed in the previous section, a supersymmetric WIMP is a well motivated particle candidate for dark matter. Furthermore, the observed thermal relic abundance constrains the supersymmetric parameter space. Therefore the question arises whether this constraint is consistent with various accelerator based measurements which affect also the parameter space, like searches for sparticle production. A prominent example of a recent result that affects the parameter space is the discovery of the Higgs boson at the *Large Hadron Collider* (LHC).

This section starts with a short review of the relevant supersymmetric parameters in the most common models. Afterwards, we will list the most recent global fits [85, 137, 182, 302] to results from direct dark matter searches, thermal relic abundance, and results from the LHC. Finally, we note the implications for future direct searches for dark matter.

The general soft supersymmetry-breaking Lagrangian of the MSSM that is consistent with gauge invariance and R -parity conservation has 105 free parameter [240, Ref. 77]. Consequently, usually simplified phenomenological SUSY models are used

to interpret experimental results, like the *Constrained Minimal Supersymmetric Standard Model* (CMSSM) which serves as canonical model for supersymmetric studies [174]. In the CMSSM, the supersymmetry breaking is mediated by gravity, hence it is also called *minimal supergravity* (MSUGRA) [240, Refs. 152,153]. The number of free parameter is reduced to 5 (m_0 , $M_{1/2}$, A_0 , $\tan\beta$, $\text{sign } \mu$) at the GUT scale $\approx 2 \times 10^{16}$ GeV, under the three assumptions of [208]: a universal gaugino mass $M_{1/2}$, a universal scalar mass m_0 , and a common trilinear scalar coupling A_0 .

Some regions of the parameter space are named according to the possible interactions that could contribute to the LSP self-annihilation [240]: a resonance annihilation with the neutral Higgs scalar A^0 of the MSSM is possible in the *A-funnel*, a coannihilation with the lightest stau or stop is possible in the *sfermion coannihilation region*, *t*-channel squark or slepton exchange and coannihilation can occur in the *focus point*.

Global fits of the CMSSM parameter space consider as inputs [85, 137, 182, 302]: the thermal WIMP relic abundance from CMB observations (see Sect. 2.1.2), limits from direct dark matter searches which will be discussed in Sects. 2.2 and 2.3, and constraints from accelerator results. Usually all of the following three categories of accelerator based observations are used to fit the CMSSM parameter space⁷:

As already mentioned in the previous section, the mass of the lightest Higgs boson is sensitive to the supersymmetric particle spectrum via radiative corrections [206]. Additional, SUSY may open new, invisible channels for the Higgs decay [139]. Recently, the ATLAS [2] and CMS [147] experiments discovered at the LHC a new particle at ≈ 126 GeV, consistent with evidence from the D0 and CDF experiments [11], and in agreement with the Higgs boson of the standard model. It is therefore an important test to reproduce this Higgs mass within the CMSSM.

It is expected that a hadron collider like the LHC will produce mainly colored supersymmetric particles [174] e.g. stops. As astronomical observation favours a weakly interacting LSP, the strong interaction particles have to decay. Their cascade decay to the LSP would cause a high jet (j) multiplicity as signature [174, 221]. The signature for the LSP would be missing transverse energy (\cancel{E}_T) in the final state accompanied by standard model particles [174]. Both ATLAS and CMS searched for these signatures in several final states, e.g. $(\cancel{E}_T + j)$ [3, 83, 146, 211], $(\cancel{E}_T + l)$ [1], $(\cancel{E}_T + \gamma)$ [149], $(\cancel{E}_T + l^+ l^-)$ [148], but found no signal so far.

Also precision measurements of electroweak interactions, e.g. the anomalous magnetic moment of the muon $a_\mu = (g_\mu - 2)/2$ [102], and b-physics is used to constrain the CMSSM parameters. An example for the latter category is the exclusive dimuon decay of B_s^0 , B^0 mesons which are helicity suppressed in the standard model, but its branching ratios are enhanced in SUSY models [82]. Therefore, the CMSSM parameter space is sensitive to the limits on $BR(B^0 \rightarrow \mu^+ \mu^-)$ [4, 82] and the observation of $B_s^0 \rightarrow \mu^+ \mu^-$ at the LHC [4].

⁷The examples we give in the text may differ from the specific data set used in [137, 182, 302] as we try to select the common and recent references. For the actually used data sets we refer to the references in [137, 182, 302].

For the following review, we will focus on the global fits from O. Buchmueller et al. [137], C. Strege et al. [302], and A. Fowlie et al. [182], as they contain predictions for the elastic WIMP-nucleon scattering cross section (Sect. 2.1.5), an important parameter for the direct dark matter searches listed in Sect. 2.2. Here, O. Buchmueller et al. and C. Strege et al. used the most recent results.

The actual best-fit values of these studies are less robust and depend on the used technique (frequentist or Bayesian with logarithmic or flat prior), however the contours seem more robust [182, 302], see Fig. 2.8: to some extent all fit contours enclose the stau coannihilation region ($m_0 c^2 \lesssim 0.5 \text{ TeV}$) and the A-funnel region ($m_{1/2} c^2 \simeq 1.2 \text{ TeV}$). O. Buchmueller et al. [137] found in the frequentist approach a best fit value in the stau coannihilation region, but the contour also encloses the A-funnel, this is confirmed by C. Strege et al. [302] in the Bayesian approach. A. Fowlie et al. [182] has the best-fit point in the A-funnel, but the contour also enclose the coannihilation region. However, the A-funnel is excluded in the frequentist approach of C. Strege et al. According to C. Strege et al. and O. Buchmueller et al. (as cited in [302]), the deviation between the frequentist approaches in [137, 302] can be explained by differences in the used code. C. Strege et al. accuse A. Fowlie et al. to have used unreliable code settings, resulting in the different best-fit points in [182, 302].

Therefore, we will not discuss actual predictions for sparticle masses or spin-independent WIMP nucleon scattering cross section, but reproduce some of the discussed contours in the $m_0 - m_{1/2}$ - and $\sigma_{\chi, N}^{\text{SI}} - m_\chi$ -plane in Fig. 2.8. The results of O. Buchmueller et al. for $\sigma_{\chi, N}^{\text{SI}}(m_\chi)$ are shown in Fig. 2.11. However, by comparing the results some general tendencies can be stated:

The rather high mass of the discovered Higgs has a significant impact, as pre-Higgs constraints favoured a lower best-fit value of $m_h c^2 \approx 116 \text{ GeV}$ [302]. The measured value can be fitted either by including radiative corrections or allowing maximal mixing scenarios. The first is most sensitive to the stop mass and favours large m_0 in the A-funnel, the second favours small $m_{1/2}$ in the stau coannihilation region [137, 182, 302], but the best-fit for the Higgs mass of all three studies is below the experimental value [137, 182, 302].

However, the A-funnel is disfavoured in the frequentist approach by the measured anomalous magnetic moment a_μ . Its strong deviation from the standard model prediction favours new physics, e.g. in form of a significant SUSY contribution. Therefore, small masses in the coannihilation region are favoured by a_μ [137, 302].

This is in tension with the results for $BR(B^0 \rightarrow \mu^+ \mu^-)$, $BR(B_s^0 \rightarrow \mu^+ \mu^-)$ which are consistent with the standard model prediction and disfavour new physics at low masses [137, 182]. Also the null-result of SUSY particle production at the LHC is in tension with a_μ [137, 302]. A. Fowlie et al. and C. Strege et al. argued that remaining uncertainties in the modelling of a_μ may justify to remove it from the constraints. By doing so, they found a greatly improved goodness of fit [182, 302].

Higher m_0 values are limited by the XENON100 direct dark matter search [68], which disfavor the complete focus-point region (large m_0 and small $m_{1/2}$) [137, 302]. The more sensitive result of the LUX experiment [42] may further strengthen this exclusion, but it is not yet included in global fits.

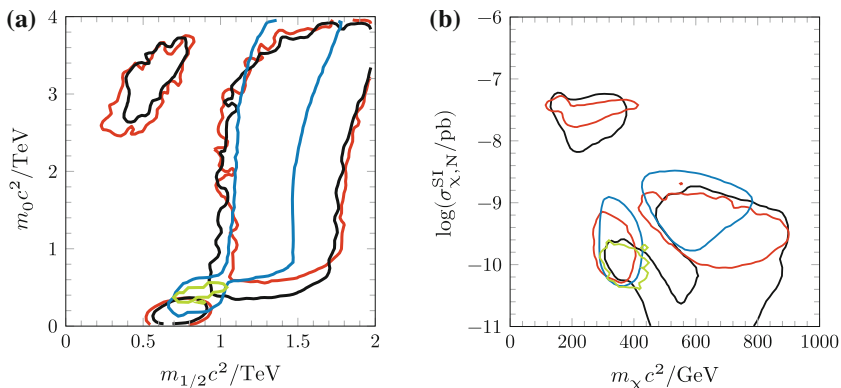


Fig. 2.8 Overview of current global fits of the CMSSM, 95 % CL regions in **a** the $m_0 - m_{1/2}$ -plane and **b** $\sigma_{\chi,N}^{\text{SI}} - m_\chi$ -plane: [302] Bayesian with logarithmic prior including a_μ (blue), [302] Profile likelihood including a_μ (green), [182] Bayesian with logarithmic prior including a_μ (red), [182] Bayesian with logarithmic prior excluding a_μ (black)

All three studies discussed have different best-fit values and different 95 % CL contours. However, all three contours overlap in one region of the $\sigma_{\chi,N}^{\text{SI}} - m_\chi$ -plane, see Figs. 2.8b and 2.11. Therefore, a WIMP with $m_\chi c^2 \approx 400 \text{ GeV}$ at $\sigma_{\chi,N}^{\text{SI}} \approx 10^{-10} \text{ pb}$ seems in agreement with all three studies [137, 182, 302] at 95 % CL.

The question whether the CMSSM is still a reliable model to fit the data is open: O. Buchmueller et al. state a p -value of 0.085 and emphasize the tension between a_μ and null-results for SUSY production at LHC. Consequently, they call to look for alternatives beyond CMSSM [137]. C. Stenge et al. state a p -value of 0.21 and argue that the CMSSM is not ruled out by any statistical significance [302]. However, they admit that the parameter space is shrinking [302]. The underestimation of the Higgs mass in all three studies increase the pressure on CMSSM. The MSSM may be an alternative, but it seems to need fine tuning to get a suitable Higgs mass. Such fine tuning could be avoided in the *next to minimal supersymmetric standard model* (NMSSM) [138].

2.1.4 Limits on the WIMP Self-annihilation Cross Section by Astroparticle Data

As shown in the Sect. 2.1.2, the WIMP miracle can lead to the observed relic abundance of non-baryonic, cold dark matter if WIMPs are self-annihilating. To match the thermal relic density (Eq. 2.4b) an annihilation cross section of $\langle \sigma_a v \rangle \approx 3 \times 10^{-26} \text{ cm}^3 \text{ s}^{-1}$ (Eq. 2.10) would be needed. This prediction can be tested by searching for particles produced in present day WIMP annihilation. Signatures for annihilation products are predicted for various astroparticle data, including cosmic rays, gamma rays, and neutrinos. In this section we will follow the reviews [206, 264] and will

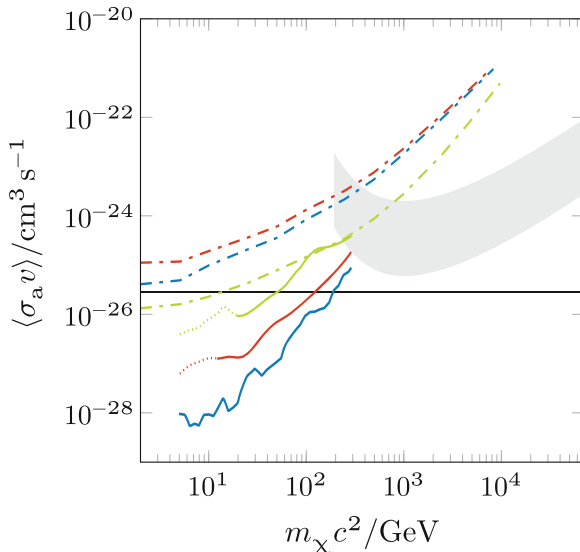


Fig. 2.9 Compilation of exclusion limits at 95% CL on $\langle\sigma_a v\rangle$ as function of m_χ . The results from AMS [108, Fig. 3] (solid lines) and from FermiLAT [26, Fig. 5] (dashed-dot lines) are shown for the final states e^-e^+ (blue), $\mu^-\mu^+$ (red) $\tau^-\tau^+$ (green). The gray area indicates the uncertainty due to the dark halo model in the H.E.S.S. exclusion limit [34, Fig. 1]. The dotted parts of the AMS results are potentially affected by solar modulation [108]. The black solid line indicates $\langle\sigma_a v\rangle = 3 \times 10^{-26} \text{cm}^3 \text{s}^{-1}$, the value necessary to match the WIMP relic abundance, often called *natural scale*

briefly list the most recent results, the associated techniques, and report the obtained limits on σ_a in Fig. 2.9.

Searching for a dark matter signal via the potential annihilation products is commonly known as *indirect search*. The *direct search* for scattering of galactic dark matter off terrestrial targets will be discussed in Sect. 2.1.5.

The type of annihilation products depends on the dark matter candidate and its interaction with standard model particles. Therefore, only given dark matter models are testable. Within the MSSM, the annihilation products depend on the LSP, its mass, and the MSSM mass spectrum. In principal, the dark matter particle may annihilate to any standard model particle as final state: Z , W^\pm , g , l , q , ν [264]. Even an annihilation to monochromatic γ -rays is possible, but suppressed to loop level, as the parent particle is by definition *dark* matter [206]. The source spectrum for standard model particles is the convolution of the annihilation final states and the branching ratios. To be more independent from the involved dark matter physics, most searches express the limits for specific final states like γ , $\mu^+\mu^-$, or $b\bar{b}$.

Assuming the final state particle to be unstable, it will decay or hadronize until reaching a stable particle like γ , e^- , ν_e , ν_μ , ν_τ , p , d , and their respective anti-particles. Each of these particles can undergo secondary processes like inverse-Compton scattering in case of γ . These messengers can be divided in three categories: cosmic rays

(e^-/e^+ , p/\bar{p} , d/\bar{d}), γ -rays, and neutrinos (ν_e , ν_μ , $\nu_\tau\nu_\tau$). For each category we will shortly report the results from the most recent experiments.

Besides being directly the final states, e^\pm can be produced via μ^\pm - and τ^\pm -decay and via π^\pm -decay subsequent to W^\pm - and Z -decay or hadronization. Charged hadrons (p/\bar{p} , d/\bar{d}) can be produced via W^\pm -, and Z -decay or hadronization.

Charged cosmic rays scatter on magnetic fields in the interstellar medium and the galactic halo, therefore their incident direction get mostly randomized. Furthermore, energy loss via inverse-Compton scattering limits the sources of e^\pm with $\lesssim 100$ GeV to a few kiloparsec around the Earth. Therefore, the propagation through and interaction with the interstellar medium has to be considered, adding additional model dependence to potential signals.

As little directional information is available for charged cosmic rays, one relies on the spectral shape to distinguish it from background. In most scenarios it is a hard continuum spectrum on top of the background, with a bump or edge near the WIMP mass [264].

The *Advanced Thin Ionization Calorimeter* (ATIC) [145] and the *Balloon-borne Electron Telescope with Scintillating fibers* on the *Polar Patrol Balloon* (PPB-BETS) [310] found a bump in the combined $e^- + e^+$ spectrum at $\approx 300\text{--}800$ GeV [264]. This bump was not confirmed with the more precise data of the satellite experiment *Fermi Large Area Telescope* (FermiLAT), but it found a smaller excess at ≈ 200 GeV [13]. However, these excesses can be explained with additional, non-exotic sources like pulsars [266].

As the WIMP annihilation produces the same amounts of matter and anti-matter, anti-matter is a potentially better signal due to its lower astrophysical background [264]. A positron background arises from the collision of cosmic ray protons with the interstellar medium [108]. The space-based *Payload for Antimatter Matter Exploration and Light-nuclei Astrophysics* (PAMELA) [29, 30] observed a positron excess in the e^+/e^- -fraction at $\gtrsim 100$ GeV over the background. Contrary, the \bar{p}/p -fraction is in agreement with the prediction. The observation may be explained as a dark matter signal, but it would require an exotic scenario where the dark matter annihilates predominantly into leptons, e.g. [155]. Contrary, also additional, yet unknown nearby pulsars are proposed to explain the excess, e.g. [163].

The positron excess is confirmed by the *Alpha Magnetic Spectrometer* (AMS) on the International Space Station [108]. However, a fit of the observed spectral shape found no indication of the expected sharp, edge-like feature from dark matter annihilation. Consequently, AMS data can be used to set limits on $\langle\sigma_a v\rangle$, depending on the final states of the decay [108], see Fig. 2.9.

A γ -ray signal may be produced directly as final state of the annihilation, but also via π^0 -decay subsequent to W^\pm -, Z -, and hadronic τ^\pm -decay; or hadronization [264]. As γ -rays are unaffected by magnetic fields, they indicate the direction of their source.

Contrary to the case of charged cosmic rays, γ -ray signals can be distinguish from background by their directional information. As the annihilation rate is proportional to the density squared, an increased signal from dark matter self-annihilation is expected from regions with high dark matter densities, like the centre of the galaxy, the

centers of galaxy clusters, or dark matter dominated dwarf galaxies [264]. Therefore, the predicted γ -flux due to annihilation is strongly affected by uncertainties in the dark matter distribution from N-body simulations. A background of diffuse γ -emission arises from propagation and interaction of cosmic rays: inelastic collision of nuclei with the interstellar gas can produce π^0 , and its subsequent decay leads to γ -rays; e^\pm can produce γ -rays via bremsstrahlung and inverse-Compton scattering with the interstellar radiation field. Searches for γ -signals therefore also strongly depend on a correct modelling of the propagation and interaction of cosmic rays.

The FermiLAT experiment searched for monochromatic γ -lines from the galactic centre [15] and studied also the diffuse galactic [14] and extragalactic [16, 18] γ -emission. C. Weniger [316] found in 43 months of FermiLAT data an indication of a γ -line at ≈ 130 GeV and stated a significance of 3.2σ , considering the look-elsewhere effect. However, reanalysis with data of 4.4 years and including the systematic effect of different data selection chains reduces the global significance to less than 1.0σ [197]. In case of diffuse galactic emission, the proposed excess in the data of the older EGRET experiment [125] was not confirmed by FermiLAT. Based on the absence of a galactic monochromatic γ -line, an upper limit on the γ -flux from annihilation could be set. Depending on the used dark matter halo model it corresponds to $\langle\sigma_a v\rangle \lesssim 10^{-27} \text{cm}^3 \text{s}^{-1}$ [15].

Dwarf galaxies, especially *dwarf spheroidals* (dSph), have a high mass-to-light ratio and thus a presumably high abundance of dark matter [291]. They have probably a low γ -background and only a few pulsars [264]. Three imaging atmospheric Cherenkov telescopes searched for dark matter signal in dwarf galaxies: MAGIC observed the Draco [49] and Segue 1 [51]; VERITAS observed also Segue 1 [53] and the galaxies Draco, Ursa Minor, Boötes 1, and Willman 1 [24]; and H.E.S.S. observed Sagittarius [32, 34] and Canis Major [33] Sculptor and Carina dSph [21]. No dark matter signal was found and exclusion limits on $\langle\sigma_a v\rangle$ were set. A simultaneous fit to 15 Milky Way dwarf spheroidal satellite galaxies out of 25 observed by FermiLAT set the most competitive limit on $\langle\sigma_a v\rangle$ [17, 26], see Fig. 2.9, as FermiLAT has a lower threshold than the imaging atmospheric Cherenkov telescopes [264].

A search in galaxy clusters by MAGIC [50] and FermiLAT [22, 25] found also no dark matter signal. FermiLAT set an exclusion limit which can go down to $\langle\sigma_a v\rangle < 10^{-24} \text{cm}^3 \text{s}^{-1}$, depending on the used halo model [25]. Searches in galaxy clusters are difficult due to the strong γ -background from e.g. active galactic nuclei [264].

Neutrinos may be produced via μ^\pm -, τ^\pm -decay, in addition to direct production as final states. Due to their low interaction probability, neutrinos, like γ -rays, provide the direction of their source. The direction is used to search for neutrinos capture inside the Sun or Earth. Due to scattering during passing through celestial bodies, WIMPs may lose enough energy to get gravitationally bound to them. Consequently, a neutrino signal from dark matter annihilation in the Sun or Earth is not only sensitive to the annihilation cross section σ_a , but also on the scattering cross section $\sigma_{\chi,N}$ (Eq. 2.20a). Depending on the theory, the energy of the neutrino signal can reach up to 1/3 of the WIMP mass [206]. Thus, WIMPs annihilating inside the sun would produce a high energy neutrino signal which is clearly distinct from solar neutrinos.

The IceCube neutrino telescope at the South Pole search for Cherenkov light caused by neutrino-induced interactions in the ice. Including its denser subarray DeepCore, the IceCube experiment searched for neutrinos from the sun caused by WIMP annihilation in the range $20 \text{ GeV} < m_\chi c^2 < 500 \text{ GeV}$. The measurement was consistent with atmospheric muon and neutrino background, and IceCube set limits on the spin-dependent and spin-independent cross section for elastic WIMP-proton scattering [12]. Its results are therefore comparable to the direct searches, see Fig. 2.11, which we will discuss in Sect. 2.2.

In Fig. 2.9 we compiled the exclusion limits from FermiLAT [26], AMS [108], and from the H.E.S.S. observation of the Sagittarius dwarf [34]. As far as we know, the latter is the leading exclusion limit for imaging atmospheric Cherenkov telescopes. AMS and FermiLAT already reached the $\langle \sigma_a v \rangle$ value needed to match the WIMP relic density (Eqs. 2.4b and 2.10), assuming $e^- e^+$ in the final state. Thus, they indicate WIMPs with $m_\chi c^2 \gtrsim 10\text{--}100 \text{ GeV}$.

2.1.5 WIMP Signature in Direct Searches for Dark Matter

Astronomical and cosmological observations strongly indicate the existence of dark matter (see Sect. 2.1.1), and *indirect searches* try to further constrain its properties (Sect. 2.1.4). Possible particle candidates for dark matter are motivated by extensions of the standard model of particle physics (Sect. 2.1.2) and their existence is tested at accelerators (Sect. 2.1.3). However, even if a particle candidate exists and its properties match the astronomical observations, this is no unambiguous proof that the constituent of cosmic dark matter is identical to the candidate. *Direct searches* try to establish this identity by searching for scatterings between galactic dark matter and terrestrial targets. In this controlled conditions, a more detailed comparison with possible candidates is possible.

In this section we review the connection between the microscopic physics of supersymmetric WIMP candidates, the galactic WIMP distribution, and the signatures in direct searches. This will prepare the discussion of the results of current direct searches in Sects. 2.2 and 2.3.

Assuming the lightest neutralino as WIMP candidate, in direct searches one usually restricts WIMP interaction with ordinary matter to WIMP-quark coupling.⁸ Consequently, scattering of WIMPs off target nuclei leads finally to recoiling nuclei in the detector [206]. The energy of the recoiling nucleus E_r with mass m_{nucl} can be given as function of the scattering angle in the centre of mass frame θ [120]:

$$E_r = \frac{\mu^2 v^2 (1 - \cos \theta)}{m_{\text{nucl}}}, \quad \mu = \frac{m_\chi m_{\text{nucl}}}{m_\chi + m_{\text{nucl}}}. \quad (2.17)$$

⁸However, we note that also WIMP coupling to leptons is studied, e.g. [115] and references therein.

In general the WIMP-nucleus cross section has contributions from spin-dependent (SD) and spin-independent (SI) interactions and can be expressed as [120]:

$$\frac{d\sigma_{\chi,nucl}}{dE_r} = \frac{m_{nucl}}{2\mu^2 v^2} \left(\sigma_0^{SI} F_{SI}^2(E_r) + \sigma_0^{SD} F_{SD}^2(E_r) \right), \quad (2.18)$$

with the spin-independent (σ_0^{SI}) and spin-dependent (σ_0^{SD}) cross sections at zero momentum transfer and v denoting the WIMP velocity relative to the nucleus. The dependence on the momentum transfer and the loss of coherence for heavy WIMPs or nuclei are considered by the form factors⁹ F_{SI}, F_{SD} .

The spin-dependent contribution arises from the coupling of the WIMP to the axial-current of the quark, which leads to [120, 206]:

$$\sigma_0^{SD} \propto (a_p \langle S_p \rangle + a_n \langle S_n \rangle) (J + 1), \quad (2.19)$$

where $\langle S_p \rangle$ ($\langle S_n \rangle$) are the expectation values of the spin content of the proton (neutron) group of the nucleus and J is the nucleus spin. The a_n, a_p depend on the theoretical WIMP-quark coupling and the quark spin distribution in the nucleon, which has to be experimentally determined from polarized deep inelastic scattering.

The spin-independent contribution arises via scalar-scalar and vector-vector coupling leading to [120, 206]:

$$\sigma_0^{SI} \propto (f^p Z + f^n (A - Z))^2 \quad (2.20a)$$

$$\approx A^2. \quad (2.20b)$$

Similar to the a_n, a_p , the terms f^p, f^n depend on the theoretical WIMP-quark coupling and the experimental quark densities in the nucleon. In most cases $f^p \approx f^n$, i.e. the WIMP couples in a similar way to neutrons and protons, and the cross section scales with the atomic weight A^2 of the target.

Both, the nucleon number and the form factor, have to be considered by selecting a target for direct searches. In example, on one side xenon has a higher spin-independent cross section than germanium due to its higher atomic mass, but on the other side it has a larger form factor suppression of events with high momentum transfer [186].

Finally, the properties of the galactic WIMP distribution affects the differential event rate dR/dE_r of recoiling target nuclei [97, 120, 227]:

$$\frac{dR}{dE_r} = \frac{\rho_0}{m_{nucl} m_\chi} \int_{v_{min}}^{v_{esc}} v f(\vec{v}, \vec{v}_E) \frac{d\sigma_{\chi,nucl}}{dE_r}(v, E_r) d\vec{v} \quad (2.21a)$$

$$v_{min} = \sqrt{\frac{m_{nucl} E_r}{2\mu^2}}, \quad (2.21b)$$

⁹For the spin-independent case, the form factor of R.H. Helm [199] is usually used in direct searches.

resulting in a quasi-exponentially falling spectrum. Here, $f(\vec{v}, \vec{v}_E)$ is the distribution of the WIMP velocity \vec{v} in the reference frame of the detector and \vec{v}_E is the velocity of the detector relative to the galactic frame. The local WIMP density is ρ_0 . The distribution $f(\vec{v}, \vec{v}_E)$ is limited by the escape velocity for gravitationally bound WIMPs, v_{esc} , and by the minimal velocity v_{min} that is needed to induce a recoil with E_r above an experimental threshold.

Because the actual galactic WIMP distribution is still unknown and numerical simulation results are not commonly accepted, see Sect. 2.1.1, a canonical distribution is assumed in context of direct dark matter searches. This is the *isothermal* halo (Eq. 2.2a with $\alpha = 2.0$, $\beta = 2.0$, $\gamma = 1.0$, $R = 3.5$ kpc) [121]. The isothermal halo leads to a Maxwellian velocity distribution [120]:

$$f(\vec{v}, \vec{v}_E) = \frac{1}{\sqrt{2\pi}\sigma} \exp\left(-\frac{|\vec{v} + \vec{v}_E|^2}{2\sigma^2}\right), \quad \sigma = \sqrt{\frac{3}{2}}v_0 \quad (2.22)$$

with the local circular speed v_0 . Most of the direct detection experiments listed in Sect. 2.2 apply the following standard values [120]¹⁰:

$$v_{\text{esc}} = 544 \text{ km s}^{-1}, \quad v_0 = 220 \text{ km s}^{-1}, \quad \rho_0 c^2 = 0.3 \text{ GeV cm}^{-3}. \quad (2.23)$$

Reasonable variations of the halo model may affect the detection rate by about ten percent [207].

Earth's absolute velocity projected on the galactic plane [97] can be parametrized as

$$v_E = v_{\text{sun}} + v_{\text{rot}} \cos \gamma \cos\left(\frac{2\pi}{T}(t - t_0)\right) \quad (2.24)$$

where v_{sun} is the proper motion of the sun and v_{rot} is the rotation velocity around the sun with a period of $T = 1$ year, a phase of $t_0 \sim 2$ nd June, and an inclination of γ relative to the galactic plane.

Therefore, nuclear recoils induced by galactic WIMPs features an annual modulated event rate following a cosine [120, 227]. However, the cosine may be distorted in the presence of halo substructures such as streams [281]. Additionally, the incident WIMP flux in the lab frame is peaked in the direction of Earth's motion due to the motion of the detector relative to the galactic restframe. This produces a directional dependence of a potential WIMP signal. As both, the annual modulation and the directional dependence, do not depend on the assumption of the WIMP physics,

¹⁰J.D. Lewin and P.F. Smith [227] originally proposed slightly different values: $v_{\text{esc}} = 600 \text{ km s}^{-1}$, $v_0 = 230 \text{ km s}^{-1}$. Within the stated uncertainties, they agree with the more recent values from [120].

potential signals with these characteristics are regarded as *model independent*. An overview of experiments using these characteristics as detection signature are given in Sects. 2.2.1 and 2.2.7.

Without such characteristic features, one has to search for an excess in the measured event rate over the known background of the experiment. For $\sigma^{\text{SI}} \approx 10^{-10}$ pb as expected in some theoretical models, see Fig. 2.8b, only one event within an exposure of 3 t.yr is expected [76]. This event has to be identified against the background, especially neutrons which also induce nuclear recoils. Possible sources for neutron background in direct dark matter searches are [181]: neutrons from uranium/thorium decay or (α , n)-reactions near the detector, and neutrons induced by atmospheric muons. The latter ones can reach kinetic energies up to several hundred GeV, which makes a passive shielding of the detector difficult. Instead, one has to use active muon vetos to reject events associated with tagged muons and to go deep underground to reduce the muon flux.

Another difficulty, maybe even a final background for direct searches is the coherent scattering of neutrinos on the target nucleus which starts at $\sigma^{\text{SI}} \approx 10^{-13}$ pb [123]. However, this is no limitation for running experiments, as this magnitude of cross section is only reachable for the most ambitious future experiments, see Sect. 2.2 and especially Sect. 2.2.4.

In any case, direct dark matter experiments search for a very rare signal and need therefore a good knowledge of the expected background where muon-induced neutrons are a central component.

2.2 Overview of Direct Searches for Galactic WIMPs

In the previous section, we motivated the existence of dark matter and introduced the WIMP as possible particle candidate. This section will give an overview of current results of direct searches for WIMPs.¹¹ We will focus on running experiments and their obtained exclusion limits or claimed signals for elastic, spin-independent WIMP-nucleon scattering. Detailed reviews of finished, running, and planned direct dark matter searches can be found in e.g. [45, 88, 120, 151, 179, 284, 297]. An overview of already finished experiments from mid-1980s till mid-2000, e.g. IGEX, UKDMC, and HDMS, is given in [186, Tables 1 and 2].

Most theories predict a very weak signal, e.g. in CMSSM a cross section of roughly $\sigma^{\text{SI}} \approx 10^{-10}$ pb is expected for elastic WIMP-nucleon scattering (Sect. 2.1.3). Therefore, the experiments aim to measure signals as rare as one WIMP-induced nuclear recoil event within an exposure of 3 t.yr, see Sect. 2.1.5. To reach this sensitivity, a low background is important. Typical background sources are β - and γ -decays which result in electron recoils. Neutrons, either from (α , n) reactions or induced by cosmic muons, cause nuclear recoils [186]. Especially neutrons are an important background,

¹¹ We note that planned experiments searching for neutrinoless double beta decay, like MAJORANA [10] and CUORE [265], will be also sensitive to dark matter [190, 315].

as they can mimic WIMP induced nuclear recoils (Sect. 2.1.5). Active and passive techniques are used to suppress these kinds of background. On the active side, most of the experiments feature some kind of rejection for electron recoils, like pulse shape analysis (e.g. GoGeNT [9] and COUPP [91]) or a dedicated detector design using the simultaneous measurement of two signal channels (e.g. EDELWEISS [76] and XENON [68]). Also a muon veto to tag muon-induced background produced inside the veto is not unusual, e.g. [7, 63, 283]. On the passive side, most experiments have neutron and gamma shields, and usually they are located at deep underground sites to reduce the cosmogenic background. An overview of the underground laboratories where most of the experiments are located is given in [122], their shielding power being expressed in *meter water equivalent* (mwe). The physics of this shielding and the creation of muon-induced neutrons will be discussed in detail in Chap. 3.

We will first shortly introduce the experiments and their latest results, classified by the used technique: scintillators (Sect. 2.2.1), ionisation detectors (Sect. 2.2.2), cryogenic detectors like EDELWEISS (Sect. 2.2.3), two-phase and single-phase noble liquids (Sects. 2.2.4 and 2.2.5), superheated liquids (Sect. 2.2.6), and directional experiments (Sect. 2.2.7). If not stated otherwise, the results are given for a standard isothermal halo [227], (Eq. 2.23).

Most of the experiments set upper limits on the cross section for elastic WIMP-nucleon scattering, but some claimed also indication for a WIMP signal. Due to the A^2 -enhancement, the limits on spin-independent scattering are lower than the limits on spin-dependent scattering, see Sect. 2.1.5. In the following we will focus on limits on the spin-independent cross section for WIMP-nucleon scattering $\sigma_{\chi,N}^{\text{SI}}(m_\chi)$ (Eq. 2.20a). An overview of the possible signals is shown in Fig. 2.10. The upper limits on $\sigma_{\chi,N}^{\text{SI}}(m_\chi)$ at 90 % CL, hereafter called *exclusion limits*, of the discussed experiment are shown on Fig. 2.11. The tension between the possible signals and the exclusion limits will be discussed in Sect. 2.2.8. Section 2.3 will then discuss the experimental aspects and possible background contributions based on the example of the EDELWEISS experiment.

2.2.1 Scintillators

Scintillators are in principle capable to discriminate events with high stopping power dE/dX like nuclear recoils via pulse shape analysis. However, the low light yield prevents an event-by-event discrimination at low energy [297].

The DAMA [109, 116] experiment claims a discovery of galactic dark matter interacting with their target based on an annual modulation of the count rate statistic. As stated above, this is extracted without specifying the kind of interaction on an event-by-event base. Experiments like KIMS [213, 225], ANAIS [56], and DM-ICE [152] are aimed to test this claim and possible systematic effects with similar targets but different experimental set-ups. KIMS already finished its data taking, whereas ANAIS and DM-ICE are in their prototype stages.

The *DAMA* project searched, with two experimental set-ups, for WIMP signatures in NaI(Tl) crystals at the *Laboratori Nazionali del Gran Sasso* (LNGS, Italy) at a depth of 3600 mwe [109, 117]. Until July 2002, the *DAMA/NaI* set-up collected in 7 years [111] 107,731 kg.d exposure with nine crystals of 9.7 kg mass [112]. Afterwards the set-up was upgraded to *DAMA/LIBRA* with 25 crystals of the same individual mass [114], which collected additional 317,697 kg.d until September 2009 [116]. Already in the *DAMA/NaI* data, the *DAMA* collaboration found a sinusoidal modulation of the residual hit rate at low energy with a period of 1 year and a phase equivalent to a peak in June 2nd [110], as expected for the interaction of galactic WIMPs with an Earth based detector, see also Sect. 2.1.5. As expected for the low interaction cross section of a WIMP, the modulation is only observed in single hits, i.e. when only one crystal fires [110]. This modulation persisted in the combined exposure of *DAMA/NaI* and *DAMA/LIBRA* (1.17 t.yr) at a significance of 8.9σ CL, spanning 13 annual cycles [109]. According to the *DAMA* collaboration, possible modulated backgrounds, like muon-induced neutrons, can not explain the observed topology of the events and amplitude of the modulation [109, 116, 117]. Therefore, the *DAMA* collaboration claims evidence for a dark matter induced signal [109, 116]. Since January 2011 *DAMA/LIBRA* is running in *phase 2*, using new PMTs with higher quantum efficiency. The aim of phase 2, among others, is an increased sensitivity at low energies and the investigation of the distribution of dark matter in the galactic halo [118, 119].

The *DAMA* collaboration stresses that their observation is *model independent* as far as the modulation would occur regardless of the specific dark matter particle candidate [109, 116]. To compare the *DAMA* signal with the results of other experiments in the $\sigma_{\chi,N}^{\text{SI}} - m_\chi$ -plane (Sect. 2.2.8), we use in this work the interpretation [98] as suggested by [109, 127].¹² In the *light neutralino model* [127], the observed modulation would correspond to a particle mass of $7 \text{ GeV} < m_\chi c^2 < 50 \text{ GeV}$ [98], see also Fig. 2.10. Including constraints from the LHC reduces the mass range to $18 \text{ GeV} < m_\chi c^2 < 38 \text{ GeV}$ [127].

The *Korea Invisible Mass Search* (KIMS) experiment searched for elastic scattering of WIMPs with CsI(Tl) crystals at the *Yangyang Underground Laboratory* (Republic of Korea, 2000 mwe) [224, 225]. Twelve crystals, each of 8.7 kg mass, were installed in the last stage [213]. Identifying nuclear recoils via pulse shape analysis, no excess was found in the total exposure of 24524.3 kg.d and an exclusion limit at 90 % CL is set [213].

The *Annual Modulation with NaI(Tl) Scintillators* experiment (AN AIS) at the *Canfranc Underground Laboratory* (LSC) (Spain, 2450 mwe) aims to confirm or refute the annual modulation observed by *DAMA* [109, 116] with the same target and technique [56]. It plans to operate in total 250 kg of ultrapure NaI(Tl) crystals. Currently it investigates the intrinsic background with a sample of two NaI(Tl) crystals of 12.5 kg each [56].

¹²However, the analysis used non-standard parameter for their isothermal galactic halo ($\rho_0 c^2 = 0.45 \text{ GeV cm}^{-3}$, $v_0 = 270 \text{ km s}^{-1}$, $v_{\text{esc}} = 650 \text{ km s}^{-1}$ [98]), therefore it is questionable if the analysis is really comparable to the results of other experiments.

The *DM-ICE* collaboration [165] proposed to test the DAMA signal [109, 116] with 250 kg of NaI(Tl) crystals installed at a depth of 2450 m below the IceCube neutrino detector at the south pole [152]. As seasonal effects are opposite on the northern and southern hemisphere, a dark matter induced annual modulation in DM-ICE that agrees with DAMA's signal will occur 6 months out of phase from seasonal modulated background [152]. Currently, data are taken with a prototype of two crystals of 17 kg total mass deployed at 2450 m depth [152].

2.2.2 Ionisation Detectors

Experiments like CoGeNT and TEXONO search for an ionisation signal caused by WIMP-induced recoils in diodes. By using high purity germanium (HPGe) or silicon crystals as target, these experiments have a low intrinsic background, but they lack the capability for a discrimination between nuclear recoils, as expected for WIMP interactions, and electron recoils, as expected for γ -background via Compton scattering [297]. However, the situation may be improved in future detectors: recently experiments searching for neutrinoless double beta decays, like GERDA [23] and MAJORANA [10], developed segmented diodes, enabling the active rejection of Compton background due to their multiple, spatially separated interactions [297].

The dual use of this detector techniques for dark matter searches and neutrino physics is illustrated by CoGeNT [8, 9] and TEXONO [229, 233]. Both experiments started searching for low energy neutrino interactions, but published recently results for their dark matter searches.

The *Coherent Germanium Neutrino Technology* (CoGeNT) [9] collaboration uses a p-type point contact (PPC) germanium detector (HPGe) [5], a detector design with low threshold and noise but large mass and high energy resolution, suitable for searches of coherent neutrino scattering, but also WIMP scattering [87]. First measurements were taken at the *Chicago's Tunnel And Reservoir Plan* (US, 330 mwe) [5, 6], later measurements with a 440 g detector at the *Soudan Underground Laboratory* (US, 2100 mwe) for 145 kg.d live days [7–9]. Here, the experiment reports an irreducible excess of bulk-like events above the analysis threshold of 400 eV_{ee}. Based on fits to the exponential spectrum, neither the hypothesis of pure background nor the hypothesis of an additional WIMP signal was favored [7]. However, later investigations found $\approx 2.8\sigma$ significance for an annual modulation of the event rate as one would expect for a WIMP signal, with a best fitting mass of $m_{\chi}c^2 = 7 \text{ GeV}$ [8], see also Fig. 2.10. Known backgrounds like muon-induced neutrons or α -recoils from radon contamination can not explain the measured excess [7–9]. Also a comparison with the measured annual modulation of the radon level in the laboratory and the muon flux found no correlation with the observed signal by CoGeNT [27]. The CoGeNT collaboration plans to further investigate the observation with the *C-4* upgrade. Its aims are: an increase of the target mass to four PPCs of up to 1.3 kg mass each, a lowering of the threshold, an improved muon veto, and an increased shielding against γ - and neutron background [126].

The *TEXONO* experiment is located at the *Kuo-Sheng Power Plant* in Taiwan at 30mwe. Its main objective is low energy neutrino physics, such as neutrino-nucleus coherent scattering [287]. However, the experiment searches also for elastic scattering of WIMPs [229, 233]. The latest results are obtained with a PPC of 840 g fiducial mass and an analysis threshold of 500 eV_{ee} [229]. Due to the low threshold, the obtained exclusion limit at 90 % from a fiducial exposure of 39.5 kg.d [229] is especially sensitive at low m_χ -values, see Fig. 2.11.

The dark matter search was later separated from the neutrino investigation and is continued by the CDEX-TEXONO collaboration as *China Dark Matter Experiment* (CDEX) at the *China Jin-Ping Underground Laboratory* (CJPL) (PR China, 6720 mwe [320]), taken advantage from the increased shielding against cosmic background [322]. First data are obtained with a PPC-Ge of 994 g total mass [324]. However, as the rejection of Compton and surface background is not yet applied, the obtained exclusion limit [324] is slightly worse than the latest TEXONO result [229].

2.2.3 Cryogenic Crystal Detectors

Contrary to experiments which measured only scintillation light or ionisation, experiments like EDELWEISS, CDMS, or CRESST measure two signal channels in parallel: heat and ionisation in EDELWEISS and CDMS, and heat and scintillation in CRESST.

The heat channel enables true calorimetric measurements at mK temperature as the heat capacity follows Debye's law, being proportional to T^3 , therefore the energy deposit from a single nuclear recoil can yield a measurable temperature increase [189].

The second channel, ionisation or scintillation light, is *quenched* and allows a discrimination of events with high energy loss dE/dX . For example, compared to electron recoils (low dE/dX), nuclear recoils (high dE/dX) of the same energy produce the same heat signal, but a reduced ionisation signal [189, 297]. Consequently, this technique allows an event-by-event discrimination of nuclear recoils, as expected from elastic WIMP scattering, over electron recoils as expected from γ -background. This will be discussed in detail on the example of EDELWEISS in Sect. 2.3.

The advantage of active background rejection led to intensive developments since its first proposal and is reported in detail elsewhere, see e.g. [189, 297] and references therein. Currently the experiments CDMS [37–39], EDELWEISS [38, 76, 77], and CRESST [63] published results. ROSEBUD [158] was more focused on R&D of new target materials, but was defunct in 2012 [168]. EDELWEISS and CRESST plan to merge to EURECA in the future [64, 218, 219].

The *EDELWEISS* experiment is located at the *Laboratoire Souterrain de Modane* (LSM) (France, 4850 mwe [106]). It will be discussed in detail in Sect. 2.3. As result of its second stage (EDELWEISS-II), EDELWEISS can set an upper limit of 4.4×10^{-8} pb on $\sigma_{\chi,N}^{\text{SI}}$ at 90 % CL for $m_\chi c^2 = 85$ GeV [76]. To further improve the

exclusion limits, the exposure of EDELWEISS-II [76] was combined [38] with the exposure of CDMS II (Ge) [37], also a direct search experiment using cryogenic germanium bolometers. The combined exclusion limit is with $\sigma_{\chi,N}^{\text{SI}} < 3.3 \times 10^{-8}$ pb at 90 % CL minimal at $m_\chi c^2 = 90$ GeV [38]. The obtained exclusion limits are the most sensitive limits for any germanium based experiment and third only to the xenon based experiments XENON100 [68] and LUX [42]. With a special data selection [77], the exclusion limit is extended to lower WIMP masses: $\sigma_{\chi,N}^{\text{SI}} < 10^{-5}$ pb at 90 % CL for $m_\chi c^2 = 10$ GeV [77].

For the *Cryogenic Dark Matter Search*, the most recent results are published for the second stage (CDMS-II), which was located at the Soudan Underground Laboratory [37]. It used *Z-sensitive Ionization and Phonon* detectors (ZIP) to search for WIMP-induced nuclear recoils in germanium (19 detectors with 250 g each) and silicon (11 detectors with 100 g each) [37, 39]. With the germanium detectors, an exposure of 121.3 kg.d was taken between October 2006 and July 2007 [36] and an exposure of 612 kg.d between July 2007 and September 2008 [37]. In the last period, the CDMS collaboration found two events in their WIMP search region [37]. By an estimated background of 0.8 evts from surface electron recoils and 0.1 evts from neutrons, the result is no evidence for a WIMP signal. Combining both data sets, CDMS-II set an exclusion limit with a minimum of $\sigma_{\chi,N}^{\text{SI}} < 3.8 \times 10^{-8}$ pb at $m_\chi c^2 = 70$ GeV [37]. To increase the sensitivity on $\sigma_{\chi,N}^{\text{SI}}$, the CDMS and EDELWEISS collaborations had combined their data as mentioned above. Selecting only data from germanium detectors with especially low threshold, a reanalysis [39] of the data set [36, 37] together with older data taken with germanium and silicon detectors at the shallow *Stanford Underground Facility* (SUF) (US, 17 mwe) [41] results in an improved exclusion limit below $m_\chi c^2 = 9$ GeV. Also, no evidence for a modulation in the low mass CDMS-II data [39] was found [40]. Within the 140.2 kg.d exposure taken with 8 silicon detector between July 2007 and September 2008, in total 3 event were identified in the WIMP search region [31]. Albeit a profile likelihood test favoured the hypothesis that the events were caused by a signal of a WIMP with $m_\chi c^2 = 8.6$ GeV, see also Fig. 2.10, the CDMS collaboration stated that this result does not rise to the level of a discovery [31]. CDMS-II was upgraded to *SuperCDMS* [268] with detectors of higher mass and a more efficient rejection of surface events using interleaved electrodes, similar to EDELWEISS, and additional phonon sensors. Currently, SuperCDMS is running with 15 of these new *iZIP* detectors at Soudan Underground Laboratory, aiming for a sensitivity of $\sigma_{\chi,N}^{\text{SI}} < 5 \times 10^{-9}$ pb [268]. The next stage is to move SuperCDMS to *SNOLAB* (Canada, 6000 mwe) due to the increased shielding against cosmogenic background and to further increase the individual detector mass [268].

The *Cryogenic Rare Event Search with Superconducting Thermometers* (CRESST) experiment is located at the LNGS [63]. Initially, it measured the thermal signals of sapphire crystals (Al_2O_3) (CRESST-I) [61]. In its current second stage (CRESST-II) a dual readout of phonon and scintillation signals from CaWO_4 is used [63]. Within 730 kg.d of exposure between July 2009 and March 2011, 67 events in the WIMP search region were found [63]. With a significance of 4σ , a maximum

likelihood analysis shows that the estimated background from leaking electromagnetic events, α -particle and recoiling nuclei from α -decay, and neutron scattering is not sufficient to explain the observed events. Also a dedicated Geant4 simulation confirmed that ambient and muon-induced neutrons are only a minor contribution to the observed events [285]. In case scattering WIMPs are the missing contribution and considering the different nuclei in the target, a maximum likelihood analysis found two maxima in the $\sigma_{\chi N}^{\text{SI}}-m_{\chi}$ -parameter space, corresponding to potential WIMP signals at 11.6 and 25.3 GeV, respectively [63]. Figure 2.10, shows the contours at 95.45% CL for these excesses. This is in mild tension with earlier results from CRESST-II [62], both in the analysis provided by the CRESST collaboration [63] and in the analysis by A. Brown et al. [135], as they partially exclude the potential WIMP signals from [63]. To investigate this situation further, the experiment was recently upgraded to reduce the still high background contribution: depending on the chosen likelihood maximum, a background of 37.6 events or 42.8 events remains, mainly recoiling nuclei and α -particles from α -decay [63].

The *Rare Objects SEarch with Bolometers Underground* (ROSEBUD) [142, 158] at the LSC investigated the prospects of different target materials (BGO, Al_2O_3 , LiF) for WIMP searches and in situ neutron monitoring based on the dual measurement of phonon and scintillation signals.

Finally, EDELWEISS, CRESST and new groups merged to the *European Underground Rare Event Calorimeter Array* (EURECA) [64, 218, 219], planned to be installed in the extension of the LSM [220]. In the final stage, it aims for a sensitivity of $<2 \times 10^{-11}$ pb with a target mass of ≈ 1000 kg [64, 218]. A multi-target (e.g. Ge, Al_2O_3) approach is planned to control systematic effects and to investigate the A^2 dependence (Eq. 2.20a) in case of a detected WIMP candidate [218]. To reduce the neutron background with respect to current experiments like EDELWEISS, CRESST, it is planned [218] to shield the cryostat by ≈ 3 m of water, with the cryostat immersed in a water Cherenkov detector [309], also used as muon veto. The amount of muon-induced neutrons will be further reduced by a reducing high-Z material near the detectors [283]. The mechanism of muon-induced neutron production will be discussed in Chap. 3.

2.2.4 Two-Phase Noble Liquids

Similar to cryogenic crystal detectors, existing and planned experiments based on two-phase noble liquids, like ZEPLIN, XENON, WArP, LUX, ArDM, DarkSide, XAX, MAX, LZ, or DARWIN, use the dual measurement of two signals to identify nuclear recoils as dark matter signature: the first signal is scintillation light, the second the ionisation signal which is quenched relative to the scintillation signal [45, 151].

As experimental design a time projection chamber is used, filled with noble gas in a liquid phase as target and a gaseous phase. An interaction in the liquid phase will cause scintillation light and free charge carriers via ionisation. The latter are

drifted into a gaseous phase above the noble liquid via electric fields and are mostly measured indirectly via electroluminescence [45, 151]. Only the ArDM experiment proposed to use large electron multiplier for a direct detection of the ionisation signal [273]. As target mostly liquid xenon (LXe, $A = 131.3$ [65]) is used, i.e. in XENON and LUX, as its high atomic weight makes it a suitable target for spin-independent interaction which scales like A^2 and a good kinetic match to likely WIMP masses [297]. However, also liquid argon (LAr, $A = 40.0$ [65]) is used, currently only in DarkSide, as it has three advantages: first to test the A^2 -scaling (Eq. 2.20a) of a possible dark matter signal with a lighter target, second it has better discrimination power for nuclear recoils, and third it is cheaper than LXe [297].

To suppress the background further, most of the experiments use *self-shielding* [151]. As noble liquids can be purified to high levels, the target is usually separated in an inner *fiducial* volume and an outer region. Whereas the inner fiducial volume is used to search for dark matter signals, the outer region acts as shield against ambient backgrounds, but produces little background by itself due to its high radiopurity. With respect to radiopurity, LAr has, with the long-lived radioactive isotope ^{39}Ar , an intrinsic background which requires the sourcing from special, depleted underground reservoirs [151, 179, 297].

The experiments ZEPLIN [47, 223], XENON [60, 68], WArP [101], and LUX [42] have recently published results of their search for dark matter, whereas ArDM [84, 273], and DarkSide [52, 318] are still under construction or in commissioning. Proposals for future experiments are Panda-X [231], XAX [73], MAX [72], Darwin [89], and LZ [238].

The ZEPLIN programme spans the experiments ZEPLIN I, ZEPLIN II, and ZEPLIN III, using targets of liquid xenon (LXe) at Boulby Underground Science Facility (UK, 2800 mwe) [54]. ZEPLIN I used pulse shape analysis to identify scintillation caused by nuclear recoils in ≈ 5 kg LXe [54]. Starting with ZEPLIN II (31 kg LXe), the simultaneous readout of scintillation and ionisation signals was used to identify nuclear recoils [55]. ZEPLIN III, a two-phase xenon time-projection chamber containing 12 kg LXe, collected data in two science runs: first in 2008 and later between June 2010 and May 2011 [47, 223]. During the second run, ZEPLIN III was equipped with a gadolinium based anti-coincidence veto system to reject neutron background [46]. In the combined fiducial exposure of 1344 kg.d 13 events were found in the WIMP search region in agreement with the expected background from electron recoils [47]. The resulting exclusion limit is $\sigma_{\chi, N}^{\text{SI}} < 3.9 \times 10^{-8}$ pb at $m_\chi c^2 = 52$ GeV [47].

The multi-stage experiment XENON is a dual phase liquid xenon time projection chamber at the LNGS [59]. The target mass is continuously increased over the individual stages: XENON10 had a target of 25 kg [66] (5.4 kg fiducial mass [59]), the current stage XENON100 has a target of 62 kg [67] (34 kg fiducial mass [68]), and for XENON1T a target of ≈ 2500 kg (1000 kg fiducial mass) is planned [67, 100]. Within an exposure of 7636.4 kg.d, collected by XENON100 during 2011 and 2012, two events were found in the WIMP search region [68]. The expected background, mainly leakage of β - and γ -radioactivity in the WIMP search region,

is estimated to 1.0(2) event [68]. The minor contribution from ambient and muon-induced neutrons is deduced to $0.17^{+0.12}_{-0.07}$ [69]. Therefore the observed events are no indication for a dark matter signal. Consequently a 90 % CL exclusion limit of $\sigma_{\chi,N}^{\text{SI}} < 2.0 \times 10^{-9}$ pb at $m_{\chi}c^2 = 55$ GeV [68] is set. Based on data collected during 12.5 live days in 2006 with XENON10, also an limit of $\sigma_{\chi,N}^{\text{SI}} < 7.0 \times 10^{-6}$ pb for light WIMPs with $m_{\chi}c^2 = 7$ GeV could be set [60]. With a background reduced by a factor 100 with respect to XENON100, it is planned to start data taking with XENON1T in 2015 [100]. The next stage is *XENONnT*, an upgrade to ≈ 6 t target mass [136].

The *Large Underground Xenon* (LUX) experimentally uses a two-phase detector with 370 kg LXe (250 kg active monitored volume) aiming for $\sigma_{\chi,N}^{\text{SI}} < 2 \times 10^{-10}$ pb [42, 44]. After a test run of the fully assembled detector at surface [43], the detector was installed in 2012 at the Davis laboratory (4300 mwe) of the *Sanford Underground Research Facility* (US)[317]. Over 85.3 live-days between April 2013 and August 2013, it collected first physics data with a fiducial volume of 118 kg [42]. The observed 160 events are consistent with the predicted background of electron recoils. Therefore, it could set a 90 % CL exclusion limit on $\sigma_{\chi,N}^{\text{SI}} < 7.6 \times 10^{-10}$ pb for $m_{\chi}c^2 = 33$ GeV, cutting also into the range of low mass WIMPs due to a lower threshold than XENON100 [42]. It is planned to continue the search until 2015 with an improved set-up and aiming for 300 live-days of data.

The *Wimp ARgon Programme* (WArP) at the LNGS [175] is a two-phase drift chamber searching for WIMP recoils in 2.6 kg (1.83 kg fiducial mass) liquid argon (LAr) [101]. In an exposure of 96.5 kg.d no events were found in the WIMP search region and an exclusion limit at 90 % CL was published 2008 [101]. The next stage of the programme is the WArP 100L detector, containing 100 l of LAr [303]. The project is continued as the *DarkSide* experiment [168].

The multi-stage *DarkSide* programme at LNGS uses a two-phase time projection chamber with depleted argon, to reduce background from ^{39}Ar [318]. The prototype detector DarkSide-10 with 10 kg LAr is currently running at LNGS [52, 318]. The first stage to collect physics data will be DarkSide-50 with 50 kg LAr [318], featuring a neutron veto based on boron-loaded liquid scintillator [319]. Currently, DarkSide-50 is under construction at LNGS [276]. The next stage would be DarkSide G2 with a multi-tonne target [72, 276].

The *Argon Dark Matter* experiment (ArDM) is a two-phase detector with a tonne-scale LAr target [84, 273]. Instead of relying on electroluminescence to measure the ionisation signal, it extracts the ionisation signal via large electron multipliers in the gaseous phase [273]. After detector assembling and testing at surface [239], the detector was deployed at the LSC and is currently commissioned [84].

Panda-X is a multi-stage experiment, planned to be installed at the CJPL [231]. The first stage of the LXe dual-phase detector will contain 25 kg LXe, going up to 1.5 t LXe in the final stage [231].

The $^{129/131}\text{Xenon-Argon-}^{136}\text{Xenon}$ (XAX) experiment is a proposal to use three different targets of 10 t mass each [73]: LXe enriched with ^{129}Xe , ^{131}Xe to search for spin-dependent interaction of WIMPs, LXe enriched with ^{136}Xe for spin-independent

interaction, and LAr to compare possible interactions in LXe to a target with lower atomic weight. A similar multi-target experiment is *MAX*, proposed by a consortium of the XENON and DarkSide collaborations [72].

Dark matter wimp search with noble liquids (DARWIN) is a design study for a dual-phase detector with a multi-tonne target of LAr or LXe, aiming for a sensitivity of $\sigma_{\chi,N}^{\text{SI}} < 10^{-12}$ pb [89].

The *LUX-ZEPLIN* programme (LZ) aims for a sensitivity of $\sigma_{\chi,N}^{\text{SI}} < 5 \times 10^{-13}$ pb with a two stage experiment at *Sanford Underground Research Facility* [238]: the dual-phase detector will contain 1.5–3 t LXe in the first stage (LZS) and 20 t LXe in the second stage (LZD).

2.2.5 Single-Phase Noble Liquids

Contrary to experiments using two-phase noble liquids, single-phase experiments like XMASS and CLEAN/DEAP use only the scintillation light as signal. Therefore, a gaseous phase is missing and the target consists only of a liquefied noble gas.

A passive background reduction is still possible by using the self-shielding of the target [297]. For an active background rejection and discrimination of nuclear recoils, a pulse shape analysis of the scintillation signal is possible [297].

XMASS [19, 20] is the only experiment using this technique that recently published results on dark matter search. The first detectors of the CLEAN/DEAP project dedicated to search for dark matter, i.e. MiniCLEAN and DEAP-3600 are currently under construction [129, 192, 200].

The XMASS detector is located at the Kamioka underground laboratory (Japan, 2700 mwe), using a target of 835 kg LXe [19]. Commissioning runs ended in 2012 [19]. With an exposure of 5591.4 kg.d taken in February 2012 and a low threshold of 0.3 keV_{ee}, the experiment set an exclusion limit, dedicated for low-mass WIMPs [20]. However, the systematic uncertainty of the scintillation efficiency for nuclear recoils relative to electron recoils has a large impact in the limit, see [20, Fig. 8]

The *Dark matter Experiment using Argon Pulse shape discrimination/Cryogenic Low Energy Astrophysics with Noble liquids* (DEAP/CLEAN) programme proposed and built several experiments based on single-phase detectors using LAr and noble neon (LNe) targets [192] including four prototypes: DEAP-0 and picoCLEAN were R&D prototypes, microCLEAN measured the nuclear quenching factor and DEAP-1 studied discrimination based on pulse shape analysis. The first detectors expected to deliver physics data are currently under construction at SNOLAB: MiniCLEAN and DEAP-3600 [192]. MiniCLEAN will have a LAr target of 500 kg mass (150 kg fiducial mass) [200]. DEAP-3600 will be a detector with 3.6 t LAr, its commissioning is expected for the end of 2013 [129].

2.2.6 Superheated Liquids

Experiments using superheated liquids (PICASSO [70], COUPP [91], SIMPLE [172]) detect the bubble-nucleation after interactions occur. Via tuning of temperature and pressure, the detectors become insensitive to ionising particles with low stopping power dE/dX , such as electron recoils. Only events with high stopping power, like nuclear recoils, cause nucleation [88]. All experiments have an increased sensitivity to spin-dependent interaction via ^{19}F in their targets. However, they also published limits on the spin-independent interaction cross section.

The *Project In Canada to Search for Supersymmetric Objects* (PICASSO) [70, 128] at SNOLAB uses C_4F_{10} as target. With a subset of 10 detectors, a combined exposure of 114.3 kg.d was collected [70]. A low background allowed to lower the threshold as low as 1.7 keV, resulting in an increased sensitivity for WIMPs with mass below 10 GeV with a minimum at $\sigma_{\chi,\text{N}}^{\text{SI}} < 6.1 \times 10^{-5}$ pb for $m_\chi c^2 = 20$ GeV at 90 % CL [70].

The *Superheated Instrument for Massive ParticLe Experiments* (SIMPLE) at the *Low Noise Underground Laboratory* (France, 1500 mwe) use C_2ClF as target [171, 172]. The experiment's second stage (SIMPLE-II) collected data in two runs: in the first run [171] an exposure of 14.1 kg.d was obtained with 208 g active mass and in the second run [172] an exposure of 13.67 kg.d with 215 g active mass. The combined exposure contained eleven events in the WIMP search region, in agreement with the estimated neutron background [172]. Therefore an exclusion limit of $\sigma_{\chi,\text{N}}^{\text{SI}} < 7.6 \times 10^{-6}$ pb for $m_\chi c^2 = 35$ GeV was obtained [172]. It is planned to increase the active mass by a factor of 25 and add additional neutron shielding for SIMPLE-III [191].

The *Chicagoland Observatory for Underground Particle Physics* (COUPP) uses CF_3I as target [90, 91]. Between September 2010 and August 2011 a total exposure of 553.0 kg.d was collected with a 4.0 kg-target at SNOLAB. Within the exposure 20 events in the WIMP search region were observed, with an estimated background of 5.3 events. However, the observed events show a clustering in time which is unlikely for true nuclear recoils induced by WIMPs. Therefore, no discovery is claimed, but an exclusion limit is set [91]. The upper exclusion limit at 90 % is presented as a band to consider systematic uncertainties in the nucleation efficiency due to ^{19}F and ^{12}C recoils [91]. The next stages contain a 60 kg target (COUPP-60 kg) currently installed at SNOLAB and a tonne scale detector (COUPP-500 kg) currently in R&D phase [313].

The *PICASSO-COUPP* (PiCo) experiment is a merger of both groups, aiming for a target volume of 250 l at SNOLAB [71, 159].

2.2.7 Directional Experiments

This section focuses on spin-independent interaction and thus excludes the experiments searching for a directional signal as they investigate spin-dependent interactions with targets containing ^{19}F and did not publish limits on spin-independent interactions.

Four directional experiments try to establish a correlation between the galactic motion and the track of recoiling nuclei in gaseous time projection chambers [88, 179, 297]: *Directional Recoil Identification From Tracks* (DRIFT) at Boulby Underground Science Facility [160, 247], the *Dark Matter Time Projection Chamber* (DMTPC) at the *Waste Isolation Pilot Plant* (US, 1600mwe) [35, 246], the *NEw generation WIMP search with an Advanced Gaseous tracking device Experiment* (NEWAGE) at Kamioka underground laboratory [244, 249], and the *MIMAC* experiment at LSM [195, 271]. All these experiments are using at least partially CF_4 as target, therefore they are sensitive to spin-dependent interactions. DRIFT [160], DMTPC [35], and NEWAGE [244] already published limits on the spin-dependent scattering cross section.

2.2.8 Tension Between Signal Claims and Exclusion Limits

As shown in Sects. 2.2.1–2.2.7, 13 experiments published currently results of their search for dark matter.¹³ In three cases¹⁴ an excess above the known background was found, but no discovery was claimed so far. Only DAMA/LIBRA claimed discovery of dark matter via an annually modulated signal. In twelve cases¹⁵ no excess over the known background was found and consequently exclusion limits were set. A compilation of the published signals and limits are shown¹⁶ in Figs. 2.10 and 2.11, together with a theoretical prediction [137], see Sect. 2.1.4. In Fig. 2.11 we show also the limits obtained from the indirect search by IceCube [12], see Sect. 2.1.4.

¹³In the following, an asterisk will indicate a dedicated analysis for low WIMP mass.

¹⁴CDMS II (Si) [31], CoGeNT [7, 8], CRESST-II [63].

¹⁵CDEX [324], CDMS II (Ge) [37], CDMS II (Ge) + EDELWEISS II [38], CDMS II (Ge)* [39], CDMS (SUF)* [41], COUPP [91], EDELWEISS-II [76], EDELWEISS-II* [77], KIMS [213], LUX [42], SIMPLE [172], TEXONO [229], WArP [101], XENON 10* [60], XENON 100 [68], XMASS* [20], ZEPLIN III [47].

¹⁶The data for CDMS II (Ge) [37], CDMS II (Ge)* [39], CDMS SUF* [41], CDMS II (Ge) + EDELWEISS II [38], CRESST-II [63], CoGeNT [7, 8], COUPP [91], DAMA/LIBRA [282], EDELWEISS-II [76], KIMS [213], LUX [42], SIMPLE [172], WArP [101], XENON 100 [68], XENON 10* [60], ZEPLIN-III [47], and the prediction for the coherent neutrino background [123] were obtained from the *DMTools* (<http://dmtools.brown.edu>). The data for CDMS II (Si) [31], CDEX [324], DAMA/LIBRA [98, Fig. 1, rightpanel], EDELWEISS-II* [77], IceCube [12], TEXONO [229], XMASS [20], and the theoretical model [137] were copied directly from the original publication. For PICASSO [70], no data in the logarithmical scale needed for Fig. 2.11 was found.

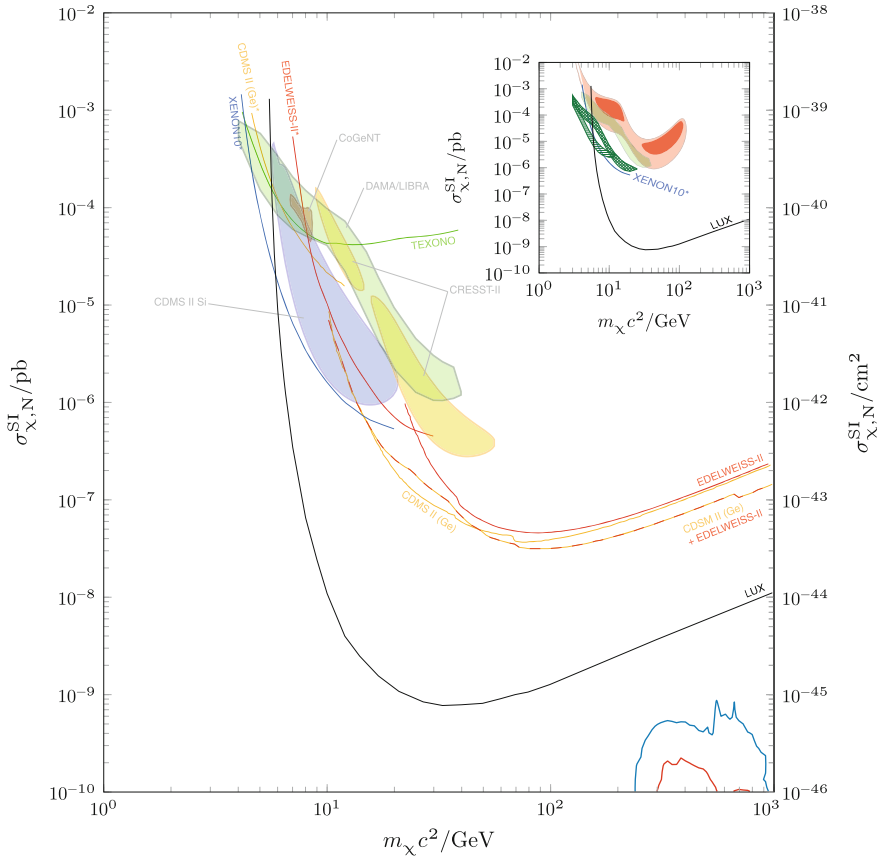


Fig. 2.10 Possible WIMP signals in the $\sigma_{\chi,N}^{\text{SI}} - m_{\chi}$ -plane: contours of the CoGeNT signal at 90 % CL [7, 8], the excess measured by CDMS II with silicon detectors at 90 % CL [31], the CRESST-II excess at 95.45 % CL [63] and of the DAMA/LIBRA signal under the assumption of light neutralino dark matter [98] (We note that this contour indicates *not* the usual CL. It “represent the domain where the likelihood-function values differ more than 7.5σ from the null hypothesis (absence of modulation)” [98, Fig. 1, right panel]. Nevertheless, we show it, as it is the analysis favoured by the DAMA/LIBRA collaboration [109, 127]. Also shown is the conventional analysis [282]). Also shown are the leading exclusion limits of LUX [42], XENON10* [60], TEXONO [229], CDMS II (Ge) [37, 39], EDELWEISS-II [76, 77], and CDMS II (Ge) + EDELWEISS-II [38]. The *inset* shows the effect of channeling (*green horizontally-hatched region*) and the effect of energy dependent Na and I quenching factors (*green cross-hatched region*) on the DAMA signal (*green filled region*) according to [98, Fig. 1, right panel]. The alternative analysis [282] is shown at 3σ CL (*dark red*) and 5σ CL (*light red*) for no channeling. Shown in the *right lower corner* are 68 % CL (*red*) and 95 % CL (*blue*) expectation for a global CMSSM fit [137]

In this section we will discuss the tension between these exclusion limits and the observed excesses/signals and give a short review on the possible solutions discussed in literature. Also a comparison between experimental findings and theoretical predictions (Sect. 2.1.2) will be given. For the exclusion limits, we will focus on LUX

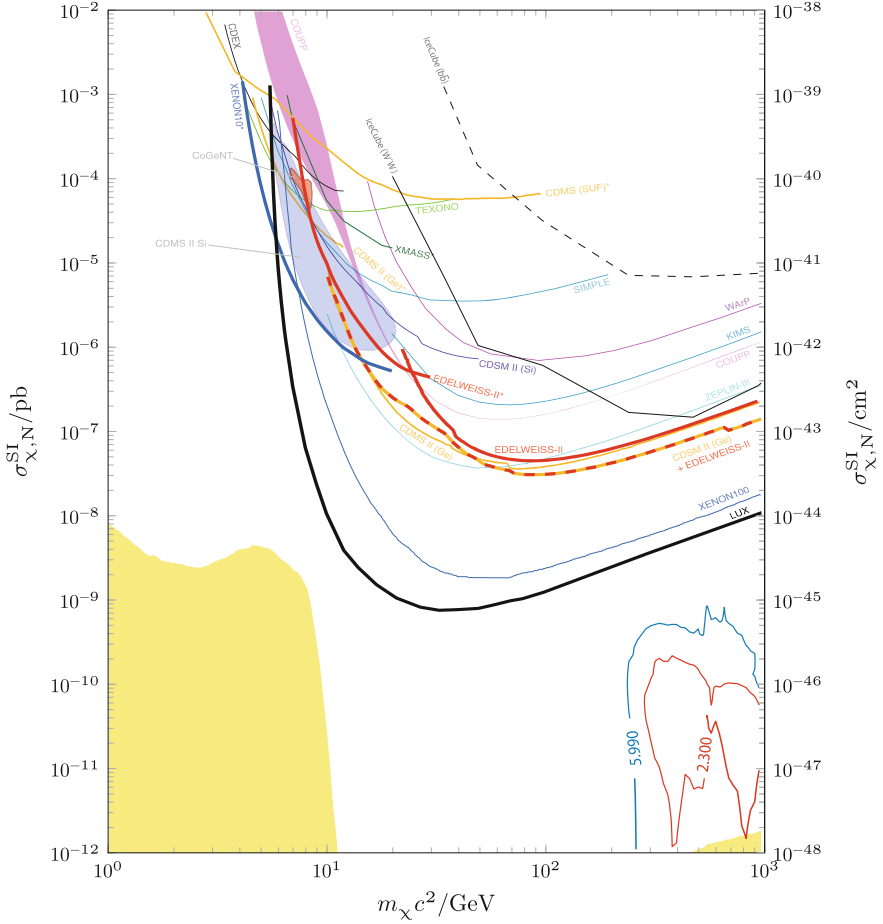


Fig. 2.11 Experimental upper limits at 90% CL on the spin-independent cross section for elastic scattering of WIMPs off various targets, $\sigma_{\chi,N}^{\text{SI}}$, normalized per nucleon, as function of the WIMP mass m_χ (CDEX [324], CDMS II (Ge) [37], CDMS II (Si) [31], CDMS II + EDELWEISS II [38], COUPP [91], EDELWEISS-II [76], KIMS [213], IceCube for $W^+ W^-$, $b \bar{b}$ final states [12], LUX [42], SIMPLE [172], TEXONO [229], WArP [101], XENON100 [68], ZEPLIN-III [47]). Dedicated analyses for low WIMP masses are indicated by an asterisk (CDMS II (Ge) [39], CDMS (SUF) [41], EDELWEISS-II [77], XENON10 [60], XMASS [20]). Also shown are the CoGeNT signal [7, 8] and the excess measured by CDMS II with silicon detectors [31], both at 90% CL. The yellow area indicate the background from coherent neutrino scattering [123]. Shown in the right lower corner are 68% CL (red) and 95% CL (blue) expectations for a global CMSSM fit [137]

[42] and the combined results of CDMS II (Ge) + EDELWEISS-II [38] as they are the leading limits for xenon and germanium targets, respectively.

If the excesses observed by CoGeNT [7, 8], CRESST [63] and CDMS II (Si) [31] and the annual modulation observed by DAMA/LIBRA [98, 114, 116] are interpreted as signals of an elastic scattered neutralino, the masses of the proposed

candidates lie between $m_\chi \approx 7$ GeV for CoGeNT and $m_\chi \approx 25$ GeV for CRESST. The leading exclusion limits of LUX ($\sigma_{\chi,N}^{\text{SI}} < 7.6 \times 10^{-10}$ pb) and CDMS II (Ge) + EDELWEISS-II ($\sigma_{\chi,N}^{\text{SI}} < 3.3 \times 10^{-8}$ pb) are less restricting for this *low mass WIMP* signal, see Fig. 2.10, as the respective experiments have their highest sensitivities between $m_\chi \approx 33$ GeV for LUX and $m_\chi \approx 90$ GeV for CDMS II (Ge) + EDELWEISS II, as the MSSM predicts *heavy* WIMPs, cf. Figs. 2.8b and 2.10.

However, reanalysis of the XENON10* [60], CDMS II (Ge)* [39], and EDELWEISS-II* [77] results, aimed for lower mass at the cost of a reduced total sensitivity, strongly limit the allowed parameter space for these light WIMPs. As Fig. 2.10 shows, the combined XENON10* and LUX limits exclude the preferred regions for the CRESST, CoGeNT, and CDSM II (Si) signal completely, and strongly limit the DAMA/LIBRA region. This strong reduction of the signal region is also confirmed by other experiments: Also CDSM II (Ge) + EDELWEISS-II, in sensitivity third only to LUX and XENON100, exclude the CRESST excess and strongly limit the parameter space for the CoGeNT, CDSM II (Si), and DAMA/LIBRA signal. This is confirmed, albeit with lower sensitivity, by experiments with a lower target mass like SIMPLE [172] or with a low threshold like TEXONO [229]. It has to be noted that possible signal is also at much lower mass and higher cross section than the predictions from the canonical CMSSM, e.g. [137], cf. Fig. 2.10.

To solve this tension between the observed excesses in some experiments and no signal in other experiments, several hypotheses are discussed in literature. They can be roughly divided into three categories: systematic effects on the experiments, alternative dark matter distribution in the galaxy like triaxial models [97] or tidal streams [210], and non-standard interactions between dark matter particles and the target such as a coupling to electrons instead to quarks [115] or iso-spin dependent interactions which suppress scattering off heavy targets like xenon [183]. However, it seems unlikely that fine tuning of the astrophysical and particle physics properties alone will yield a mutual solution for all observations [217].

Therefore, a correct understanding of possible systematic effects on the experiments is important. Exemplary, the tension between the results of DAMA/LIBRA and LUX may be removed by shifting the DAMA/LIBRA signal via channeling or energy dependent quenching factors [98, 113], see Fig. 2.10. It shows also the alternative interpretations [282] of a subset of the DAMA/LIBRA data [114]. For the tension between DAMA/LIBRA and the older XENON100 results, the tension may be reduced by relaxing the XENON limit by possible uncertainties in the relative scintillation efficiency of LXe at low energies [157, 306]. But also trivial explanations like an unknown background is possible, e.g. the CRESST excess may be caused by secondary cascades of nuclear recoils caused by ^{210}Po decay [222]. To identify such possible systematic uncertainties, it is important to maintain also in the future at least two detectors with different targets and detector designs [297]. EURECA would be an example for such a *complementary* approach within one experiment, i.e. heat and ionisation signals from germanium diodes, and heat and light from scintillators.

Future experiments with target masses up to a Multi-tonne scale will also be necessary to probe further the theoretical predictions. Increasing the target mass up to multi-tonne scale will potentially allow to observe statistically significant rates

at $\sigma_{\chi,N}^{\text{SI}} < 10^{-11}$ pb as theoretically predicted for the LSP [297], see Fig. 2.8b. At scattering cross sections below 10^{-12} pb, the background from coherent scattering of atmospheric neutrinos will limit the prospects of direct dark matter searches. For low WIMP masses ($m_\chi c^2 < 10$ GeV), coherent scattering of solar neutrinos will limit the WIMP search already at $\sigma_{\chi,N}^{\text{SI}} < 10^{-8}$ pb [123], see Fig. 2.11.

2.3 Dark Matter Search at LSM with EDELWEISS

In Sect. 2.2, we gave an overview of the current state of direct searches for WIMPs. Here, we will discuss the experimental aspects of EDELWEISS in more detail.

EDELWEISS uses cryogenic germanium bolometers to search for nuclear recoils induced by galactic WIMPs scattering off the nuclei. It is situated in the *Laboratoire Souterrain de Modane* (LSM) [76, 258]. The very first phase of the experiment started in the mid-1990s [96], developed into the EDELWEISS-I [143, 144, 280] and EDELWEISS-II [76, 77] stages. It is now in the installation phase of EDELWEISS-III [74, 258]. Continuous improvements of the detectors [258] resulted in a high power to reject background and now qualify to aim for a sensitivity of $\sigma_{\chi,N}^{\text{SI}} \lesssim 10^{-9}$ pb with EDELWEISS-III [80]. A sophisticated detector design and the simultaneous measurement of ionisation and phonon signals allows an event-by-event separation of the searched nuclear recoils from electronic recoils caused by γ - and β -radioactivity in the bulk and on the surface of the detector [133, 134].

In this section we will focus mainly on EDELWEISS-II, starting with a description of its experimental set-up in Sect. 2.3.1. Then, the rejection of electronic recoils is discussed in Sect. 2.3.2. Finally, the obtained physical results, exclusion limit and background, of EDELWEISS-II are given together with an outlook to EDELWEISS-III (Sect. 2.3.3). One kind of background, muon-induced neutrons, will then be discussed in detail in Chap. 3.

2.3.1 The Experimental Set-up at LSM

To reduce cosmogenic background, EDELWEISS is located at the Laboratoire Souterrain de Modane (LSM) besides a road tunnel below the Pointe du Fréjus in the Alps at the French-Italian boarder. Figure 2.12 shows the location of EDELWEISS in the main hall of the LSM, until 2011 [289] the NEMO 3 experiment [81] was installed next to EDELWEISS. To attenuate the remaining background, the cryostat with the germanium crystals is surrounded by passive γ - and neutron shields and an active muon veto [76]. To allow maintenance access to the cryostat, the upper part (called *Niveau 1*) of the shields and veto is divided and movable in an open and closed configuration. Contrary, the lower part (*Niveau 0*) is fixed. The exact position

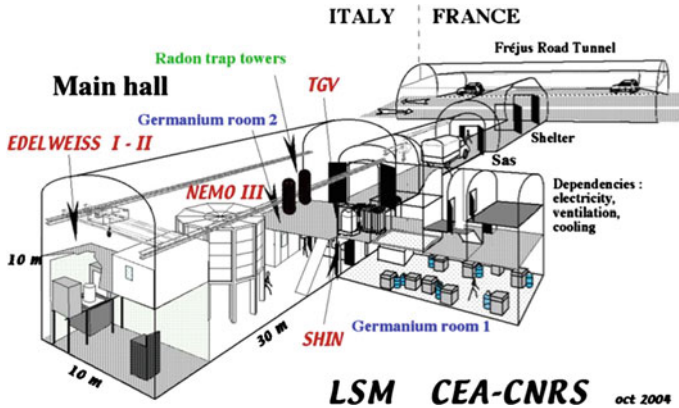


Fig. 2.12 Location of EDELWEISS in the main hall of the LSM. Until 2011 the NEMO 3 experiment was installed nearby. Figure provided by the LSM

of the movable parts are regularly monitored via laser distance measurements [283]. For an illustration of the complete set-up, see Fig. 5.1b.

To investigate sources of neutron background, additional auxiliary detectors were temporarily installed, a ^3He counter for the investigation of thermal neutrons [272], and a dedicated neutrons counter for muon-induced neutrons which is a main part of this work, see Chap. 4.

The muon flux at the LSM is attenuated by a rock overburden of 4800 mwe and measured via the EDELWEISS muon veto to $5.2 \text{ m}^{-2} \text{ D}^{-1}$ [283]. A more detailed discussion with regard to the simulation of the muon flux will be given in Sect. 5.3. The flux of ambient neutrons is $1.06 \times 10^{-6} \text{ cm}^{-2} \text{ s}^{-1} (E_n > 1 \text{ MeV})$ [180], an overview of neutron measurements at LSM will be given in Sect. 4.1.2. The radon level at LSM is $\approx 20 \text{ Bq m}^{-3}$, due to the ventilation system renewing the entire lab volume 1.5 times per hour [78]. The whole EDELWEISS set-up is surrounded by a clean room and permanently flushed with deradonized air [74], reducing the radon level to $\approx 20 \text{ mBq m}^{-3}$ [78].

The active muon veto is the outermost layer of EDELWEISS. It consists of 46 individual plastic scintillator modules (called *muon modules* hereafter) and is capable of muon track reconstruction. They are mounted in a stainless steel frame attached to the neutron shield [283]. The modules have a cross section of $65 \text{ cm} \times 5 \text{ cm}$ and lengths of 200 cm, 315 cm, 375 cm, 400 cm, for technical details of the muon modules see also Sect. 4.2.2. In total, the muon veto covers a surface of 100 m^2 [283]. Due to prominent gaps in Niveau 0 for the cryogenic supply lines and the pillars on which the experiment is mounted, the geometrical efficiency to tag throughgoing muons is 98% [283].

A throughgoing muon deposits an energy between 11.8 MeV (horizontal modules) and 24 MeV (vertical modules) [202]. Aimed for an as high as possible efficiency to tag also grazing muons, the average trigger threshold is set to $\approx 5 \text{ MeV}$ [283]. Consequently, the trigger rate of $\approx 1 \text{ s}^{-1}$ is dominated by ambient background, whereas

muon candidates, selected by requiring a coincidence between non-adjacent modules, contributes only $\approx 3.5 \times 10^{-4} \text{ s}^{-1}$ [283]. Including detector response and averaging over all muon modules, the detection efficiency for muons is 95 % [283]. MC simulation considering the geometrical coverage and the muon module efficiency results in a total muon veto efficiency for a closed Niveau 1 of 93.6(15) % in agreement with an experimental estimation of ≥ 93.5 % at 90 % CL [283].

On the inside of the muon veto follows the shield against ambient neutrons, made of polyethylene ensuring a minimal thickness of 50 cm towards the cryostat [76, 78]. The innermost shield is the γ -shield, consisting of an outer layer of 18 cm modern lead and an inner layer of 2 cm roman lead [228] with a reduced γ -activity from ^{210}Pb [78, 283].

The central part of the set-up is the cryostat, able to cool down up to 40 kg of target mass to a stabilized temperature of 18 mK [74, 75]. EDELWEISS uses a cryostat with reversed geometry, i.e. the dilution unit is below the detectors, see [78, Fig. 1]. The detectors are placed within the thermal shields at 0.01, 1, 4.2, 40, 100 K, and are shielded by 14 cm roman lead against the cold electronics, the dilution unit, and the cryogenic parts [78].

All materials in the detectors' vicinity within the 10 mK thermal shield are tested for radiopurity by dedicated HPGe detectors [74, 78], e.g. the individual casings of the detectors are of 99.99 % pure electrolytic copper [78]. Also the Teflon holders of the detectors [254] are selected for lowest possible radioactivity [255, 256]. In the EDELWEISS-III stage, also the more distant parts of the cryostat, e.g. the thermal shields at higher temperature and the vacuum chamber at 300 K are specially selected for radiopurity [78].

Within the cryostat, the detectors are arranged in an array of towers, each tower with two to three detectors, to increase the granularity of the target mass [75, 76]. The cryogenic bolometers consist of a cylindrical absorber made of a HPGe monocrystal ($< 10^{10} \text{ cm}^{-3}$ impurities [75]) equipped with sputtered aluminium electrodes and a glued Ge-NTD (Neutron Transmutation Doped) sensor [76, 256], see Fig. 2.13a. The dual readout of ionisation and phonon signal allows the rejection of electronic recoils with a power of $3(1) \times 10^{-5}$ [74], see Sect. 2.3.2 for details. An overview of the historic detector development from EDELWEISS-I to EDELWEISS-III is given in [258]. The bolometer type used in EDELWEISS-II was *InterDigit* (ID) [258], explained later in more detail. In total, ten bolometers with a diameter of 70 mm and a height of 20 mm were installed in EDELWEISS-II [75, 76, 256]. Five detectors had bevelled edges at an angle of 45° and an average mass of 370 g¹⁷ and five cylindrical detectors of 410 g [76].

The NTD measured the temperature of the crystal via the change of its resistance, $\approx 1 \text{ M } \Omega$ at 17 mK [241]. With an optimized heat exchange with the absorber [256], the reached sensitivity is 60 nV keV^{-1} [258]. The FWHM baseline resolution of this heat channel ranged from 0.6–2.0 keV_{ee} with an average of 1.2 keV_{ee} [76, 258].

¹⁷However, [75] gives 360 g.

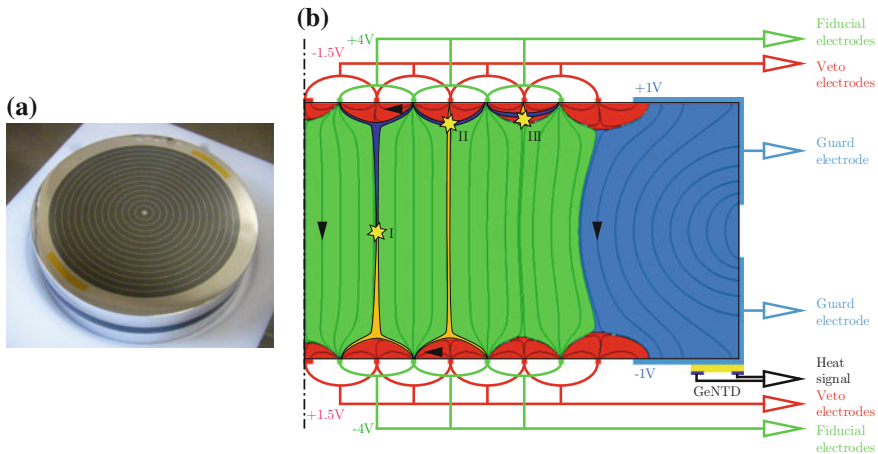


Fig. 2.13 **a** Picture of a 410g InterDigit detector. Clearly seen are the interleaved electrodes on top and the guard electrodes on side. The NTD is glued on the bottom and therefore not visible. **b** Scheme of the heat and the six ionisation channels of the InterDigit detector and the related volumes in the detector cross section: guard volume (light blue), veto volume (red), and fiducial volume (green). Illustrated are the trajectories of positive (orange) and negative (dark blue) charge carriers for three event types: I) bulk ionisation, II) ionisation in low field area, III) near surface ionisation. Figures provided by the EDELWEISS collaboration and adapted by the author according to [75], [133, Fig. 1a]

The name of the InterDigit bolometer type comes from the used electrode design. Each germanium crystal has two types of aluminium electrodes sputtered on its passivated surface [134, 288]. There are two plane electrodes at the edge, called *guard electrodes*, and on the top and bottom two sets of annular concentric electrodes. In total, each crystal has six sets of electrodes [76], which enables the rejection of near surface events [133, 134, 161, 162] with a power of 6×10^{-5} [76], see Sect. 2.3.2 for details.

The concentric electrodes are a variation of the coplanar grid design [57, 131, 237], instead of disk shape electrodes it uses four sets of interleaved strips [133, 134]. The stripes are $200 \mu\text{m}$ wide and 250 nm thick, the distance between each concentric electrode is 2 mm [133, 134]. Each electrode is connected via ultra-sonic bonding to its next but one neighbour, resulting in the earlier mentioned two sets of electrodes, called *fiducial* and *veto* electrode [133, 134].

The fiducial electrodes are biased with the highest potentials of $\pm 4 \text{ V}$ creating an axial electric field in the detector bulk [75]. The bias of $\mp 1.5 \text{ V}$ on the veto links adjacent electrodes via an electric field approximately parallel to the surface [75]. Plain guard electrodes cover the detector edges with a bias voltage of $\pm 1 \text{ V}$ [75]. See Fig. 2.13b for a map of the resulting field lines in the detector and Sect. 2.3.2 for the application in event selection. For the fiducial electrode, the chosen bias voltages and the electrode design results in a FWHM baseline resolution ranging from 0.7–1.1 keV_{ee} with an average of 0.9 keV_{ee} [76, 258].

The DAQ of the bolometers is independent from the DAQ of the muon veto, but synchronized via a common clock. The heat and ionisation signals of the bolometers are continuously sampled at 100 kS s^{-1} [75, 283]. In case the heat channel of one bolometer crosses the threshold, pulse traces of all bolometers within the given tower are stored [76]. The trigger threshold on the heat channels was continuously adjusted online to a trigger rate of a fraction of Hz [76]. To reject muon-induced background in the bolometer data, an offline search tags coincidences between any bolometer and the muon veto with a time resolution of $\approx 10 \mu\text{s}$, defined by the sampling rate of the bolometer [283]. In case of a coincidence, any bolometer within $\pm 1 \text{ ms}$ around the muon tag is rejected [283].

2.3.2 Event Categories and Event Selection

With the experimental set-up described in Sect. 2.3.1, EDELWEISS-II is able to discriminate between nuclear recoils as expected from scattering WIMPs and electronic recoils. This is a main advantage, as it provides an active rejection of background from γ - and β -radioactivity. In this section we report the basic functionality of this rejection technique, which enables EDELWEISS-II to obtain its physical results discussed in Sect. 2.3.3.

The events occurring in the cryogenic bolometers of EDELWEISS can be categorized according to their interaction type and the penetration depth [103]: Nuclear recoils are expected to be induced by elastic scattering of WIMPs, and are also induced by neutrons and recoiling nuclei from α -decays, like the $^{210}\text{Po}(\alpha)^{206}\text{Pb}$ reaction of the radon daughter nucleus ^{210}Po [103]. Whereas WIMP and neutron scattering occurs throughout the crystal, recoiling nuclei are restricted to the surface due to the short penetration depth. Similar, electronic recoils are induced by Compton scattering of ambient γ -rays throughout the crystals, whereas β -particles interact electronically near the surface.

Aiming for a sensitivity of $\sigma_{\chi, \text{N}}^{\text{SI}} < 5 \times 10^{-8} \text{ pb}$ for $20 \text{ GeV} \leq m_{\chi} c^2 \leq 100 \text{ GeV}$, the challenge is to detect a nuclear recoil rate of $< 5 \times 10^{-3} \text{ evts kg.d}^{-1}$ in germanium at $15 \text{ keV} \leq E_{\text{rec}} \leq 65 \text{ keV}$ [134]. However, already the average γ -rate within the EDELWEISS shield is $\approx 10 \text{ evts kg.d}^{-1}$, hence an active rejection of electronic recoils better than 10^{-4} is needed [134].

As electron recoils have a three times higher ionisation yield¹⁸ Q_i as nuclear recoils, the dual measurement of ionisation and phonon signals with the cryogenic bolometers allows an active, event-by-event rejection of electronic recoils [74, 133]. However, this technique is limited by surface events where poor charge collection mimics nuclear recoils in the bulk of the detector [133]. Therefore, a clean inner fiducial volume has to be defined [74]. In the following, we will first introduce the rejection of electronic recoils in the bulk and then the rejection of surface events.

¹⁸Sometimes also called *quenching factor*, see e.g. [280].

The responses E_h of the phonon channel and E_i of the ionisation channel to a nuclear recoil with energy E_{rec} is normalized to the response to an electronic recoil of the same energy. As a result, E_h and E_i are given in *electronvolt electron equivalent* (eV_{ee}) and can be parametrized as [105]:

$$E_{i,\gamma} = E_{\text{rec}} \quad (2.25a)$$

$$E_{i,n} = Q_i E_{\text{rec}} \quad (2.25b)$$

$$E_{h,\gamma} = E_{\text{rec}} \quad (2.25c)$$

$$E_{h,n} = \frac{Q_h + Q_i v}{1 + v} E_{\text{rec}} \quad v = \frac{e|V|}{\epsilon} \quad (2.25d)$$

Here, $\epsilon = 3.0 \text{ eV}$ is the energy needed to create an electron-hole pair in cryogenic germanium [105] and e is the elementary charge. Equation 2.25d also corrects the signal for the Luke-Neganov-effect [236, 257] i.e. the Joule heating of the detector via the drifting charges along the bias potential V of the electrode [75]. Also the effect of energy leakage out of the bolometer, e.g. via photon emission, is considered and experimentally described via the heat quenching factor $Q_h = 0.91$ [105].

For nuclear recoils, the ionisation yield $Q_i = Q_i(E_{\text{rec}})$ depends on the electronic and nuclear stopping power dE/dX of germanium ions in germanium [105] and is described by the Lindhard theory [234, 235]. However, instead of a theoretical description EDELWEISS [75, 241, 279] uses an experimental fit [300]:

$$Q_i = 0.16 \cdot E_{\text{rec}}^{0.18} \quad (2.26)$$

It also includes systematic effects like the heat quenching, therefore no separate Q_h values are needed [300]. Consequently, the recoil energy is [241, 280]:

$$E_{\text{rec}} = \left(1 + \frac{e|V|}{\epsilon}\right) E_h - \frac{e|V|}{\epsilon} E_i \quad (2.27a)$$

$$= \frac{E_h}{1 + Q_i \frac{e|V|}{\epsilon}} \left(1 + \frac{e|V|}{\epsilon}\right) \quad (2.27b)$$

Figure 2.14 shows the distribution of events from a neutron calibration in the $Q_i - E_{\text{rec}}$ -plane. Two clear populations from bulk events are visible: caused by the normalization of the detector response (Eq. 2.25a), the electronic recoils form a population around $Q_i = 1$ and the nuclear recoils form a population around the central line according to Eq. 2.26 [279]. Between both populations are situated electronic recoils near the surface, below the bulk nuclear recoils occur nuclear recoils near the surface [105]. The distributions of the ionisation yield Q in the electronic and nuclear recoil bands are to a good approximation Gaussian and can be calculated from the experimental baseline resolution [76, 241]. These populations are parametrized by the *gamma band* and the *nuclear recoil band*: Assuming a Gaussian fluctuation of the Q_i , the gamma band reached 99.99 % (7.72σ) below unity [76]. The nuclear

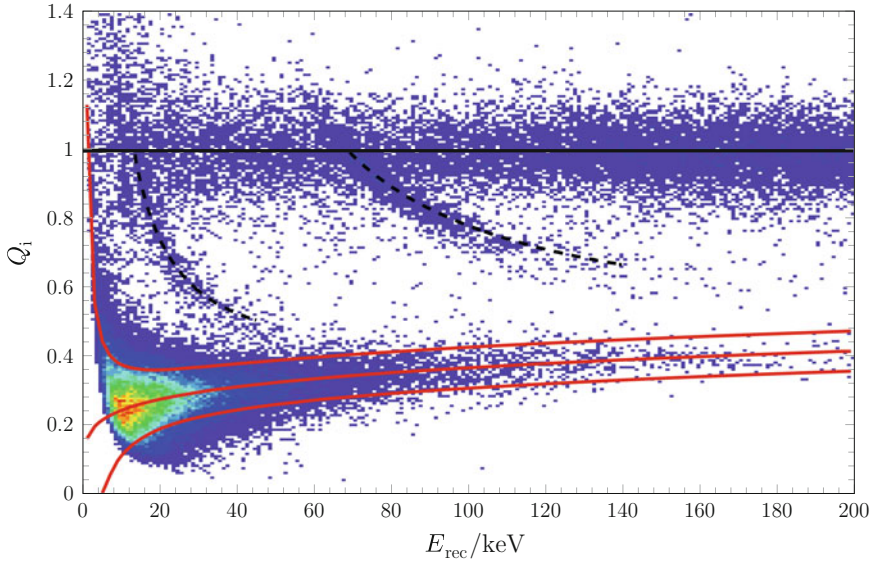


Fig. 2.14 Ionisation yield Q_i as function of the recoil energy E_{rec} of fiducial events recorded during neutron calibration. The two main populations are pure electron ($Q_i = 1$, *black solid line*) and nuclear recoils ($Q_i \approx 0.3$). The *red lines* indicate the $Q_i(E_{\text{rec}})$ -parametrization for nuclear recoils according to Eq. 2.26 together with the 90 % CL band. Deexcitation of short lived states of ^{73}Ge results in inelastic nuclear recoils with associated electromagnetic energies of 13.26 keV and 68.75 keV (*dashed black lines*). Figure adapted from [76]

recoil band is the 90 % (1.64σ) acceptance region around Eq. 2.26, considering the online-adjusted trigger threshold on the heat channel and the baseline FWHM resolution of the heat and ionisation channel [76]. The intersection of gamma band and nuclear recoil band at 10–20 keV [76], depending on the detector, defines the lower threshold the gamma rejection. Therefore, EDELWEISS used a threshold of 20 keV for the standard WIMP analysis [76].

Necessary for a great rejection power is a precise estimation of the ionisation yield via an effective charge collection. However, a long standing issue of cryogenic germanium detectors is the reduced charge collection efficiency near the surface [75]. Surface events are caused mainly by interaction of β^- -particles and X-rays in the first 20–100 μm below the electrodes where the collection of free-charge carriers is reduced due to efficient charge trapping and recombination in the electrode [253]. The reduced charge collection results in a leaking of electronic recoil events from the gamma band down in the nuclear recoil band. For instance, EDELWEISS-I was limited by the leaking of electron recoils, caused by β -decay of residual ^{210}Pb on all surfaces [258].

In EDELWEISS-II, the detector sensitivity to surface events is reduced via passive and active techniques. First, the surface is passivated by an amorphous layer of silicon or germanium, which creates a potential barrier in the band structure and prevents the charge carriers to access the electrode [256]. To increase the rejection power, three types of active techniques are possible [253]: via pulse shape discrimination or via measurements of athermal phonons¹⁹ or via an interleaved electrode design, the latter being used by EDELWEISS [75, 134].

To reject near surface events, the charge carrier trajectories in the electric field caused by the fiducial, veto, and guard electrodes are used [132]. Figure 2.13b shows the field and event topologies which are discussed in the following. Free charge carriers caused by ionisation in the bulk of the detector will follow the strong axial field between the fiducial electrodes on the top and bottom side, consequently they induce a signal on both fiducial electrodes. Charge carriers caused near the surface will be collected by the veto electrodes of the given surface and will only induce a signal there. Similarly, any interaction near the side of the cylindrical detectors give a signal on the guard electrodes. Even events in a low field volume provide signals on fiducial and veto electrodes [133, 134] due to the extension of the carrier clouds by Coulomb interaction [132].

The fiducial volume of the detector is the bulk of the detector with the volumes of reduced charge collection near the surface. Events in the fiducial volume are redundantly defined by the missing of any signal above the noise level on the veto and guard electrodes, and by requiring that the signals on the fiducial electrodes on the opposite sides have a the same timing and amplitude [75, 76]. The mass of the fiducial volume was experimentally determined to 160(5)g, averaged over all ten detectors [76]. A cut to the fiducial volume allows an experimentally determined surface rejection of 6×10^{-5} [76]. Its influence on the γ -rejection is illustrated by Fig. 2.15: out of 1.82×10^5 measured electronic interactions within $20 \text{ keV} < E_{\text{rec}} < 200 \text{ keV}$ only six events occur in the the nuclear recoil band after fiducial cut. This is a γ -rejection power of $3(1) \times 10^{-5}$ for $20 \text{ keV} < E_{\text{rec}} < 200 \text{ keV}$ [76].

Therefore, background caused by γ - and β -decays can be actively rejected due to their different event signature. In contrast, neutrons mimic the WIMP event signature: both particles induce nuclear recoils throughout the complete detector volume, the only difference is the higher scattering cross section for neutrons. The neutron background can be suppressed by rejecting coincidences between multiple bolometers. In a similar way, muon-induced neutrons can be suppressed by rejecting coincidences between any bolometer and the muon veto [283].

¹⁹As done by the CDMS experiment [37, 39], see also Sect. 2.2.3.

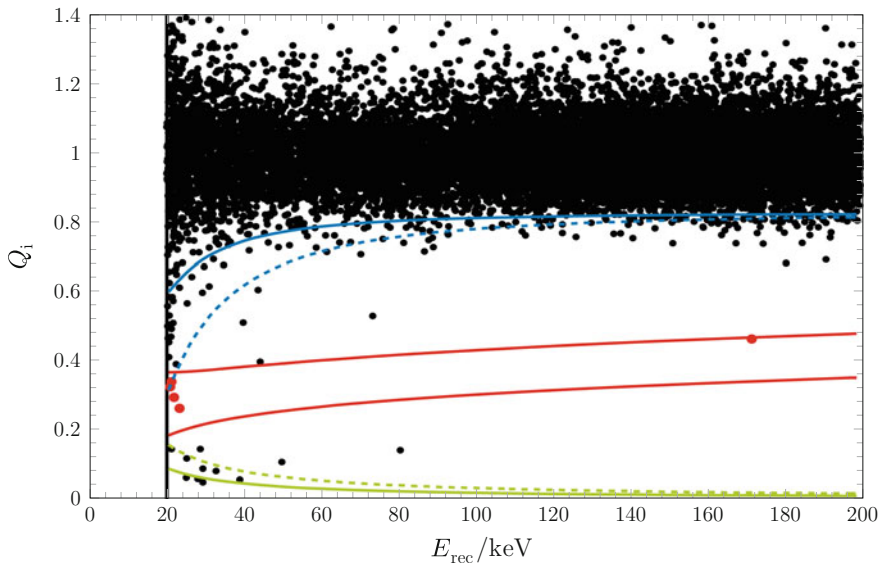


Fig. 2.15 Ionisation yield Q_i as function of the recoil energy E_{rec} of fiducial events recorded by EDELWEISS-II within an exposure of 427 kg.d. Highlighted in *red* are five WIMP candidates in the WIMP search region, i.e. in the 90 % acceptance band for nuclear recoils (*red*) and with energies between 20 and 200 keV. The *solid blue line* shows the averaged one-sided 99.99 % rejection limit for electron recoils and the *solid green line* the average ionisation threshold. *Dashed lines* indicate the worst case of the respective quality. Figure adapted from [76]

2.3.3 Results of EDELWEISS-II and Outlook on EDELWEISS-III

Having reported the experimental set-up of EDELWEISS-II in Sect. 2.3.1 and its technique of active background rejection in Sect. 2.3.2, we give the obtained physical results of EDELWEISS-II. Here, we are focusing on the spin-independent cross-section for elastic scattering of WIMPs off nucleons²⁰ [76] and estimated remaining background [78, 283]. A comparison of the EDELWEISS result with other current direct searches was given in Sect. 2.2.8 and for the set exclusion limits see Fig. 2.11.

EDELWEISS-II takes physics data from July 2008 till November 2008 and from April 2009 till May 2010 with a duty cycle of 85 % and all 10 ID detectors [76]. In total 417 live-days of WIMP data was collect [76]. This live-time is reduced by quality cuts to exclude noisy periods, pile-ups, and coincidences between the bolometers or between any bolometer and the muon veto. The total fiducial exposure after all cuts is 427 kg.d, within the 90 % nuclear recoil band the exposure is 384 kg.d [76].

²⁰However, the data of EDELWEISS-I and EDELWEISS-II was also analysed for different interaction models: for inelastic scattering [76], for spin-dependent coupling to ^{73}Ge (natural abundance of 4.8 % in the bolometers) [104], and for the sensitivity of EDELWEISS on axions [79].

For the recorded fiducial exposure, one expects a background of ≤ 5.0 evts within $20 \text{ keV} < E_{\text{rec}} < 200 \text{ keV}$, mainly caused by γ -decays and neutron scattering:

- From a surface rejection with a power of 6×10^{-5} at 90 % CL, a background of ≤ 0.3 evts from β -decays is expected [76, 78].
- The contribution of muon-induced WIMP-like events was estimated with MC simulation, considering also muon-induced neutrons. It showed that > 90 % of the muon-induced neutrons are produced in the lead of the γ -shield inside the muon veto, therefore they can be tagged by the muon veto. After rejecting muon-veto and multiple bolometer coincidences, one expects an irreducible background of ≤ 0.7 evts at 90 % CL, dominated by a small period without running muon veto [283].
- Based on calibration measurements, ≤ 0.9 evts at 90 % CL are expected from non-Gaussian fluctuations of electronic recoils out of the gamma band [76]. MC simulations indicate three source which may contribute most to the γ -background: daughter nuclei from the U/Th decay chain and ^{60}Co in the copper of the thermal shields and the 10 mK parts may contribute 39–52 %, a contamination of ^{210}Pb near the detectors or their casings may contribute 17–18 %, and the decay of ^{226}Ra and ^{228}Ra at the 300 K stage of the set-up may contribute 27–37 % [78].
- The ambient neutron background was deduced via MC simulations [78], taken into account the various shieldings and their holes due to pillars and cryogenic lines. The simulated neutron transport through the shields was checked with a strong AmBe source ($2 \times 10^5 \text{ s}^{-1}$) [78]. It showed that ambient neutrons passing through the shield make only a minor contribute of < 0.11 evts, whereas neutron sources within the shields are predominant, mostly from cables and connectors (1.5 evts). In total the estimated contribution from ambient neutrons is ≤ 3.1 evts at 90 % CL [78].
- Surface recoils from α -decay are negligible according to calibration measurements with α -source [76].

In total 1.8×10^4 evts within $20 \text{ keV} < E_{\text{rec}} < 200 \text{ keV}$ are recorded [76] in four categories in agreement with [103], see Fig. 2.15: Most events are bulk electromagnetic recoils in the gamma band. Between gamma band and nuclear recoil band ($Q < 0.65$) four events are found. However, from calibration only < 1.5 evts electronic surface events at 90 % CL are expected. Below the nuclear recoil band 11 events were found, probably induced by nuclear surface recoils of ^{210}Pb . Within the nuclear recoil band there were 5 events [76].

The number of nuclear recoils is consistent with the most recent background estimation [78]. However, even with the original background estimate of 3.0 evts [76], EDELWEISS-II does not indicate evidence for WIMPs [76]. Consequently, EDELWEISS-II sets an exclusion limit on the spin-independent WIMP-nucleon cross section $\sigma_{\chi, \text{N}}^{\text{SI}}$.

The exclusion limit was calculated with the optimal interval method [321] from the measured event rate without background subtraction. The galactic WIMP distribution is modeled as Maxwellian with $v_{\text{rms}} = 270 \text{ km s}^{-1}$, a WIMP density of $\rho_0 c^2 = 0.3 \text{ GeV cm}^{-3}$, an average earth velocity of $\bar{v}_{\text{earth}} = 235 \text{ km s}^{-1}$, and a

galactic escape velocity of $v_{\text{esc}} = 544 \text{ km s}^{-1}$ [292], see also Eq. 2.23. As result, EDELWEISS-II can exclude a minimal cross section of $\sigma_{\chi,N}^{\text{SI}} < 4.4 \times 10^{-8} \text{ pb}$ at 90 % CL for $m_{\chi}c^2 = 85 \text{ GeV}$ [76]. This is more than one order of magnitude improvement compared to EDELWEISS-I [279]. At $\approx 10^{-8} \text{ pb}$ the experiment probes already predictions from the MSSM (Sect. 2.1.5) [76]. For a comparison between theoretical predictions and experimental exclusion limits see Fig. 2.11.

To further improve the detection sensitivity, the data set of EDELWEISS-II [76] was combined [38] with the one of CDMS II (Ge) [37], also a direct search experiment using cryogenic germanium bolometer. For more information about CDMS II (Ge), see Sect. 2.2.3. The individual sets of events can simply be merged by considering the respective exposure-weighted efficiencies and applying the optimal interval method [321] on the combined event set [38]. The combined exclusion limit is with $\sigma_{\chi,N}^{\text{SI}} < 3.3 \times 10^{-8} \text{ pb}$ at 90 % CL minimal at $m_{\chi}c^2 = 90 \text{ GeV}$ [38]. The gain of the combined data set relative to the previous most sensitive data set (CDMS II) reaches 1.57 at the highest mass [38]. The obtained exclusion limits are the most sensitive limits for any germanium based experiment and third only to the xenon based experiments XENON100 [68] and LUX [42].

With a special data selection [77], the sensitivity is extended to lower WIMP masses: the base line resolution is improved from 1.2 to 0.8 keV_{ee} for the heat channel and from 0.9 to 0.7 keV_{ee} for the fiducial ionisation channel. Consequently, the exposure decreased from 384 [76] to 113 kg.d [77]. This results in an exclusion of $\sigma_{\chi,N}^{\text{SI}} < 10^{-5} \text{ pb}$ at 90 % CL for $m_{\chi}c^2 = 10 \text{ GeV}$ [77]. It excludes the WIMP interpretation of the CREST-II excess [63] and sets restrictions on the excesses of CoGeNT [8], CDMS II (Si) [31], and DAMA/LIBRA [98], see also Fig. 2.10.

EDELWEISS-III aims to improve the sensitivity by roughly one order of magnitude in two steps: in a first step the goal is $\sigma_{\chi,N}^{\text{SI}} < 5 \times 10^{-9} \text{ pb}$ within 3000 kg.d [74] and in a second step with increased target mass $\sigma_{\chi,N}^{\text{SI}} < 10^{-9} \text{ pb}$ within 12,000 kg.d [80]. To reach this improvement, two strategies are applied: Increasing the fiducial target mass and to reduce the background by active and passive techniques.

An increased fiducial mass is provided by the new *FullInterDigit* (FID) design. Figure 2.16 shows a picture of a FID detector together with a scheme of the electric field lines in the detector. The mass of the germanium crystal is roughly doubled to 800 g. The detector is equipped with two NTDs [74]. By replacing the guard electrodes of the ID design with interleaved electrodes also on the detector side of the FID, the relative fiducial volume is increased to $\approx 75 \%$ [258] compared to $\approx 40 \%$ [76] for the ID design. It is planned to install 40 FIDs with a total fiducial mass of 24 kg [74]. Large statistics gamma calibration showed also an improved rejection power for FID detector compared to ID detectors [258].

For the passive background reduction, the main sources for background in EDELWEISS-II are considered: neutrons originated within the shields and γ -radioactivity in the not-radiopure-copper of the thermal shield of the cryostat [78]. By replacing the thermal shields and the copper parts at 10 mK with new ones made from ultra pure copper, the γ -activity is expected to be reduced by at least a factor two [78]. MC simulation predicts a reduction of the neutron background

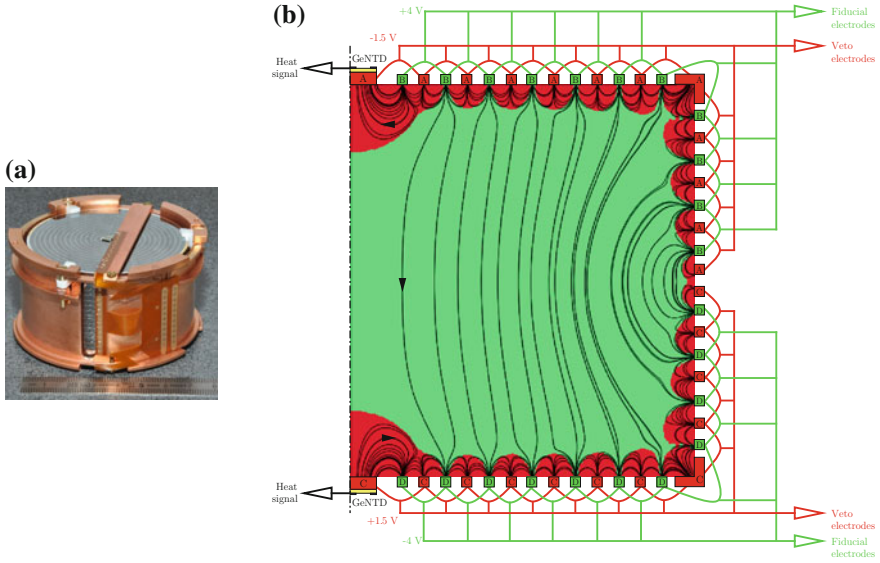


Fig. 2.16 **a** Picture of an 800 g FullInterDigit detector. Seen are the interleaved electrodes on *top* and also on *side*. Two NTDs are glued on the *top* and the *bottom* of the detector. **b** Scheme of the two heat and the four ionisation channels of the FullInterDigit detector and the related volumes in the detector cross section: veto volume (*red*) and fiducial volume (*green*). Also indicated are the two NTD sensors. Figures provided by the EDELWEISS collaboration and modified by the author

from $\leq 8.1 \times 10^{-3}$ evts kg.d $^{-1}$ in EDELWEISS-II to $\leq 1.9 \times 10^{-4}$ evts kg.d $^{-1}$ in EDELWEISS-III by new infrastructure (cabling, cold electronics, cryogenics, and acquisition) and an additional inner polyethylene shield inside the cryostat [74, 78]. The upgraded infrastructure aims also at a reduction of the microphonic noise [258]. Beyond EDELWEISS-III is the R&D work on *NbSi superconductive resistive meanders* as new heat sensors with the potential of decreased threshold and increased energy resolution [258].

A fully running muon veto and the increased granularity caused by the increased number of detectors will reduce the muon-induced WIMP-like background to $(0.6^{+0.7}_{-0.6})$ events at 90 % CL for 3000 kg.d exposure [283]. This is the same order of magnitude as the contribution of ambient neutrons: $\leq 1.9 \times 10^{-4}$ evts kg.d $^{-1}$ · 3000 kg.d = 0.57 evts [78]. Therefore, with an improved suppression of ambient backgrounds, the relative contribution of muon-induced background increases. This highlights the importance of a reliable understanding of muon interactions in the experiment, especially of muon-induced neutrons as they can mimic the WIMP signature.

In conclusion, EDELWEISS is together with CDMS, the leading experiment searching for elastic scattering of WIMPs in germanium. A further improvement by one order of magnitude in the sensitivity is planned for EDELWEISS-III. Due

to the improved reduction of ambient background, the relative importance of muon-induced background and its understanding will increase.

References

1. Aad G et al [ATLAS Collaboration] (2012) Search for supersymmetry in final states with jets, missing transverse momentum and one isolated lepton in $\sqrt{s}=7$ TeV pp collisions using 1 fb^{-1} of ATLAS data. Phys Rev D 85(1):012006. doi:[10.1103/PhysRevD.85.012006](https://doi.org/10.1103/PhysRevD.85.012006). arXiv:[1109.6606](https://arxiv.org/abs/1109.6606) [hep-ex]
2. Aad G et al [ATLAS Collaboration] (2012) Observation of a new particle in the search for the standard model Higgs boson with the ATLAS detector at the LHC. Phys Lett B 716(1):1–29. doi:[10.1016/j.physletb.2012.08.020](https://doi.org/10.1016/j.physletb.2012.08.020). arXiv:[1207.7214](https://arxiv.org/abs/1207.7214) [hep-ex]
3. Aad G et al [ATLAS Collaboration] (2013) Search for squarks and gluinos with the ATLAS detector in final states with jets and missing transverse momentum using 4.7 fb^{-1} of $\sqrt{s} = 7$ TeV proton-proton collision data. Phys Rev D 87(1):012008. doi:[10.1103/PhysRevD.87.012008](https://doi.org/10.1103/PhysRevD.87.012008). arXiv:[1208.0949](https://arxiv.org/abs/1208.0949) [hep-ex]
4. Aaij R et al [LHCb Collaboration] (2013) First evidence for the decay $b_s^0 \rightarrow \mu^+ \mu^-$. Phys Rev Lett 110(2):021801. doi:[10.1103/PhysRevLett.110.021801](https://doi.org/10.1103/PhysRevLett.110.021801). arXiv:[1211.2674](https://arxiv.org/abs/1211.2674) [hep-ex]
5. Aalseth CE et al [CoGeNT Collaboration] (2008) Experimental constraints on a dark matter origin for the DAMA annual modulation effect. Phys Rev Lett 101(25):251301. doi:[10.1103/PhysRevLett.101.251301](https://doi.org/10.1103/PhysRevLett.101.251301). arXiv:[0807.0879v3](https://arxiv.org/abs/0807.0879v3) [astro-ph]
6. Aalseth CE et al (2009) Erratum: Experimental constraints on a dark matter origin for the DAMA annual modulation effect [Phys Rev Lett 101:251301 (2008)]. Phys Rev Lett 102(10):109903. doi:[10.1103/PhysRevLett.102.109903](https://doi.org/10.1103/PhysRevLett.102.109903)
7. Aalseth CE et al [CoGeNT Collaboration] (2011) Results from a search for lightmass dark matter with a p -type point contact germanium detector. Phys Rev Lett 106(13):131301. doi:[10.1103/PhysRevLett.106.131301](https://doi.org/10.1103/PhysRevLett.106.131301). arXiv:[1002.4703](https://arxiv.org/abs/1002.4703) [astro-ph]
8. Aalseth CE et al [CoGeNT Collaboration] (2011) Search for an annual modulation in a p -type point contact germanium dark matter detector. Phys Rev Lett 107(14):141301. doi:[10.1103/PhysRevLett.107.141301](https://doi.org/10.1103/PhysRevLett.107.141301). arXiv:[1106.0650](https://arxiv.org/abs/1106.0650) [astro-ph.CO]
9. Aalseth CE et al [CoGeNT Collaboration] (2013) CoGeNT: a search for low-mass dark matter using p -type point contact germanium detectors. Phys Rev D 88(1):012002. doi:[10.1103/PhysRevD.88.012002](https://doi.org/10.1103/PhysRevD.88.012002). arXiv:[1208.5737](https://arxiv.org/abs/1208.5737) [astro-ph.CO]
10. Aalseth C et al [Majorana Collaboration] (2004) The majorana neutrinoless doublebeta decay experiment. Phys At Nucl 67(11):2002–2010. doi:[10.1134/1.1825519](https://doi.org/10.1134/1.1825519)
11. Aaltonen T et al [CDF and D0 Collaborations] (2012) Evidence for a particle produced in association with weak bosons and decaying to a bottom-antibottom quark pair in higgs boson searches at the tevatron. Phys Rev Lett 109(7):071804. doi:[10.1103/PhysRevLett.109.071804](https://doi.org/10.1103/PhysRevLett.109.071804). arXiv:[1207.6436](https://arxiv.org/abs/1207.6436) [hep-ex]
12. Aartsen MG et al [IceCube Collaboration] (2012) Search for dark matter annihilations in the Sun with the 79-string IceCube detector. Phys Rev Lett 110(13):131302. doi:[10.1103/PhysRevLett.110.131302](https://doi.org/10.1103/PhysRevLett.110.131302). arXiv:[1212.4097](https://arxiv.org/abs/1212.4097) [astro-ph.HE]
13. Abdo AA et al [Fermi LAT Collaboration] (2009) Measurement of the cosmic ray e^+ plus e^- spectrum from 20 GeV to 1 TeV with the Fermi Large Area Telescope. Phys Rev Lett 102(18):181101. doi:[10.1103/PhysRevLett.102.181101](https://doi.org/10.1103/PhysRevLett.102.181101). arXiv:[0905.0025](https://arxiv.org/abs/0905.0025) [astro-ph.HE]
14. Abdo AA et al [Fermi LAT Collaboration] (2009) Fermi large area telescope measurements of the diffuse gamma-ray emission at Intermediate Galactic Latitudes. Phys Rev Lett 103(25):251101. doi:[10.1103/PhysRevLett.103.251101](https://doi.org/10.1103/PhysRevLett.103.251101). As cited in Ref. [264]
15. Abdo AA et al [Fermi LAT Collaboration] (2010) Fermi large area telescope search for photon lines from 30 to 200 GeV and dark matter implications. Phys Rev Lett 104(9):091302. doi:[10.1103/PhysRevLett.104.091302](https://doi.org/10.1103/PhysRevLett.104.091302). As cited in Ref. [264]

16. Abdo AA et al [Fermi LAT Collaboration] (2010) Spectrum of the isotropic diffuse gamma-ray emission derived from first-year Fermi Large Area Telescope data. *Phys Rev Lett* 104(10):101101. doi:[10.1103/PhysRevLett.104.101101](https://doi.org/10.1103/PhysRevLett.104.101101). As cited in Ref. [264]
17. Abdo AA et al (2010) Observations of milky way dwarf spheroidal galaxies with the Fermi-Large Area Telescope detector and constraints on dark matter models. *Astrophys J* 712(1):147–158. doi:[10.1088/0004-637X/712/1/147](https://doi.org/10.1088/0004-637X/712/1/147)
18. Abdo AA et al (2010) Constraints on cosmological dark matter annihilation from the Fermi-LAT isotropic diffuse gamma-ray measurement. *J Cosmol Astropart Phys* 2010(4):014. doi:[10.1088/1475-7516/2010/04/014](https://doi.org/10.1088/1475-7516/2010/04/014)
19. Abe K et al (2013) XMASS detector. *Nucl Instrum Methods Phys Res Sect A* 716:78–85. doi:[10.1016/j.nima.2013.03.059](https://doi.org/10.1016/j.nima.2013.03.059)
20. Abe K et al (2013) Light WIMP search in XMASS. *Phys Lett B* 719(1–3):78–82. doi:[10.1016/j.physletb.2013.01.001](https://doi.org/10.1016/j.physletb.2013.01.001)
21. Abramowski A et al (2011) H.E.S.S. constraints on dark matter annihilations towards the sculptor and carina dwarf galaxies. *Astropart Phys* 34(8):608–616. doi:[10.1016/j.astropartphys.2010.12.006](https://doi.org/10.1016/j.astropartphys.2010.12.006)
22. Abramowski A et al (2012) Search for dark matter annihilation signals from the fornax galaxy cluster with H.E.S.S. *Astrophys J* 750(2):123. doi:[10.1088/0004-637X/750/2/123](https://doi.org/10.1088/0004-637X/750/2/123). arXiv:[1202.5494](https://arxiv.org/abs/1202.5494) [astro-ph.HE]
23. Abt I et al (2007) Background reduction in neutrinoless double beta decay experiments using segmented detectors-A Monte Carlo study for the GERDA setup. *Nucl Instrum Methods Phys Res Sect A* 570(3):479–486. doi:[10.1016/j.nima.2006.10.188](https://doi.org/10.1016/j.nima.2006.10.188)
24. Acciari VA et al (2010) VERITAS search for VHE gamma-ray emission from dwarf spheroidal galaxies. *Astrophys J* 720(2):1174–1180. doi:[10.1088/0004-637X/720/2/1174](https://doi.org/10.1088/0004-637X/720/2/1174)
25. Ackermann M et al (2010) Constraints on dark matter annihilation in clusters of galaxies with the Fermi large area telescope. *J Cosmol Astropart Phys* 2010(5):025. doi:[10.1088/1475-7516/2010/05/025](https://doi.org/10.1088/1475-7516/2010/05/025)
26. Ackermann M et al [Fermi-LAT Collaboration] (2013) Dark matter constraints from observations of 25 Milky Way satellite galaxies with the Fermi Large Area Telescope. *Phys Rev D* 89(4):042001. doi:[10.1103/PhysRevD.89.042001](https://doi.org/10.1103/PhysRevD.89.042001). arXiv:[1310.0828](https://arxiv.org/abs/1310.0828) [astro-ph.HE]
27. Adamson P et al [MINOS Collaboration] (2013) Comparisons of annual modulations in MINOS with the event rate modulation in CoGeNT. *Phys Rev D* 87(3):032005. doi:[10.1103/PhysRevD.87.032005](https://doi.org/10.1103/PhysRevD.87.032005). arXiv:[1212.1776](https://arxiv.org/abs/1212.1776) [hep-ex]
28. Ade PAR et al [Planck Collaboration] (2013) Planck 2013 results: XVI. Cosmological parameters. *Astron Astrophys* 571:A16. doi:[10.1051/0004-6361/201321591](https://doi.org/10.1051/0004-6361/201321591). arXiv:[1303.5076](https://arxiv.org/abs/1303.5076) [astro-ph.CO]
29. Adriani O et al [PAMELA Collaboration] (2009) An anomalous positron abundance in cosmic rays with energies 1.5–100 GeV. *Nature* 458:607–609. doi:[10.1038/nature07942](https://doi.org/10.1038/nature07942). arXiv:[0810.4995](https://arxiv.org/abs/0810.4995) [astro-ph]
30. Adriani O et al (2013) Cosmic-ray positron energy spectrum measured by PAMELA. *Phys Rev Lett* 111(8):081102. doi:[10.1103/PhysRevLett.111.081102](https://doi.org/10.1103/PhysRevLett.111.081102). arXiv:[1308.0133](https://arxiv.org/abs/1308.0133) [astro-ph.HE]
31. Agnese R et al [CDMS Collaboration] (2013) Dark matter search results using the silicon detectors of CDMS II. arXiv:[1304.4279](https://arxiv.org/abs/1304.4279) [hep-ex]
32. Aharonian F et al (2008) Observations of the Sagittarius dwarf galaxy by the HESS experiment and search for a dark matter signal. *Astropart Phys* 29(1):55–62. doi:[10.1016/j.astropartphys.2007.11.007](https://doi.org/10.1016/j.astropartphys.2007.11.007)
33. Aharonian F et al (2009) A search for a dark matter annihilation signal toward the canis major overdensity with H.E.S.S. *Astrophys J* 691(1):175–181. doi:[10.1088/0004-637X/691/1/175](https://doi.org/10.1088/0004-637X/691/1/175)
34. Aharonian F et al (2010) Erratum to Observations of the Sagittarius dwarf galaxy by the HESS experiment and search for a dark matter signal [*Astropart. Phys.* 29(1) (2008) 55–62]. *Astropart Phys* 33(4):274–275. doi:[10.1016/j.astropartphys.2010.01.007](https://doi.org/10.1016/j.astropartphys.2010.01.007)
35. Ahlen S et al [DMTPC Collaboration] (2011) First dark matter search results from a surface run of the 10-L DMTPC directional dark matter detector. *Phys Lett B* 695(1–4):124–129. doi:[10.1016/j.physletb.2010.11.041](https://doi.org/10.1016/j.physletb.2010.11.041). arXiv:[1006.2928](https://arxiv.org/abs/1006.2928)

36. Ahmed Z et al [CDMS Collaboration] (2009) Search for weakly interacting massive particles with the first five-tower data from the cryogenic dark matter search at the soudan underground laboratory. *Phys Rev Lett* 102(1):011301. doi:[10.1103/PhysRevLett.102.011301](https://doi.org/10.1103/PhysRevLett.102.011301)
37. Ahmed Z et al [CDMS II Collaboration] (2010) Dark matter search results from the CDMS II experiment. *Science* 327(5973):1619–1621. doi:[10.1126/science.1186112](https://doi.org/10.1126/science.1186112)
38. Ahmed Z et al [CDMS and EDELWEISS collaborations] (2011) Combined limits on WIMPs from the CDMS and EDELWEISS experiments. *Phys Rev D* 84(1):011102. doi:[10.1103/PhysRevD.84.011102](https://doi.org/10.1103/PhysRevD.84.011102). arXiv:[1105.3377](https://arxiv.org/abs/1105.3377) [astro-ph.CO]
39. Ahmed Z et al [CDMS Collaboration] (2011) Results from a low-energy analysis of the CDMS II germanium data. *Phys Rev Lett* 106(13):131302. doi:[10.1103/PhysRevLett.106.131302](https://doi.org/10.1103/PhysRevLett.106.131302). arXiv:[1011.2482](https://arxiv.org/abs/1011.2482) [astro-ph.CO]
40. Ahmed Z et al [CDMS Collaboration] (2012) Search for annual modulation in lowenergy CDMS-II data. arXiv:[1203.1309](https://arxiv.org/abs/1203.1309) [astro-ph.CO]
41. Akerib DS et al [CDMS Collaboration] (2010) Low-threshold analysis of CDMS shallow-site data. *Phys Rev D* 82(12):122004. doi:[10.1103/PhysRevD.82.122004](https://doi.org/10.1103/PhysRevD.82.122004). arXiv:[1010.4290](https://arxiv.org/abs/1010.4290) [astro-ph.CO]
42. Akerib DS et al [LUX Collaboration] (2013) First results from the LUX dark matter experiment at the Sanford Underground Research Facility. arXiv:[1310.8214](https://arxiv.org/abs/1310.8214) [astro-ph.CO]
43. Akerib D et al (2013) Technical results from the surface run of the LUX dark matter experiment. *Astropart Phys* 45:34–43. doi:[10.1016/j.astropartphys.2013.02.001](https://doi.org/10.1016/j.astropartphys.2013.02.001). arXiv:[1210.4569](https://arxiv.org/abs/1210.4569) [astro-ph.IM]
44. Akerib D et al (2013) The large underground xenon (LUX) experiment. *Nucl Instrum Methods Phys Res, Sect A* 704:111–126. doi:[10.1016/j.nima.2012.11.135](https://doi.org/10.1016/j.nima.2012.11.135). arXiv:[1211.3788](https://arxiv.org/abs/1211.3788) [physics.ins-det]
45. Akimov D (2011) Techniques and results for the direct detection of dark matter (review). In: VCI 2010—proceedings of the 12th international Vienna conference on instrumentation, special issue. *Nucl Instrum Methods Phys Res Sect A* 628(1):50–58. doi:[10.1016/j.nima.2010.06.283](https://doi.org/10.1016/j.nima.2010.06.283)
46. Akimov D et al (2010) The ZEPLIN-III anti-coincidence veto detector. *Astropart Phys* 34(3):151–163. doi:[10.1016/j.astropartphys.2010.06.010](https://doi.org/10.1016/j.astropartphys.2010.06.010)
47. Akimov D et al (2012) WIMP-nucleon cross-section results from the second science run of ZEPLIN-III. *Phys Lett B* 709(1–2):14–20. doi:[10.1016/j.physletb.2012.01.064](https://doi.org/10.1016/j.physletb.2012.01.064). arXiv:[1110.4769](https://arxiv.org/abs/1110.4769) [astro-ph.CO]
48. van Albada TS et al (1985) Distribution of dark matter in the spiral galaxy NGC 3198. *Astrophys J* 295:305–313. doi:[10.1086/163375](https://doi.org/10.1086/163375). ADS: 1985ApJ...295..305V
49. Albert J et al (2008) Upper limit for γ -ray emission above 140 GeV from the Dwarf Spheroidal Galaxy Draco. *Astrophys J* 679(1):428–431. doi:[10.1086/529135](https://doi.org/10.1086/529135)
50. Aleksic J et al [MAGIC Collaboration] (2010) MAGIC gamma-ray telescope observation of the perseus cluster of galaxies: Implications for cosmic rays, dark matter, and NGC 1275. *Astrophys J* 710(1):634–647. doi:[10.1088/0004-637X/710/1/634](https://doi.org/10.1088/0004-637X/710/1/634)
51. Aleksic J et al [MAGIC Collaboration] (2011) Searches for dark matter annihilation signatures in the Segue 1 satellite galaxy with the MAGIC-I telescope. *J Cosmol Astropart Phys* 2011(6):035. doi:[10.1088/1475-7516/2011/06/035](https://doi.org/10.1088/1475-7516/2011/06/035)
52. Alexander T et al (2013) Light yield in DarkSide-10: a prototype two-phase argon TPC for dark matter searches. *Astropart Phys* 49:44–51. doi:[10.1016/j.astropartphys.2013.08.004](https://doi.org/10.1016/j.astropartphys.2013.08.004)
53. Aliu E et al [VERITAS Collaboration] (2012) VERITAS deep observations of the dwarf spheroidal galaxy Segue 1. *Phys Rev D* 85(6):062001. doi:[10.1103/PhysRevD.85.062001](https://doi.org/10.1103/PhysRevD.85.062001)
54. Alner G et al (2005) First limits on nuclear recoil events from the ZEPLIN I galactic dark matter detector. *Astropart Phys* 23(5):444–462. doi:[10.1016/j.astropartphys.2005.02.004](https://doi.org/10.1016/j.astropartphys.2005.02.004)
55. Alner G et al [ZEPLIN] (2007) First limits on WIMP nuclear recoil signals in ZEPLINII: a two-phase xenon detector for dark matter detection. *Astropart Phys* 28(3):287–302. doi:[10.1016/j.astropartphys.2007.06.002](https://doi.org/10.1016/j.astropartphys.2007.06.002)
56. Amarè J et al (2013) Preliminary results of ANAIS-25. arXiv:[1308.3478](https://arxiv.org/abs/1308.3478)

57. Amman M, Luke P (2000) Three-dimensional position sensing and field shaping in orthogonal-strip germanium gamma-ray detectors. *Nucl Instrum Methods Phys Res Sect A* 452(1–2):155–166. doi:[10.1016/S0168-9002\(00\)00351-X](https://doi.org/10.1016/S0168-9002(00)00351-X). As cited in Ref. [133]
58. Anderson L et al (2012) The clustering of galaxies in the SDSS-III baryon oscillation spectroscopic survey: baryon acoustic oscillations in the data release 9 spectroscopic galaxy sample. *Mon Not R Astron Soc* 427(4):3435–3467. doi:[10.1111/j.1365-2966.2012.22066.x](https://doi.org/10.1111/j.1365-2966.2012.22066.x). arXiv:[1203.6594](https://arxiv.org/abs/1203.6594) [astro-ph.CO]
59. Angle J et al [XENON10 Collaboration] (2008) Limits on spin-dependent wimp-nucleon cross sections from the XENON10 experiment. *Phys Rev Lett* 101(9):091301. doi:[10.1103/PhysRevLett.101.091301](https://doi.org/10.1103/PhysRevLett.101.091301)
60. Angle J et al [XENON10 Collaboration] (2011) Search for light dark matter in XENON10 data. *Phys Rev Lett* 107(5):051301. doi:[10.1103/PhysRevLett.107.051301](https://doi.org/10.1103/PhysRevLett.107.051301)
61. Angloher G et al (2002) Limits on WIMP dark matter using sapphire cryogenic detectors. *Astropart Phys* 18(1):43–55. doi:[10.1016/S0927-6505\(02\)00111-1](https://doi.org/10.1016/S0927-6505(02)00111-1)
62. Angloher G et al (2009) Commissioning run of the CRESST-II dark matter search. *Astropart Phys* 31(4):270–276. doi:[10.1016/j.astropartphys.2009.02.007](https://doi.org/10.1016/j.astropartphys.2009.02.007). arXiv:[0809.1829v2](https://arxiv.org/abs/0809.1829v2) [astro-ph]
63. Angloher G et al (2012) Results from 730 kg days of the CRESST-II dark matter search. *Eur Phys J C* 72:1971. doi:[10.1140/epjc/s10052-012-1971-8](https://doi.org/10.1140/epjc/s10052-012-1971-8). arXiv:[1109.0702](https://arxiv.org/abs/1109.0702)
64. Angloher G et al (2014) EURECA conceptual design report. *Phys Dark Universe* 3:41–74. doi:[10.1016/j.dark.2014.03.004](https://doi.org/10.1016/j.dark.2014.03.004)
65. Aprile E, Baudis L (2010) Liquid noble gases. In: Bertone G (ed) *Particle dark matter: observations, models and searches*. Cambridge University Press, Cambridge (Chap 21)
66. Aprile E et al (2010) Design and performance of the XENON10 dark matter experiment. arXiv:[1001.2834](https://arxiv.org/abs/1001.2834) [astro-ph.IM]
67. Aprile E et al [XENON100 Collaboration] (2012) The XENON100 dark matter experiment. *Astropart Phys* 35(9):573–590. doi:[10.1016/j.astropartphys.2012.01.003](https://doi.org/10.1016/j.astropartphys.2012.01.003). arXiv:[1107.2155](https://arxiv.org/abs/1107.2155) [astro-ph.IM]
68. Aprile E et al [XENON100 Collaboration] (2012) Dark matter results from 225 live days of XENON100 data. *Phys Rev Lett* 109(18):181301. doi:[10.1103/PhysRevLett.109.181301](https://doi.org/10.1103/PhysRevLett.109.181301). arXiv:[1207.5988](https://arxiv.org/abs/1207.5988) [astro-ph.CO]
69. Aprile E et al (2013) The neutron background of the XENON100 dark matter experiment. *J Phys G Nucl Part Phys* 40(11):115201. doi:[10.1088/0954-3899/40/11/115201](https://doi.org/10.1088/0954-3899/40/11/115201). arXiv:[1306.2303](https://arxiv.org/abs/1306.2303) [astro-ph.IM]
70. Archambault S et al (2012) Constraints on low-mass WIMP interactions on 19F from PICASSO. *Phys Lett B* 711(2):153–161. doi:[10.1016/j.physletb.2012.03.078](https://doi.org/10.1016/j.physletb.2012.03.078). arXiv:[1202.1240](https://arxiv.org/abs/1202.1240) [hep-ex]
71. Ardid M (2013) Dark matter searches with COUPP bubble chambers. Presented at the 21st international conference on supersymmetry and unification of fundamental interactions (SUSY2013), Trieste, Italy, 26–31 Aug 2013. http://susy2013.ictp.it/lecturenotes/04_Thursday/Dark_Matter_and_Cosmology/Ardid.pdf
72. Arisaka K (2012) MAX and XAX: dark matter and neutrino observatory based on multi-ton liquid xenon and liquid argon. Presented at the 9th international conference: identification of dark matter (IDM2012), Chicago, IL, US, 23–27 July 2012. <http://kicp-workshops.uchicago.edu/IDM2012/depot/talkarisaka-katsushi.pdf>
73. Arisaka K et al (2009) XAX: a multi-ton, multi-target detection system for dark matter, double beta decay and pp solar neutrinos. *Astropart Phys* 31(2):63–74. doi:[10.1016/j.astropartphys.2008.11.007](https://doi.org/10.1016/j.astropartphys.2008.11.007)
74. Armengaud E [For the EDELWEISS Collaboration] (2012) Searching for WIMPs with EDELWEISS. In: 12th international conference on topics in astroparticle and underground physics (TAUP 2011), special issue. *J Phys Conf Ser* 375(1):012004. doi:[10.1088/1742-6596/375/1/012004](https://doi.org/10.1088/1742-6596/375/1/012004)
75. Armengaud E et al [EDELWEISS Collaboration] (2010) First results of the EDELWEISS-II WIMP search using Ge cryogenic detectors with interleaved electrodes. *Phys Lett B* 687(4–5):294–298. doi:[10.1016/j.physletb.2010.03.057](https://doi.org/10.1016/j.physletb.2010.03.057). arXiv:[0912.0805](https://arxiv.org/abs/0912.0805) [astro-ph.CO]

76. Armengaud E et al [EDELWEISS Collaboration] (2011) Final results of the EDELWEISS-II WIMP search using a 4-kg array of cryogenic germanium detectors with interleaved electrodes. *Phys Lett B* 702(5):329–335. doi:[10.1016/j.physletb.2011.07.034](https://doi.org/10.1016/j.physletb.2011.07.034). arXiv:[1103.4070](https://arxiv.org/abs/1103.4070) [astro-ph.CO]
77. Armengaud E et al [EDELWEISS Collaboration] (2012) Search for low-mass WIMPs with EDELWEISS-II heat-and-ionization detectors. *Phys Rev D* 86(5):051701(R). doi:[10.1103/PhysRevD.86.051701](https://doi.org/10.1103/PhysRevD.86.051701). . arXiv:[1207.1815](https://arxiv.org/abs/1207.1815) [astroph.CO]
78. Armengaud E et al [EDELWEISS Collaboration] (2013) Background studies for the EDELWEISS dark matter experiment. *Astropart Phys* 47:1–9. doi:[10.1016/j.astropartphys.2013.05.004](https://doi.org/10.1016/j.astropartphys.2013.05.004). arXiv:[1305.3628](https://arxiv.org/abs/1305.3628) [physics.insdet]
79. Armengaud E et al [EDELWEISS Collaboration] (2013) Axion searches with the EDELWEISS-II experiment. *J Cosmol Astropart Phys* 2013(11):067. doi:[10.1088/1475-7516/2013/11/067](https://doi.org/10.1088/1475-7516/2013/11/067). arXiv:[1307.1488](https://arxiv.org/abs/1307.1488) [astro-ph.CO]
80. Arnaud Q [For the EDELWEISS collaboration] (2014) The EDELWEISS experiment status. In: Augè E, Dumarchez J, Trân Thanh Vân J (eds) *Proceedings of the 49th RENCONTRES DE MORIOND. Cosmology*, (La Thuile, Aosta Valley, Italy, 22–29 March 2014. ARISF. pp 175–178. http://moriond.in2p3.fr/Proceedings/2014/Moriond_Cosmo_2014.pdf
81. Arnold R et al (2005) Technical design and performance of the NEMO 3 detector. *Nucl Instrum Methods Phys Res Sect A* 536(1–2):79–122. doi:[10.1016/j.nima.2004.07.194](https://doi.org/10.1016/j.nima.2004.07.194)
82. ATLAS, CMS, and LHCb Collaborations (2012) Search for the rare decays $B_{(s)}^0 \rightarrow \mu^+ \mu^-$ at the LHC with the ATLAS, CMS and LHCb experiments. Scientific report LHCb-CONF-2012-017, CMS-PAS-BPH-12-009, ATLAS-CONF-2012-061. European Organization for Nuclear Research. <http://cds.cern.ch/record/1452186/files/LHCb-CONF-2012-017.pdf>
83. ATLAS Collaboration (2012) Search for squarks and gluinos with the ATLAS detector using final states with jets and missing transverse momentum and 5.8 fb⁻¹ of $\sqrt{s} = 8$ TeV proton-proton collision data. Presented at the 20th international conference on supersymmetry and unification of fundamental interactions (SUSY2012), Beijing, China, 13–18 Aug 2012. Peking University. <http://cds.cern.ch/record/1472710>. ATLAS-CONF-2012-109
84. Badertscher A et al [ArDM Collaboration] (2013) Status of the ArDM experiment: first results from gaseous argon operation in deep underground environment. arXiv:[1307.0117](https://arxiv.org/abs/1307.0117) [physics.ins-det]
85. Baer H, Barger V, Mustafayev A (2012) Implications of a 125 GeV higgs scalar for the LHC supersymmetry and neutralino dark matter searches. *Phys Rev D* 85(7):075010. doi:[10.1103/PhysRevD.85.075010](https://doi.org/10.1103/PhysRevD.85.075010). arXiv:[1112.3017](https://arxiv.org/abs/1112.3017)[hep-ph]
86. Bahcall JN, Tremaine S (1981) Methods for determining the masses of spherical systems: I - test particles around a point mass. *Astrophys J* 244(1981):805–819. doi:[10.1086/158756](https://doi.org/10.1086/158756). ADS: 1981ApJ...244..805B
87. Barbeau P, Collar J, Whaley P (2007) Design and characterization of a neutron calibration facility for the study of sub-keV nuclear recoils. *Nucl Instrum Methods Phys Res Sect A* 574(2):385–391. doi:[10.1016/j.nima.2007.01.169](https://doi.org/10.1016/j.nima.2007.01.169)
88. Baudis L (2012) Direct dark matter detection: the next decade. In next decade in dark matter and dark energy, special issue. *Phys Dark Universe* 1(1–2):94–108. doi:[10.1016/j.dark.2012.10.006](https://doi.org/10.1016/j.dark.2012.10.006). arXiv:[1211.7222](https://arxiv.org/abs/1211.7222)
89. L. Baudis [DARWIN Consortium] (2012) DARWIN: dark matter WIMP search with noble liquids. *J Phys Conf Ser* 375:012028. doi:[10.1088/1742-6596/375/1/012028](https://doi.org/10.1088/1742-6596/375/1/012028). arXiv:[1201.2402](https://arxiv.org/abs/1201.2402) [astro-ph.IM]
90. Behnke E et al [COUPP Collaboration] (2011) Improved limits on spin-dependent wimp-proton interactions from a two liter CF3I bubble chamber. *Phys Rev Lett* 106(2):021303. doi:[10.1103/PhysRevLett.106.021303](https://doi.org/10.1103/PhysRevLett.106.021303)
91. Behnke E et al (2012) [COUPP Collaboration] First dark matter search results from a 4-kg CF3I bubble chamber operated in a deep underground site. *Phys Rev D* 86(5):052001. doi:[10.1103/PhysRevD.86.052001](https://doi.org/10.1103/PhysRevD.86.052001)
92. Bekenstein J, Milgrom M (1984A) Does the missing mass problem signal the breakdown of Newtonian gravity? *Astrophys J* 286(1984):7–14. doi:[10.1086/162570](https://doi.org/10.1086/162570). ADS: 1984ApJ...286....7B

93. Bekenstein JD (2004) Relativistic gravitation theory for the MOND paradigm. *Phys Rev D* 70(8):083509. doi:[10.1103/PhysRevD.70.083509](https://doi.org/10.1103/PhysRevD.70.083509). arXiv:[astro-ph/0403694](https://arxiv.org/abs/astro-ph/0403694). As cited in Refs. [95, 156]
94. Bekenstein JD (2006) The modified Newtonian dynamics-MOND and its implications for new physics. *Contemp Phys* 47(6):387–403. doi:[10.1080/00107510701244055](https://doi.org/10.1080/00107510701244055)
95. Bekenstein JD (2009) Relativistic MOND as an alternative to the dark matter paradigm. *Nucl Phys A* 827(1–4):555c–560c. doi:[10.1016/j.nuclphysa.2009.05.122](https://doi.org/10.1016/j.nuclphysa.2009.05.122). arXiv:[0901.1524](https://arxiv.org/abs/0901.1524) [astro-ph]
96. de Bellefon A et al (1996) Dark matter search in the Frejus Underground Laboratory EDELWEISS experiment. *Nucl Instrum Methods Phys Res Sect A* 370(1):230–232. doi:[10.1016/0168-9002\(95\)01093-9](https://doi.org/10.1016/0168-9002(95)01093-9)
97. Belli P et al (2002) Effect of the galactic halo modeling on the DAMA-NaI annual modulation result: an extended analysis of the data for weakly interacting massive particles with a purely spin-independent coupling. *Phys Rev D* 66(4):043503. doi:[10.1103/PhysRevD.66.043503](https://doi.org/10.1103/PhysRevD.66.043503)
98. Belli P et al (2011) Observations of annual modulation in direct detection of relic particles and light neutralinos. *Phys Rev D* 84(5):055014. doi:[10.1103/PhysRevD.84.055014](https://doi.org/10.1103/PhysRevD.84.055014). arXiv:[1106.4667](https://arxiv.org/abs/1106.4667) [hep-ph]
99. Belokurov V et al (2007) Cats and dogs, hair and a hero: a quintet of new milky way companions. *Astrophys J* 654(2):897–906. doi:[10.1086/509718](https://doi.org/10.1086/509718). arXiv:[astro-ph/0608448v1](https://arxiv.org/abs/astro-ph/0608448v1)
100. Beltrame P [On behalf of the XENON Collaboration] (2013) Direct dark matter search with the XENON program. arXiv:[1305.2719](https://arxiv.org/abs/1305.2719) [astro-ph.CO]
101. Benetti P et al [WARP Collaboration] (2008) First results from a dark matter search with liquid argon at 87 K in the Gran Sasso underground laboratory. *Astropart Phys* 28(6):495–507. doi:[10.1016/j.astropartphys.2007.08.002](https://doi.org/10.1016/j.astropartphys.2007.08.002). arXiv:[astro-ph/0701286](https://arxiv.org/abs/astro-ph/0701286)
102. Bennett GW et al [Muon (g-2) Collaboration] (2006) Final report of the E821 muon anomalous magnetic moment measurement at BNL. *Phys Rev D* 73(7):072003. doi:[10.1103/PhysRevD.73.072003](https://doi.org/10.1103/PhysRevD.73.072003). arXiv:[hep-ex/0602035](https://arxiv.org/abs/hep-ex/0602035). As cited in Ref. [137]
103. Benoit A et al (2000) Event categories in the EDELWEISS WIMP search experiment. *Phys Lett B* 479(1–3):8–14. doi:[10.1016/S0370-2693\(00\)00264-1](https://doi.org/10.1016/S0370-2693(00)00264-1)
104. Benoit A et al [EDELWEISS Collaboration] (2005) Sensitivity of the EDELWEISS WIMP search to spin-dependent interactions. *Phys Lett B* 616(1–2):25–30. doi:[10.1016/j.physletb.2005.04.052](https://doi.org/10.1016/j.physletb.2005.04.052)
105. Benoit A et al [EDELWEISS Collaboration] (2007) Measurement of the response of heat-and-ionization germanium detectors to nuclear recoils. *Nucl Instrum Methods Phys Res, Sect A* 577(3):558–568. doi:[10.1016/j.nima.2007.04.118](https://doi.org/10.1016/j.nima.2007.04.118)
106. Berger C et al [Fréjus Collaboration] (1989) Experimental study of muon bundles observed in the Fréjus detector. *Phys Rev D* 40(7):2163–2171. doi:[10.1103/PhysRevD.40.2163](https://doi.org/10.1103/PhysRevD.40.2163)
107. Bergström L, Edsjo J, Ullio P (1998) Possible indications of a clumpy dark matter halo. *Phys Rev D* 58(8):083507. doi:[10.1103/PhysRevD.58.083507](https://doi.org/10.1103/PhysRevD.58.083507) arXiv:[astro-ph/9804050](https://arxiv.org/abs/astro-ph/9804050)
108. Bergström L et al (2013) New limits on dark matter annihilation from alpha magnetic spectrometer cosmic ray positron data. *Phys Rev Lett* 111(17):171101. doi:[10.1103/PhysRevLett.111.171101](https://doi.org/10.1103/PhysRevLett.111.171101)
109. Bernabei R (2012) Dark matter particles in the galactic halo: DAMA/LIBRA results and perspectives. *Ann Phys* 524(9–10):497–506. doi:[10.1002/andp.201200094](https://doi.org/10.1002/andp.201200094)
110. Bernabei R et al (1998) Searching for WIMPs by the annual modulation signature. *Phys Lett B* 424(1–2):195–201. doi:[10.1016/S0370-2693\(98\)00172-5](https://doi.org/10.1016/S0370-2693(98)00172-5)
111. Bernabei R et al (2003) Dark Matter search. *Rivista Nuovo Cim* 26(1):1–74. arXiv:[astro-ph/0307403](https://arxiv.org/abs/astro-ph/0307403). As cited in Ref. [114]
112. Bernabei R et al (2004) Dark matter particles in the galactic halo: Results and implications from DAMA/NaI. *Int J Mod Phys D* 13(10):2127–2159. doi:[10.1142/S0218271804006619](https://doi.org/10.1142/S0218271804006619) arXiv:[astro-ph/0501412](https://arxiv.org/abs/astro-ph/0501412)
113. Bernabei R et al (2008) Possible implications of the channeling effect in NaI(Tl) crystals. *Eur Phys J C* 53(2):205–213. doi:[10.1140/epjc/s10052-007-0479-0](https://doi.org/10.1140/epjc/s10052-007-0479-0)

114. Bernabei R et al (2008) First results from DAMA/LIBRA and the combined results with DAMA/NaI. *Eur Phys J C* 56(3):333–355. doi:[10.1140/epjc/s10052-008-0662-y](https://doi.org/10.1140/epjc/s10052-008-0662-y)
115. Bernabei R et al (2008) Investigating electron interacting dark matter. *Phys Rev D* 77(2):023506. doi:[10.1103/PhysRevD.77.023506](https://doi.org/10.1103/PhysRevD.77.023506)
116. Bernabei R et al (2010) New results from DAMA/LIBRA. *Eur Phys J C* 67(1–2):39–49. doi:[10.1140/epjc/s10052-010-1303-9](https://doi.org/10.1140/epjc/s10052-010-1303-9)
117. Bernabei R et al (2012) No role for muons in the DAMA annual modulation results. *Eur Phys J C* 72(7):2064. doi:[10.1140/epjc/s10052-012-2064-4](https://doi.org/10.1140/epjc/s10052-012-2064-4)
118. Bernabei R et al (2013) DAMA/LIBRA results and perspectives of the second stage. *Nucl Phys At Energ* 14(2):113–120. http://jnpae.kinr.kiev.ua/14.2/Articles_PDF/jnpae-2013-14-0113-Bernabei.pdf
119. Bernabei R et al (2013) Dark matter investigation by DAMA at Gran Sasso. *Int J Mod Phys A* 28(16):1330022. doi:[10.1142/S0217751X13300226](https://doi.org/10.1142/S0217751X13300226). arXiv:[1306.1411](https://arxiv.org/abs/1306.1411) [astro-ph.GA]
120. Bertone G (ed) (2010) Particle dark matter: observations models and searches. Cambridge University Press, Cambridge
121. Bertone G, Hooper D, Silk J (2005) Particle dark matter: evidence, candidates and constraints. *Phys Rep* 405(5–6):279–390. doi:[10.1016/j.physrep.2004.08.031](https://doi.org/10.1016/j.physrep.2004.08.031)
122. Bettini A (2011) Underground laboratories. *Nucl Instrum Methods Phys Res Sect A* 626–627(Supplement):S64–S68. doi:[10.1016/j.nima.2010.05.017](https://doi.org/10.1016/j.nima.2010.05.017)
123. Billard J, Strigari L, Figueroa-Feliciano E (2013) Implication of neutrino backgrounds on the reach of next generation dark matter direct detection experiments. arXiv:[1307.5458](https://arxiv.org/abs/1307.5458) [hep-ph]
124. Blumenthal GR et al (1984) Formation of galaxies and large-scale structure with cold dark matter. *Nature* 311:517–525. doi:[10.1038/311517a0](https://doi.org/10.1038/311517a0)
125. de Boer W et al (2005) EGRET excess of diffuse galactic gamma rays as tracer of dark matter. *Astron Astrophys* 444(1):51–67. doi:[10.1051/0004-6361:20053726](https://doi.org/10.1051/0004-6361:20053726). arXiv:[astro-ph/0508617](https://arxiv.org/abs/astro-ph/0508617). As cited in Ref. [264]
126. Bonicalzi R et al (2013) The C-4 dark matter experiment. *Nucl Instrum Methods Phys Res Sect A* 712:27–33. doi:[10.1016/j.nima.2013.02.012](https://doi.org/10.1016/j.nima.2013.02.012)
127. Bottino A, Fornengo N, Scopel S (2012) Phenomenology of light neutralinos in view of recent results at the CERN Large Hadron Collider. *Phys Rev D* 85(9):095013. doi:[10.1103/PhysRevD.85.095013](https://doi.org/10.1103/PhysRevD.85.095013)
128. Boukhira N et al (2000) Suitability of superheated droplet detectors for dark matter search. *Astropart Phys* 14(3):227–237. doi:[10.1016/S0927-6505\(00\)00123-7](https://doi.org/10.1016/S0927-6505(00)00123-7)
129. Boulay MG [For the DEAP Collaboration] (2012) DEAP-3600 dark matter search at SNO-LAB. *J Phys Conf Ser* 375(1):012027. doi:[10.1088/1742-6596/375/1/012027](https://doi.org/10.1088/1742-6596/375/1/012027)
130. Bradač M et al (2008) Revealing the properties of dark matter in the merging cluster MACS j0025.4–1222. *Astrophys J* 687(2):959–967. doi:[10.1086/591246](https://doi.org/10.1086/591246)
131. Brink P et al (2006) First test runs of a dark-matter detector with interleaved ionization electrodes and phonon sensors for surface-event rejection. In proceedings of the 11th international workshop on low temperature detectors (LTD-11), special issue. *Nucl Instrum Methods Phys Res, Sect A* 559(2):414–416. doi:[10.1016/j.nima.2005.12.026](https://doi.org/10.1016/j.nima.2005.12.026)
132. Broniatowski A (2004) A simulation code for the ionization and heat signals in low temperature germanium detectors for Dark Matter research. In proceedings of the 10th international workshop on low temperature detectors, special issue. *Nucl Instrum Methods Phys Res Sect A* 520(1–3):178–181. doi:[10.1016/j.nima.2003.11.287](https://doi.org/10.1016/j.nima.2003.11.287)
133. Broniatowski A et al [EDELWEISS Collaboration] (2008) Cryogenic Ge detectors with interleaved electrodes: Design and modeling. *J Low Temp Phys* 151(3):830–834. doi:[10.1007/s10909-008-9754-1](https://doi.org/10.1007/s10909-008-9754-1)
134. Broniatowski A et al [EDELWEISS Collaboration] (2009) A new high-background-rejection dark matter Ge cryogenic detector. *Phys Lett B* 681(4):305–309. doi:[10.1016/j.physletb.2009.10.036](https://doi.org/10.1016/j.physletb.2009.10.036). arXiv:[0905.0753](https://arxiv.org/abs/0905.0753) [astro-ph.IM]
135. Brown A et al (2012) Extending the CRESST-II commissioning run limits to lower masses. *Phys Rev D* 85(2):021301. doi:[10.1103/PhysRevD.85.021301](https://doi.org/10.1103/PhysRevD.85.021301). arXiv:[1109.2589](https://arxiv.org/abs/1109.2589) [astro-ph.CO]

136. Brown E (2013) Searching for dark matter with XENON100 and XENON1T. In: Presented at the 13th international conference on topics in astroparticle and underground physics (TAUP2013), Asilomar, CA, US, 8–13 Sept 2013. <https://conferences.lbl.gov/event/36/session/11/contribution/86/material/slides/>
137. Buchmueller O et al (2012) The CMSSM and NUHM1 in light of 7 TeV LHC, $B_s \rightarrow \mu^+ \mu^-$ and XENON100 data. *Eur Phys J C* 72(11):2243. doi:[10.1140/epjc/s10052-012-2243-3](https://doi.org/10.1140/epjc/s10052-012-2243-3)
138. Cao J et al (2012) A SM-like Higgs near 125 GeV in low energy SUSY: a comparative study for MSSM and NMSSM. *J High Energy Phys* 2012(3):1–22. doi:[10.1007/JHEP03\(2012\)086](https://doi.org/10.1007/JHEP03(2012)086)
139. J. Cao et al (2013) A light SUSY dark matter after CDMS-II, LUX and LHC Higgs data. arXiv:[1311.0678](https://arxiv.org/abs/1311.0678) [hep-ph]
140. Carlberg R et al (1996A) Galaxy cluster virial masses and Ω . *Astrophys J* 462(1):32–49. doi:[10.1086/177125](https://doi.org/10.1086/177125). ADS: 1996ApJ...462...32C
141. Carr B (1994) Baryonic dark matter. *Ann Rev Astron Astrophys* 32(1):531–590. doi:[10.1146/annurev.aa.32.090194.002531](https://doi.org/10.1146/annurev.aa.32.090194.002531)
142. Cebrián S et al (2001) First results of the ROSEBUD dark matter experiment. *Astropart Phys* 15(1):79–85. doi:[10.1016/S0927-6505\(00\)00138-9](https://doi.org/10.1016/S0927-6505(00)00138-9). arXiv:[astro-ph/0004292](https://arxiv.org/abs/astro-ph/0004292)
143. Censier B [For the EDELWEISS Collaboration] (2006) Final results of the EDELWEISSI dark matter search with cryogenic heat-and-ionization Ge detectors. In: Proceedings of the 11th international workshop on low temperature detectors—LTD-11, special issue. *Nucl Instrum Methods Phys Res Sect A* 559(2):381–383. doi:[10.1016/j.nima.2005.12.171](https://doi.org/10.1016/j.nima.2005.12.171)
144. Censier B [For the EDELWEISS Collaboration] (2006) Erratum to: final results of the EDELWEISS-I dark matter search with cryogenic heat-and-ionization Ge detectors : [Nucl Instrum Methods A 559:381]. *Nucl Instrum Methods Phys Res Sect A* 564(1):614–614. doi:[10.1016/j.nima.2006.04.027](https://doi.org/10.1016/j.nima.2006.04.027)
145. Chang J et al (2008) An excess of cosmic ray electrons at energies of 300–800 GeV. *Nature* 456(7220):362–365. doi:[10.1038/nature07477](https://doi.org/10.1038/nature07477). As cited in Refs. [13,264]
146. Chatrchyan S et al [CMS Collaboration] (2011) Search for supersymmetry at the LHC in events with jets and missing transverse energy. *Phys Rev Lett* 107(22):221804. doi:[10.1103/PhysRevLett.107.221804](https://doi.org/10.1103/PhysRevLett.107.221804). arXiv:[1109.2352](https://arxiv.org/abs/1109.2352) [hep-ex]
147. Chatrchyan S et al [CMS Collaboration] (2012) Observation of a new boson at a mass of 125 GeV with the CMS experiment at the LHC. *Phys Lett B* 716(1):30–61. doi:[10.1016/j.physletb.2012.08.021](https://doi.org/10.1016/j.physletb.2012.08.021). arXiv:[1207.7235](https://arxiv.org/abs/1207.7235) [hep-ex]
148. Chatrchyan S et al [CMS Collaboration] (2013) Search for supersymmetry in events with opposite-sign dileptons and missing transverse energy using an artificial neural network. *Phys Rev D* 87(7):072001. doi:[10.1103/PhysRevD.87.072001](https://doi.org/10.1103/PhysRevD.87.072001). arXiv:[1301.0916](https://arxiv.org/abs/1301.0916) [hep-ex]
149. Chatrchyan S et al [CMS Collaboration] (2013) Search for supersymmetry in events with photons and low missing transverse energy in pp collisions at. *Phys Lett B* 719(1–3):42–61. doi:[10.1016/j.physletb.2012.12.055](https://doi.org/10.1016/j.physletb.2012.12.055). arXiv:[1210.2052](https://arxiv.org/abs/1210.2052) [hep-ex]
150. Chen D-M (2008) Strong lensing probability in TeVeS (tensor-vector-scalar) theory. *J Cosmol Astropart Phys* 2008(1):006. doi:[10.1088/1475-7516/2008/01/006](https://doi.org/10.1088/1475-7516/2008/01/006). As cited in Ref. [95]
151. Chepel V, Araújo H (2013) Liquid noble gas detectors for low energy particle physics. *J Instrum* 8(04):R04001. doi:[10.1088/1748-0221/8/04/R04001](https://doi.org/10.1088/1748-0221/8/04/R04001). arXiv:[1207.2292](https://arxiv.org/abs/1207.2292) [physics.ins-det]
152. Cherwinka J et al (2012) A search for the dark matter annual modulation in South Pole ice. *Astropart Phys* 35(11):749–754. doi:[10.1016/j.astropartphys.2012.03.003](https://doi.org/10.1016/j.astropartphys.2012.03.003). arXiv:[1106.1156](https://arxiv.org/abs/1106.1156) [astro-ph.HE]
153. Chiu H-Y (1966) Symmetry between particle and anti-particle populations in the universe. *Phys Rev Lett* 17:712–714. doi:[10.1103/PhysRevLett.17.712](https://doi.org/10.1103/PhysRevLett.17.712). As cited in Refs. [173, 206]
154. Chiu MC, Tian Y, Ko CM (2008) Necessity of dark matter in modified Newtonian dynamics within galactic scales?—Testing the covariant MOND in elliptical lenses. In: Zhang SN, Li Y, Yu QJ (eds) APRIM 2008: Proceedings of the 10th Asian-Pacific Regional IAU Meeting, Kunming, China, 3–6 Aug 2008. National Observatories of China Press, Beijing, pp 1–2. arXiv:[0812.5011](https://arxiv.org/abs/0812.5011) [astro-ph]. As cited in Ref. [95]

155. Cirelli M et al (2009) Model-independent implications of the cosmic ray spectra on properties of dark matter. *Nucl Phys B* 813(1–2):1–21. doi:[10.1016/j.nuclphysb.2008.11.031](https://doi.org/10.1016/j.nuclphysb.2008.11.031). As cited in Ref. [30]
156. Clowe D et al (2006) A direct empirical proof of the existence of dark matter. *Astrophys J Lett* 648(2):L109–L113. doi:[10.1086/508162](https://doi.org/10.1086/508162)
157. Collar JI (2010) Light WIMP searches: the effect of the uncertainty in recoil energy scale and quenching factor. arXiv:[1010.5187](https://arxiv.org/abs/1010.5187) [astro-ph.IM]
158. Coron N et al (2011) 2010 update on the ROSEBUD project. In: Identification of dark matter 2010. 8th international workshop on the identification of dark matter (IDM 2010). Proceedings of Science IDM2010, Montpellier, France, 26–30 July 2010. SISSA, Trieste. p 054. http://pos.sissa.it/archive/conferences/110/054/IDM2010_054.pdf
159. Crisler MB (2013) PICO 250-liter bubble chamber dark matter experiment. Presented at the SNOLAB future projects workshop, 21 Aug 2013. http://www.snolab.ca/sites/default/files/Crisler_PICO.pdf
160. Daw E et al (2012) Spin-dependent limits from the DRIFT-IIId directional dark matter detector. *Astropart Phys* 35(7):397–401. doi:[10.1016/j.astropartphys.2011.11.003](https://doi.org/10.1016/j.astropartphys.2011.11.003)
161. Defay X (2008) Recherche de matière noire au sein de l'expérience EDELWEISS avec des bolomètres germanium à double composante Ionisation/Chaleur, rejet des événements de surface avec la voie ionisation' [in French]. PhD dissertation, Université Montpellier II, Sciences et Techniques du Languedoc. <http://tel.archives-ouvertes.fr/tel-00369460/fr/>. As cited in Ref. [133]
162. Defay X et al [EDELWEISS Collaboration] (2008) Cryogenic Ge detectors for dark matter search: surface event rejection with ionization signals. *J Low Temp Phys* 151(3–4):896–901. doi:[10.1007/s10909-008-9762-1](https://doi.org/10.1007/s10909-008-9762-1)
163. Delahaye T et al (2010) Galactic electrons and positrons at the Earth: new estimate of the primary and secondary fluxes. *Astron Astrophys* 524:A51. doi:[10.1051/0004-6361/201014225](https://doi.org/10.1051/0004-6361/201014225). As cited in Ref. [30]
164. Dietrich JP et al (2012) A filament of dark matter between two clusters of galaxies. *Nature* 487:202–204. doi:[10.1038/nature11224](https://doi.org/10.1038/nature11224)
165. DM-Ice homepage. <http://dm-ice.physics.wisc.edu/>
166. D'Onghia E et al (2010) Substructure depletion in the Milky Way halo by the disk. *Astrophys J* 709(2):1138–1147. <http://stacks.iop.org/0004-637X/709/i=2/a=1138>
167. Einasto J, Kaasik A, Saar E (1974) Dynamic evidence on massive coronas of galaxies. *Nature* 250:309–310. doi:[10.1038/250309a0](https://doi.org/10.1038/250309a0)
168. K. Eitel. Private communication, November 2013
169. Fairbairn M, Douce T, Swift J (2013) Quantifying astrophysical uncertainties on dark matter direct detection results. *Astropart Phys* 47:45–53. doi:[10.1016/j.astropartphys.2013.06.003](https://doi.org/10.1016/j.astropartphys.2013.06.003)
170. Feix M, Fedeli C, Bartelmann M (2008) Asymmetric gravitational lenses in TeVeS and application to the bullet cluster. *Astron Astrophys* 480(2):313–325. doi:[10.1051/0004-6361:20078224](https://doi.org/10.1051/0004-6361:20078224). As cited in Ref. [95]
171. Felizardo M et al [SIMPLE Collaboration] (2010) First results of the phase II SIMPLE dark matter search. *Phys Rev Lett* 105(21):211301. doi:[10.1103/PhysRevLett.105.211301](https://doi.org/10.1103/PhysRevLett.105.211301)
172. Felizardo M et al [SIMPLE Collaboration] (2012) Final analysis and results of the phase II SIMPLE dark matter search. *Phys Rev Lett* 108(20):201302. doi:[10.1103/PhysRevLett.108.201302](https://doi.org/10.1103/PhysRevLett.108.201302). arXiv:[1106.3014](https://arxiv.org/abs/1106.3014) [astro-ph.CO]
173. Feng JL (2010) Dark matter candidates from particle physics and methods of detection. *Ann Rev Astron Astrophys* 48(1):495–545. doi:[10.1146/annurev-astro-082708-101659](https://doi.org/10.1146/annurev-astro-082708-101659)
174. Feng JL, Grivaz J-F, Nachtman J (2010) Searches for supersymmetry at highenergy colliders. *Rev Mod Phys* 82(1):699–727. doi:[10.1103/RevModPhys.82.699](https://doi.org/10.1103/RevModPhys.82.699)
175. Ferrari N [WARP Collaboration] (2006) WARP: a double phase argon programme for dark matter detection. *J Phys Conf Ser* 39(1):111. doi:[10.1088/1742-6596/39/1/022](https://doi.org/10.1088/1742-6596/39/1/022)
176. Ferreras I, Sakellariadou M, Yusaf M (2008) Necessity of dark matter in modified newtonian dynamics within galactic scales. *Phys Rev Lett* 100(3):031302. doi:[10.1103/PhysRevLett.100.031302](https://doi.org/10.1103/PhysRevLett.100.031302)

177. Ferreras I, Saha P, Burles S (2008) Unveiling dark haloes in lensing galaxies. *Mon Not R Astron Soc* 383(3):857–863. doi:[10.1111/j.1365-2966.2007.12606.x](https://doi.org/10.1111/j.1365-2966.2007.12606.x). arXiv:[0710.3159](https://arxiv.org/abs/0710.3159)
178. Ferreras I et al (2012) Confronting MOND and TeVeS with strong gravitational lensing over galactic scales: an extended survey. *Phys Rev D* 86(8):083507. doi:[10.1103/PhysRevD.86.083507](https://doi.org/10.1103/PhysRevD.86.083507). arXiv:[1205.4880](https://arxiv.org/abs/1205.4880) [astro-ph.CO]
179. Figueroa-Feliciano E (2011) Direct detection searches for WIMP dark matter. *Prog Part Nucl Phys* 66(3):661–673. doi:[10.1016/j.pnpnp.2011.01.003](https://doi.org/10.1016/j.pnpnp.2011.01.003)
180. Fiorucci S et al [EDELWEISS Collaboration] (2007) Identification of backgrounds in the EDELWEISS-I dark matter search experiment. *Astropart Phys* 28(1):143–153. doi:[10.1016/j.astropartphys.2007.05.003](https://doi.org/10.1016/j.astropartphys.2007.05.003)
181. Formaggio JA, Martoff CJ (2004) Backgrounds to sensitive experiments underground. *Annu Rev Nucl Part Sci* 54:361–412. doi:[10.1146/annurev.nucl.54.070103.181248](https://doi.org/10.1146/annurev.nucl.54.070103.181248)
182. Fowlie A et al [BayesFITS Group] (2012) Constrained MSSM favoring new territories: the impact of new LHC limits and a 125 GeV Higgs boson. *Phys Rev D* 86(7):075010. doi:[10.1103/PhysRevD.86.075010](https://doi.org/10.1103/PhysRevD.86.075010). arXiv:[1206.0264](https://arxiv.org/abs/1206.0264) [hep-ph]
183. Frandsen MT et al (2013) The unbearable lightness of being: CDMS versus XENON. *J Cosmol Astropart Phys* 2013(7):023. doi:[10.1088/1475-7516/2013/07/023](https://doi.org/10.1088/1475-7516/2013/07/023). arXiv:[1304.6066](https://arxiv.org/abs/1304.6066) [hep-ph]
184. Freeman KC (1970) On the disks of spiral and S0 galaxies. *Astrophys J* 160(1970):811–830. doi:[10.1086/150474](https://doi.org/10.1086/150474). ADS:1970ApJ...160..811F
185. Freeman KC (1970) Erratum: on the disks of spiral and S0 galaxies. *Astrophys J* 161(1970):802. doi:[10.1086/150583](https://doi.org/10.1086/150583). ADS:1970ApJ...161..802F
186. Gaitskell RJ (2004) Direct detection of dark matter. *Annu Rev Nucl Part Sci* 54(1):315–359. doi:[10.1146/annurev.nucl.54.070103.181244](https://doi.org/10.1146/annurev.nucl.54.070103.181244)
187. Gavazzi R et al (2007) The Sloan lens ACS survey: IV. The mass density profile of early-type galaxies out to 100 effective radii. *Astrophys J* 667(1):176. doi:[10.1086/519237](https://doi.org/10.1086/519237). ADS:2007ApJ...667..176G
188. GeHa M (2010) Galaxy formation: gone with the wind? *Nature* 463(7278):167–168. doi:[10.1038/463167a](https://doi.org/10.1038/463167a)
189. Gerbier G, Gascon J (2010) Cryogenic detectors. In: Bertone G (ed) *Particle dark matter: observations, models and searches*. Cambridge University Press, Cambridge (Chap. 20)
190. Giovanetti GK et al (2012) Dark matter sensitivities of the Majorana Demonstrator. *J Phys Conf Ser* 375(1):012014. doi:[10.1088/1742-6596/375/1/012014](https://doi.org/10.1088/1742-6596/375/1/012014)
191. Girard TA et al (2012) Prospects for a phase III SIMPLE measurement. *J Phys Conf Ser* 375(1):012017. doi:[10.1088/1742-6596/375/1/012017](https://doi.org/10.1088/1742-6596/375/1/012017)
192. Giuliani F [DEAP/CLEAN collaboration] (2010) Hunting the dark matter with DEAP/CLEAN. In: Alverson G, Nath P, Nelson B (eds) *SUSY09. 7th international conference on supersymmetry and the unification of fundamental interactions*. AIP conference proceedings, vol 1200, Boston, MA, USA, 5–10 June 2008. AIP Publishing, Melville, pp 985–988. doi:[10.1063/1.3327779](https://doi.org/10.1063/1.3327779)
193. Gonzalez AH, Zaritsky D, Zabludoff AI (2007) A census of baryons in galaxy clusters and groups. *Astrophys J* 666(1):147–155. doi:[10.1086/519729](https://doi.org/10.1086/519729). arXiv:[0705.1726](https://arxiv.org/abs/0705.1726) [astro-ph]
194. Governato F et al (2010) Bulgeless dwarf galaxies and dark matter cores from supernova-driven outflows. *Nature* 463(7278):203–206. doi:[10.1038/nature08640](https://doi.org/10.1038/nature08640)
195. Grignon C et al (2009) A prototype of a directional detector for non-baryonic dark matter search: MIMAC (Micro-TPC Matrix of Chambers). *J Instrum* 4(11):P11003. arXiv:[0909.0654](https://arxiv.org/abs/0909.0654)[astro-ph.IM]
196. Guedes J et al (2011) Forming realistic late-type spirals in a Λ CDM Universe: the eris simulation. *Astrophys J* 742(2):76. doi:[10.1088/0004-637X/742/2/76](https://doi.org/10.1088/0004-637X/742/2/76). arXiv:[1103.6030](https://arxiv.org/abs/1103.6030) [astro-ph.CO]
197. Gustafsson M [For the Fermi-LAT Collaboration] (2013) Fermi-LAT and the gamma-ray line search. arXiv:[1310.2953](https://arxiv.org/abs/1310.2953) [astro-ph.HE]
198. Harvard-Smithsonian Center for Astrophysics (2006) 1E 0657–56: NASA Finds Direct Proof of Dark Matter. <http://chandra.harvard.edu/photo/2006/1e0657/index.html>

199. Helm RH (1956) Inelastic and elastic scattering of 187-MeV electrons from selected even-even nuclei. *Phys Rev (2nd ser)* 104(5):1466–1475. doi:[10.1103/PhysRev.104.1466](https://doi.org/10.1103/PhysRev.104.1466). As cited in Ref. [42]
200. Hime A (2012) CLEAN detection of dark matter. Presented at the 9th international conference: identification of dark matter, IDM2012, Chicago, IL, USA, July 23–27, 2012. <http://kicp-workshops.uchicago.edu/IDM2012/depot/plenary-talk-hime-andrew.pdf>
201. Hoekstra H, Jain B (2008) Weak gravitational lensing and its cosmological applications. *Annu Rev Nucl Part Sci* 58(1):99–123. doi:[10.1146/annurev.nucl.58.110707.171151](https://doi.org/10.1146/annurev.nucl.58.110707.171151)
202. Horn OM (2007) Simulations of the muon-induced neutron background of the EDELWEISS-II experiment for dark matter search. Scientific report FZKA 7391. Forschungszentrum Karlsruhe. <http://bibliothek.fzk.de/zb/berichte/FZKA7391.pdf>. Orig. pub. as PhD dissertation, Universität Karlsruhe (TH), 2007. <http://digbib.ubka.uni-karlsruhe.de/volltexte/1000007402>
203. Hu W, Dodelson S (2002) Cosmic microwave background anisotropies. *Annu Rev Astron Astrophys* 40(1):171–216. doi:[10.1146/annurev.astro.40.060401.093926](https://doi.org/10.1146/annurev.astro.40.060401.093926)
204. Identification of Dark Matter 2010 (2011) 8th international workshop on the identification of dark matter, IDM 2010, Montpellier, France, July 26–30, 2010. Proceedings of science IDM2010. SISSA, Trieste. <http://pos.sissa.it/cgi-bin/reader/conf.cgi?confid=110>
205. Jee MJ et al (2007) Discovery of a ringlike dark matter structure in the core of the galaxy cluster Cl 0024+17. *Astrophys J* 661(2):728–749. doi:[10.1086/517498](https://doi.org/10.1086/517498). arXiv:[0705.2171](https://arxiv.org/abs/0705.2171) [astro-ph]
206. Jungman G, Kamionkowski M, Griest K (1996) Supersymmetric dark matter. *Phys Rep* 267(5–6):195–373. doi:[10.1016/0370-1573\(95\)00058-5](https://doi.org/10.1016/0370-1573(95)00058-5)
207. Kamionkowski M, Kinkhabwala A (1998) Galactic halo models and particle dark matter detection. *Phys Rev D* 57(6):3256–3263. doi:[10.1103/PhysRevD.57.3256](https://doi.org/10.1103/PhysRevD.57.3256). arXiv:[hep-ph/9710337](https://arxiv.org/abs/hep-ph/9710337)
208. Kane GL et al (1994) Study of constrained minimal supersymmetry. *Phys Rev D* 49(11):6173–6210. doi:[10.1103/PhysRevD.49.6173](https://doi.org/10.1103/PhysRevD.49.6173). arXiv:[hep-ph/9312272](https://arxiv.org/abs/hep-ph/9312272)
209. Karachentsev I (2005) The local group and other neighboring galaxy groups. *Astron J* 129(1):178–188. doi:[10.1086/426368](https://doi.org/10.1086/426368)
210. Kelso C, Hooper D, Buckley MR (2012) Toward a consistent picture for CRESST, CoGeNT, and DAMA. *Phys Rev D* 85(4):043515. doi:[10.1103/PhysRevD.85.043515](https://doi.org/10.1103/PhysRevD.85.043515). arXiv:[1110.5338](https://arxiv.org/abs/1110.5338) [astro-ph.CO]
211. Khachatryan V et al [CMS Collaboration] (2011) Search for supersymmetry in pp collisions at 7 TeV in events with jets and missing transverse energy. *Phys Lett B* 698(3):196–218. doi:[10.1016/j.physletb.2011.03.021](https://doi.org/10.1016/j.physletb.2011.03.021). arXiv:[1101.1628](https://arxiv.org/abs/1101.1628) [hep-ex]
212. Kim JE, Carosi G (2010) Axions and the strong CP problem. *Rev Mod Phys* 82(1):557–601. doi:[10.1103/RevModPhys.82.557](https://doi.org/10.1103/RevModPhys.82.557)
213. Kim SC et al [KIMS Collaboration] (2012) New limits on interactions between weakly interacting massive particles and nucleons obtained with CsI(Tl) crystal detectors. *Phys Rev Lett* 108(18):181301. doi:[10.1103/PhysRevLett.108.181301](https://doi.org/10.1103/PhysRevLett.108.181301)
214. Klypin A, Zhao H, Somerville RS (2002) Λ CDM-based models for the Milky Way and M31: I. Dynamical models. *Astrophys J* 573(2):597–613. doi:[10.1086/340656](https://doi.org/10.1086/340656)
215. Klypin A et al (1999) Where are the missing galactic satellites? *Astrophys J* 522:82–92. doi:[10.1086/307643](https://doi.org/10.1086/307643)
216. Klypin A et al (2003) Constrained simulations of the real universe: the local supercluster. *Astrophys J* 596(1):19–33. doi:[10.1086/377574](https://doi.org/10.1086/377574)
217. Kopp J, Schwetz T, Zupan J (2012) Light dark matter in the light of CRESST-II. *J Cosmol Astropart Phys* 2012(3):001. doi:[10.1088/1475-7516/2012/03/001](https://doi.org/10.1088/1475-7516/2012/03/001)
218. Kraus H [EURECA Collaboration] (2012) EURECA. Presented at the 9th international conference: identification of dark matter, IDM2012, Chicago, IL, USA, July 23–27, 2012. <http://kicp-workshops.uchicago.edu/IDM2012/depot/talk-kraus-hans.pdf>
219. Kraus H et al (2006) EURECA—the European future of cryogenic dark matter searches. *J Phys Conf Ser* 39(1):139. doi:[10.1088/1742-6596/39/1/031](https://doi.org/10.1088/1742-6596/39/1/031)
220. Kraus H et al (2010) EURECA. In: Identification of dark matter. 8th international workshop on the identification of dark matter, IDM 2010, Montpellier, France, 26–30 July 2010. Proceedings of science IDM2010. SISSA, Trieste, p 109. http://pos.sissa.it/archive/conferences/110/109/IDM2010_109.pdf

221. Kumar J (2012) Large jet multiplicities and natural supersymmetry at the LHC. In: Limosani A (ed) 36th international conference on high energy physics, ICHEP2012. Melbourne, Australia, 4–11 July 2012. Proceedings of science ICHEP2012. SISSA, Trieste, p 103. arXiv:[1211.6503](#) [hep-ph]
222. Kuźniak M, Boulay M, Pollmann T (2012) Surface roughness interpretation of 730 kg days CRESST-II results. *Astropart Phys* 36(1):77–82. doi:[10.1016/j.astropartphys.2012.05.005](#)
223. Lebedenko VN et al (2009) Results from the first science run of the ZEPLIN-III dark matter search experiment. *Phys Rev D* 80(5):052010. doi:[10.1103/PhysRevD.80.052010](#)
224. Lee HS et al [KIMS Collaboration] (2007) Limits on interactions between weakly interacting massive particles and nucleons obtained with CsI(Tl) crystal detectors. *Phys Rev Lett* 99(9):091301. doi:[10.1103/PhysRevLett.99.091301](#). arXiv:[0704.0423](#) [astro-ph]
225. Lee H et al (2006) [KIMS Collaboration] First limit on WIMP cross section with low background crystal detector. *Phys Lett B* 633(2–3):201–208. doi:[10.1016/j.physletb.2005.12.035](#) arXiv:[astro-ph/0509080](#)
226. Lesgourgues J et al (2006) Probing neutrino masses with CMB lensing extraction. *Phys Rev D* 73:045021. doi:[10.1103/PhysRevD.73.045021](#) arXiv:[astro-ph/0511735](#)
227. Lewin JD, Smith PF (1996) Review of mathematics, numerical factors, and corrections for dark matter experiments based on elastic nuclear recoil. *Astropart Phys* 6(1):87–112. doi:[10.1016/S0927-6505\(96\)00047-3](#)
228. L’Hour M (1987) *Rev Archeol Ouest* 4:113–131. As cited in Ref. [283]
229. Li HB et al [TEXONO Collaboration] (2013) Limits on spin-independent couplings of WIMP dark matter with a p -type point-contact germanium detector. *Phys Rev Lett* 110(26):261301. doi:[10.1103/PhysRevLett.110.261301](#). arXiv:[1303.0925](#) [hep-ex]
230. Li Y-S, White SDM (2008) Masses for the local group and the Milky Way. *Mon Not R Astron Soc* 384(4):1459–1468. doi:[10.1111/j.1365-2966.2007.12748.x](#)
231. Li Z et al (2013) The cryogenic system for the Panda-X dark matter search experiment. *J Instrum* 8:P01002. doi:[10.1088/1748-0221/8/01/P01002](#). arXiv:[1207.5100](#) [astro-ph.IM]
232. Liang H et al (2000) A powerful radio Halo in the hottest known cluster of Galaxies 1E 0657–56. *Astrophys J* 544(2):686. doi:[10.1086/317223](#). arXiv:[astro-ph/0006072](#)
233. Lin ST et al [TEXONO Collaboration] (2009) New limits on spin-independent and spin-dependent couplings of low-mass WIMP dark matter with a germanium detector at a threshold of 220 eV. *Phys Rev D* 79(6):061101. doi:[10.1103/PhysRevD.79.061101](#). arXiv:[0712.1645](#) [hep-ex]
234. Lindhard J (1968) Approximation method in classical scattering by screened Coulomb fields. *Mat Fys Medd Dan Vid Selsk* 36(10):1–44. <http://www.sdu.dk/media/bibpdf/Bind%2030-39/Bind/mfm-36-10.pdf>. As cited in Ref. [105]
235. Lindhard J et al (1963) Integral equations governing radiation effects: notes on atomic collisions, III. *Mat Fys Medd Dan Vid Selsk* 33(10):1–44. <http://www.sdu.dk/media/bibpdf/Bind%2030-39/Bind/mfm-33-10.pdf>. As cited in Ref. [105]
236. Luke PN (1988) Voltage-assisted calorimetric ionization detector. *J Appl Phys* 64(12):6858–6860. doi:[10.1063/1.341976](#). As cited in Ref. [77]
237. Luke PN (1995) Unipolar charge sensing with coplanar electrodes-application to semiconductor detectors. *IEEE Trans Nucl Sci* 42(4):207–213. doi:[10.1109/23.467848](#). As cited in Ref. [133]
238. Malling DC et al (2011) After LUX: the LZ program. arXiv:[1110.0103](#) [astro-ph.IM]
239. Marchionni A et al (2011) ArDM: a ton-scale LAr detector for direct Dark Matter searches. *J Phys Conf Ser* 308(1):012006. doi:[10.1088/1742-6596/308/1/012006](#)
240. Martin SP (2008) A supersymmetry primer. arXiv:[hep-ph/9709356](#)
241. Martineau O et al [EDELWEISS Collaboration] (2004) Calibration of the EDELWEISS cryogenic heat-and-ionization germanium detectors for dark matter search. *Nucl Instrum Methods Phys Res Sect A* 530(3):426–439. doi:[10.1016/j.nima.2004.04.218](#)
242. Milgrom M (1983) A modification of the Newtonian dynamics as a possible alternative to the hidden mass hypothesis. *Astrophys J* 270:365–370. doi:[10.1086/161130](#)

243. Milgrom M (1983) A modification of the Newtonian dynamics—implications for galaxies. *Astrophys J* 270:371–383. doi:[10.1086/161131](https://doi.org/10.1086/161131). ADS:1983ApJ...270..371M
244. Miuchi K et al (2010) First underground results with NEWAGE-0.3a direction-sensitive dark matter detector. *Phys Lett B* 686(1):11–17. doi:[10.1016/j.physletb.2010.02.028](https://doi.org/10.1016/j.physletb.2010.02.028). arXiv:[1002.1794](https://arxiv.org/abs/1002.1794) [astro-ph.CO]
245. Moffat JW (2006) Gravitational lensing in modified gravity and the lensing of merging clusters without dark matter. arXiv:[astro-ph/0608675v1](https://arxiv.org/abs/astro-ph/0608675v1)
246. Monroe J [For the DMTPC Collaboration] (2012) Status and prospects of the DMTPC directional dark matter experiment. In: Steadman SG, Stephans GS, Taylor FE (eds) 19th particles and nuclei international conference, PANIC11, Cambridge, MA, USA, 24–29 July 2011. AIP conference proceedings, vol 1441. AIP Publishing, Melville, pp 515–517. doi:[10.1063/1.3700603](https://doi.org/10.1063/1.3700603). arXiv:[1111.0220](https://arxiv.org/abs/1111.0220) [physics.ins-det]
247. Morgan B [On behalf of the DRIFT and UK Dark Matter collaborations] (2003) DRIFT: a directionally sensitive dark matter detector. In: Proceedings of the 6th international conference on position-sensitive detectors, special issue. *Nucl Instrum Methods Phys Res Sect A* 513 (1–2):226–230. doi:[10.1016/j.nima.2003.08.037](https://doi.org/10.1016/j.nima.2003.08.037)
248. Mulchaey JS (2000) X-ray properties of groups of galaxies. *Annu Rev Astron Astrophys* 38(1):289–335. doi:[10.1146/annurev.astro.38.1.289](https://doi.org/10.1146/annurev.astro.38.1.289)
249. Nakamura K et al (2012) NEWAGE. *J Phys Conf Ser* 375(1):012013. doi:[10.1088/1742-6596/375/1/012013](https://doi.org/10.1088/1742-6596/375/1/012013). arXiv:[1109.3099](https://arxiv.org/abs/1109.3099) [astro-ph.IM]
250. Navarro JF, Frenk CS, White SDM (1996) The structure of cold dark matter halos. *Astrophys J* 462(1996):563–575. doi:[10.1086/177173](https://doi.org/10.1086/177173). ADS:1996ApJ...462..563N
251. Navarro JF, Frenk CS, White SDM (1997) A universal density profile from hierarchical clustering. *Astrophys J* 490:493–508. doi:[10.1086/304888](https://doi.org/10.1086/304888) arXiv:[astro-ph/9611107](https://arxiv.org/abs/astro-ph/9611107)
252. Navarro JF, White SDM (1994) Simulations of dissipative galaxy formation in hierarchically clustering universes: II. Dynamics of the baryonic component in galactic haloes. *Mon Not R Astron Soc* 267:401–412. ADS:1994MNRAS.267..401N
253. Navick X-F [For the EDELWEISS Collaboration] (2009) Status of the development of surface event rejection for ionization-heat detectors in the EDELWEISS collaboration. In: PSD8—proceedings of the 8th international conference on position sensitive detectors, special issue. *Nucl Instrum Methods Phys Res Sect A* 604(1–2):45–47. doi:[10.1016/j.nima.2009.01.199](https://doi.org/10.1016/j.nima.2009.01.199)
254. Navick X-F, L'Hôte D, Tourbot R (2000) Ionization measurement at very low temperature for nuclear and electron recoils discrimination by ionization-heat simultaneous measurement for dark matter research. *Nucl Instrum Methods Phys Res Sect A* 442(1–3):267–274. doi:[10.1016/S0168-9002\(99\)01232-2](https://doi.org/10.1016/S0168-9002(99)01232-2)
255. Navick X-F et al (2004) Fabrication of ultra-low radioactivity detector holders for Edelweiss-II. In: Proceedings of the 10th international workshop on low temperature detectors, special issue. *Nucl Instrum Methods Phys Res Sect A* 520(1–3):189–192. doi:[10.1016/j.nima.2003.11.290](https://doi.org/10.1016/j.nima.2003.11.290)
256. Navick X-F et al [EDELWEISS Collaboration] (2006) Twenty-three ionization heat detectors for the Dark Matter search with EDELWEISS-II. In: Proceedings of the 11th international workshop on low temperature detectors—LTD-11, special issue. *Nucl Instrum Methods Phys Res Sect A* 559(2):483–485. doi:[10.1016/j.nima.2005.12.081](https://doi.org/10.1016/j.nima.2005.12.081)
257. Neganov B, Trofimov V (1985) *Otkrytia i izobretenia* 146:215. As cited in Ref. [77]
258. Nones C [On behalf of the Edelweiss Collaboration] (2012) EDELWEISS detectors: from R & D to dark matter search. *J Phys Conf Ser* 375(1):012024. doi:[10.1088/1742-6596/375/1/012024](https://doi.org/10.1088/1742-6596/375/1/012024)
259. Oort JH (1932) The force exerted by the stellar system in the direction perpendicular to the galactic plane and some related problems. *Bull Astron Inst Netherlands* 6:249–287. ADS:1932BAN.....6..249O
260. Ostriker JP, Peebles PJE, Yahil A (1974) The size and mass of galaxies, and the mass of the universe. *Astrophys J* 193:L1–L4. doi:[10.1086/181617](https://doi.org/10.1086/181617). ADS:1974ApJ...193L...1O
261. Peccei RD, Quinn HR (1977) CP conservation in the presence of instantons. *Phys Rev Lett* 38:1440–1443. doi:[10.1103/PhysRevLett.38.1440](https://doi.org/10.1103/PhysRevLett.38.1440). As cited in Ref. [174, 186]

262. Persic M, Salucci P (1991) The universal galaxy rotation curve. *Astrophys J* 368:60–65. doi:[10.1086/169670](https://doi.org/10.1086/169670). ADS:1991ApJ...368...60P
263. Persic M, Salucci P, Stel F (1996) The universal rotation curve of spiral galaxies: I. The dark matter connection. *Mon Not R Astron Soc* 281:27–47. ADS:1996MNRAS.281...27P
264. Porter TA, Johnson RP, Graham PW (2011) Dark matter searches with astroparticle data. *Annu Rev Astron Astrophys* 49(1):155–194. doi:[10.1146/annurev-astro-081710-102528](https://doi.org/10.1146/annurev-astro-081710-102528)
265. E. Previtali [On behalf of the CUORE Collaboration] (2013) Search for neutrinoless double beta decay with CUORE. In: Proceedings of the 12th Pisa meeting on advanced detectors (La Biodola, Isola d’Elba, Italy, 20–26 May 2012), special issue. *Nucl Instrum Methods Phys Res, Sect A* 718:522–523. doi:[10.1016/j.nima.2012.11.141](https://doi.org/10.1016/j.nima.2012.11.141)
266. Profumo S (2012) Dissecting cosmic-ray electron-positron data with Occam’s razor: The role of known pulsars. *Cent Eur J Phys* 10(1):1–31. doi:[10.2478/s11534-011-0099-z](https://doi.org/10.2478/s11534-011-0099-z). arXiv:[0812.4457](https://arxiv.org/abs/0812.4457) [astro-ph]. As cited in Ref. [13]
267. Randall SW et al (2008) Constraints on the self-interaction cross section of dark matter from numerical simulations of the merging galaxy cluster 1E 0657–56. *Astrophys J* 679(2):1173–1180. doi:[10.1086/587859](https://doi.org/10.1086/587859)
268. Rau W [For the CDMS and SuperCDMS collaborations] (2012) CDMS and Super-CDMS. *J Phys Conf Ser* 375(1):012005. doi:[10.1088/1742-6596/375/1](https://doi.org/10.1088/1742-6596/375/1)
269. Rich J (2010) Fundamentals of cosmology, 2nd ed. Springer, Berlin. doi:[10.1007/978-3-642-02800-7](https://doi.org/10.1007/978-3-642-02800-7)
270. Richard M et al (2007) Dark matter maps reveal cosmic scaffolding. *Nature* 445:286–290. doi:[10.1038/nature05497](https://doi.org/10.1038/nature05497)
271. Riffard Q et al (2013) Dark matter directional detection with MIMAC. arXiv:[1306.4173](https://arxiv.org/abs/1306.4173) [astro-ph.IM]
272. Rozov S et al (2010) Monitoring of the thermal neutron flux in the LSM underground laboratory. arXiv:[1001.4383v1](https://arxiv.org/abs/1001.4383v1) [astro-ph.IM]
273. Rubbia A (2006) ArDM: a ton-scale liquid Argon experiment for direct detection of Dark Matter in the Universe. *J Phys Conf Ser* 39(1):129. doi:[10.1088/1742-6596/39/1/028](https://doi.org/10.1088/1742-6596/39/1/028)
274. Rubin VC, Thonnard N, Ford WK Jr (1980) Rotational properties of 21 SC galaxies with a large range of luminosities and radii, from NGC 4605 ($R = 4$ kpc) to UGC 2885 ($R = 122$ kpc). *Astrophys J* 238:471–487. doi:[10.1086/158003](https://doi.org/10.1086/158003)
275. Rubin VC et al (1985) Rotation velocities of 16 SA galaxies and a comparison of Sa, Sb, and SC rotation properties. *Astrophys J* 289:81–104. doi:[10.1086/162866](https://doi.org/10.1086/162866)
276. Saldanha RN (2012) Status of darkside. Presented at the 9th international conference: identification of dark matter, IDM2012, Chicago, IL, USA, July 23–27, 2012. <http://kicp-workshops.uchicago.edu/IDM2012/depot/plenary-talk-saldanha-richard.pdf>
277. Samtleben D, Staggs S, Winstein B (2007) The cosmic microwave background for pedestrians: a review for particle and nuclear physicists. *Annu Rev Nucl Part Sci* 57(1):245–283. doi:[10.1146/annurev.nucl.54.070103.181232](https://doi.org/10.1146/annurev.nucl.54.070103.181232)
278. Sanders RH (1996) The published extended rotation curves of spiral galaxies: confrontation with modified dynamics. *Astrophys J* 473(1):117–129. doi:[10.1086/178131](https://doi.org/10.1086/178131). arXiv:[astro-ph/9606089v1](https://arxiv.org/abs/astro-ph/9606089v1). As cite in Ref. [176]
279. Sanglard V (2005) Recherche de la matière noire non-baryonique à l’aide de détecteurs cryogéniques à double composante ionisation et chaleur: analyse et interprétation des données de l’expérience EDELWEISS-I’ [in French]. PhD dissertation, Université Claude Bernard - Lyon I. <http://tel.archives-ouvertes.fr/tel-00178567/fr/>. As cite in Ref. [202]
280. Sanglard V et al [EDELWEISS Collaboration] (2005) Final results of the EDELWEISSI dark matter search with cryogenic heat-and-ionization Ge detectors. *Phys Rev D* 71(12):122002. doi:[10.1103/PhysRevD.71.122002](https://doi.org/10.1103/PhysRevD.71.122002)
281. Savage C, Freese K, Gondolo P (2006) Annual modulation of dark matter in the presence of streams. *Phys Rev D* 74(4):043531. doi:[10.1103/PhysRevD.74.043531](https://doi.org/10.1103/PhysRevD.74.043531)
282. Savage C et al (2009) Compatibility of DAMA/LIBRA dark matter detection with other searches. *J Cosmol Astropart Phys* 2009(4):010. doi:[10.1088/1475-7516/2009/04/010](https://doi.org/10.1088/1475-7516/2009/04/010). arXiv:[0808.3607](https://arxiv.org/abs/0808.3607) [astro-ph]

283. Schmidt B et al [EDELWEISS collaboration] (2013) Muon-induced background in the EDELWEISS dark matter search. *Astropart Phys* 44:28–39. doi:[10.1016/j.astropartphys.2013.01.014](https://doi.org/10.1016/j.astropartphys.2013.01.014). arXiv:[1302.7112](https://arxiv.org/abs/1302.7112) [astro-ph.CO]
284. Schnee RW (2011) Introduction to dark matter experiments. In: Csaki C, Dodelson S (ed) *Physics of the large and the small. Proceedings of the theoretical advanced study institute in elementary particle physics, TASI 2009, Boulder, CO, USA, June 1–26, 2009*. World Scientific, Singapore, pp 629–681. doi:[10.1142/9789814327183_fmatter](https://doi.org/10.1142/9789814327183_fmatter). arXiv:[1101.5205](https://arxiv.org/abs/1101.5205) [astro-ph.CO]
285. Scholl S, Jochum J (2012) Neutron background simulation for the CRESST-II experiment. *J Phys Conf Ser* 375(1):012020. doi:[10.1088/1742-6596/375/1/012020](https://doi.org/10.1088/1742-6596/375/1/012020)
286. Shimwell TW et al (2014) Deep radio observations of the radio halo of the bullet cluster 1E 0657–55.8. *Mon Not R Astron Soc* 440(4):2901–2915. doi:[10.1093/mnras/stu467](https://doi.org/10.1093/mnras/stu467). arXiv:[1403.2393](https://arxiv.org/abs/1403.2393) [astro-ph.CO]
287. Shin-Ted L [TEXONO Collaboration] (2008) Neutrino physics and dark matter physics with ultra-low-energy germanium detector. In: Lee D-S, Lee W, Xue S-S (ed) *Relativistic astrophysics. 5th Sino-Italian workshop on relativistic astrophysics, Taipei-Hualien, Taiwan, May 28–June 1, 2008*. AIP conference proceedings, vol 1059. AIP Publishing, Melville, pp 164–171. doi:[10.1063/1.3012272](https://doi.org/10.1063/1.3012272)
288. Shutt T et al (2000) A solution to the dead-layer problem in ionization and phonon-based dark matter detectors. *Nucl Instrum Methods Phys Res Sect A* 444(1–2):340–344. doi:[10.1016/S0168-9002\(99\)01379-0](https://doi.org/10.1016/S0168-9002(99)01379-0). As cited in Refs. [134, 253]
289. Simard L [On behalf of the NEMO-3 Collaboration] (2012) The NEMO-3 results after completion of data taking. *J Phys Conf Ser* 375(4):042011. doi:[10.1088/1742-6596/375/1/042011](https://doi.org/10.1088/1742-6596/375/1/042011)
290. Simionescu A et al (2011) Baryons at the edge of the X-ray-brightest galaxy cluster. *Science* 331(6024):1576–1579. doi:[10.1126/science.1200331](https://doi.org/10.1126/science.1200331)
291. Simon JD, Geha M (2007) The kinematics of the ultra-faint Milky Way satellites: solving the missing satellite problem. *Astrophys J* 670(1):313–331. doi:[10.1086/521816](https://doi.org/10.1086/521816)
292. Smith MC et al (2007) The RAVE survey: constraining the local Galactic escape speed. *Mon Not R Astron Soc* 379(2):755–772. doi:[10.1111/j.1365-2966.2007.11964.x](https://doi.org/10.1111/j.1365-2966.2007.11964.x). As cited in Ref. [39, 76]
293. Sofue Y (2012) A grand rotation curve and dark matter halo in the Milky Way galaxy. *Publ Astron Soc Jpn* 64(4):75. arXiv:[1110.4431](https://arxiv.org/abs/1110.4431) [astro-ph.GA]. <http://www.iao.s.u-tokyo.ac.jp/sofue/htdocs/2012DarkHalo/>
294. Space Telescope Science Institute. Picture album: Einstein ring gravitational lens (SDSS J120540.43+491029.3). <http://hubblesite.org/gallery/album/pr2005032d/>
295. Space Telescope Science Institute. Hubble Finds Ring of Dark Matter. 2007. <http://hubblesite.org/newscenter/archive/releases/2007/17/>. News release STScI-2007-17
296. Spergel DN et al (2003) First-year Wilkinson microwave anisotropy probe (WMAP) observations: determination of cosmological parameters. *Astrophys J Suppl Ser* 148(1):175–194. doi:[10.1086/377226](https://doi.org/10.1086/377226)
297. Spooner NJC (2007) Direct dark matter searches. *J Phys Soc Jpn* 76(11):111016. doi:[10.1143/JPSJ.76.111016](https://doi.org/10.1143/JPSJ.76.111016)
298. Springel V, Frenk CS, White SDM (2006) The large-scale structure of the Universe. *Nature* 440:1137–1144. doi:[10.1038/nature04805](https://doi.org/10.1038/nature04805). arXiv:[astro-ph/0604561](https://arxiv.org/abs/astro-ph/0604561)
299. Steadman SG, Stephans GS, Taylor FE (eds) (2012) 19th particles and nuclei international conference, PANIC11, Cambridge, MA, US, 24–29 July 2011. AIP conference proceedings, vol 1441. AIP Publishing, Melville. <http://scitation.aip.org/content/aip/proceeding/aipcp/1441>
300. Stefano PD et al [EDELWEISS Collaboration] (2001) Background discrimination capabilities of a heat and ionization germanium cryogenic detector. *Astropart Phys* 14(4):329–337. doi:[10.1016/S0927-6505\(00\)00127-4](https://doi.org/10.1016/S0927-6505(00)00127-4)
301. Steigman G (2007) Primordial nucleosynthesis in the precision cosmology era. *Annu Rev Nucl Part Sci* 57(1):463–491. doi:[10.1146/annurev.nucl.56.080805.140437](https://doi.org/10.1146/annurev.nucl.56.080805.140437)
302. Strece C et al (2013) Global fits of the cMSSM and NUHM including the LHC Higgs discovery and new XENON100 constraints. *J Cosmol Astropart Phys* 2013(4):013. doi:[10.1088/1475-7516/2013/04/013](https://doi.org/10.1088/1475-7516/2013/04/013). arXiv:[1212.2636](https://arxiv.org/abs/1212.2636) [hep-ph]

303. Szelc AM [WArP Collaboration] (2009) Current status of the WArP experiment. In: Khalil S (ed) The dark side of the universe. 4th international workshop on the dark side of the universe. Cairo, Egypt, 1–5 June 2008. AIP conference proceedings, vol 1115. AIP Publishing, Melville. pp 105–110. doi:[10.1063/1.3131480](https://doi.org/10.1063/1.3131480)
304. Takahashi R, Chiba T (2007) Weak lensing of galaxy clusters in modified Newtonian dynamics. *Astrophys J* 671(1):45–52. doi:[10.1086/522564](https://doi.org/10.1086/522564)
305. Tegmark M (2005) Cosmological neutrino bounds for non-cosmologists. *Phys Scr T* 121:153–155. doi:[10.1088/0031-8949/2005/T121/023](https://doi.org/10.1088/0031-8949/2005/T121/023). arXiv:[hep-ph/0503257](https://arxiv.org/abs/hep-ph/0503257)
306. The XENON100 Collaboration (2010) Reply to the comments on the XENON100 first dark matter results. arXiv:[1005.2615](https://arxiv.org/abs/1005.2615) [astro-ph.CO]
307. Tisserand P et al (2007) [EROS-2 Collaboration] Limits on the macho content of the galactic halo from the EROS-2 survey of the magellanic clouds. *Astron Astrophys* 469:387–404. doi:[10.1051/0004-6361:20066017](https://doi.org/10.1051/0004-6361:20066017). arXiv:[astro-ph/0607207](https://arxiv.org/abs/astro-ph/0607207)
308. Tollerud EJ et al (2008) Hundreds of Milky Way satellites? Luminosity bias in the satellite luminosity function. *Astrophys J* 688(1):277–289. doi:[10.1086/592102](https://doi.org/10.1086/592102)
309. Tomasello V, Robinson M, Kudryavtsev V (2010) Radioactive background in a cryogenic dark matter experiment. *Astropart Phys* 34(2):70–79. doi:[10.1016/j.astropartphys.2010.05.005](https://doi.org/10.1016/j.astropartphys.2010.05.005)
310. Torii S et al (2008) High-energy electron observations by PPB-BETS flight in Antarctica. arXiv:[0809.0760](https://arxiv.org/abs/0809.0760) [astro-ph]. As cited in Ref. [13, 264]
311. Treu T (2010) Strong lensing by galaxies. *Annu Rev Astron Astrophys* 48(1):87–125. doi:[10.1146/annurev-astro-081309-130924](https://doi.org/10.1146/annurev-astro-081309-130924)
312. Trimble V (1987) Existence and nature of dark matter in the universe. *Annu Rev Astron Astrophys* 25:425–472. doi:[10.1146/annurev.aa.25.090187.002233](https://doi.org/10.1146/annurev.aa.25.090187.002233)
313. Vazquez-Jauregui E (2012) COUPP500: a 500kg bubble chamber for dark matter detection. Presented at the 9th international conference: identification of dark matter, IDM2012, Chicago, IL, USA, 23–27 July 2012. http://kipc-workshops.uchicago.edu/IDM2012/depot/talk-vazquez-jauregui-eric__1.pdf
314. Vegetti S et al (2012) Gravitational detection of a low-mass dark satellite galaxy at cosmological distance. *Nature* 481:341–343. doi:[10.1038/nature10669](https://doi.org/10.1038/nature10669)
315. Vignati S [On behalf of the CUORE Collaboration] (2012) Direct dark matter and axion detection with CUORE. In: Steadman SG, Stephans GS, Taylor FE (eds) 19th particles and nuclei international conference, PANIC11, Cambridge, MA, USA, 24–29 July 2011. AIP conference proceedings, vol 1441. AIP Publishing, Melville, pp 512–514. doi:[10.1063/1.3700602](https://doi.org/10.1063/1.3700602)
316. Weniger C (2012) A tentative gamma-ray line from dark matter annihilation at the Fermi large area telescope. *J Cosmol Astropart Phys* 2012(8):007. doi:[10.1088/1475-7516/2012/08/007](https://doi.org/10.1088/1475-7516/2012/08/007). arXiv:[1204.2797](https://arxiv.org/abs/1204.2797) [hep-ph]
317. Woods M [For the LUX Collaboration] (2013) Underground commissioning of LUX. arXiv:[1306.0065](https://arxiv.org/abs/1306.0065) [astro-ph.IM]
318. Wright A [For the DarkSide Collaboration] (2011) The DarkSide program at LNGS. arXiv:[1109.2979](https://arxiv.org/abs/1109.2979) [physics.ins-det]
319. Wright A et al (2011) A highly efficient neutron veto for dark matter experiments. *Nucl Instrum Methods Phys Res Sect A* 644(1):18–26. doi:[10.1016/j.nima.2011.04.009](https://doi.org/10.1016/j.nima.2011.04.009). arXiv:[1010.3609](https://arxiv.org/abs/1010.3609) [nucl-ex]
320. Wu Y-C et al (2013) Measurement of cosmic ray flux in China JinPing underground laboratory. arXiv:[1305.0899](https://arxiv.org/abs/1305.0899) [physics.ins-det]
321. Yellin S (2002) Finding an upper limit in the presence of an unknown background. *Phys Rev D* 66(3):032005. doi:[10.1103/PhysRevD.66.032005](https://doi.org/10.1103/PhysRevD.66.032005). As cited in Refs. [39, 76]
322. Yue Q, Wong HT [and the Cdex-TeXono Collaboration] (2012) Dark matter search with sub-keV germanium detectors at the China Jinping Underground Laboratory. *J Phys Conf Ser* 375(4):042061. doi:[10.1088/1742-6596/375/1/042061](https://doi.org/10.1088/1742-6596/375/1/042061). arXiv:[1201.5373](https://arxiv.org/abs/1201.5373) [physics.ins-det]
323. Zel'dovich YB (1965) Survey of modern cosmology. In: Kopal Z (ed) *Advances in astronomy and astrophysics*, vol 3. Elsevier, Amsterdam, pp 241–379. doi:[10.1016/B978-1-4831-9921-4.50011-9](https://doi.org/10.1016/B978-1-4831-9921-4.50011-9). As cited in Refs. [173, 206]

- 324. Zhao W et al [CDEX Collaboration] (2013) First results on low-mass WIMP from the CDEX-1 experiment at the China Jinping underground Laboratory. arXiv:[1306.4135](#) [hep-ex]
- 325. Zwicky F (1933) Die Rotverschiebung von extragalaktischen Nebeln [in German]. *Helv Phys Acta* 6(2):110–127. doi:[10.5169/seals-110267](#)
- 326. Zwicky F (1937) On the masses of nebulae and of clusters of nebulae. *Astrophys J* 86(1937):217–246. doi:[10.1086/143864](#). ADS:1937ApJ....86..217Z

Production Yield of Muon-Induced Neutrons in Lead
Measured at the Modane Underground Laboratory

Kluck, H.

2015, XXV, 382 p. 91 illus., 65 illus. in color., Hardcover

ISBN: 978-3-319-18526-2